

**UV/OXIDANT DEGRADATION OF PRE-TREATED PALM OIL MILL  
EFFLUENT IN A PHOTOCATALYTIC FUEL CELL**

**JOYEE YAP CHUN TING**

**A project report submitted in partial fulfilment of the  
requirements for the award of the degree of  
Bachelor of Engineering (Hons) Environmental Engineering**

**Faculty of Engineering and Green Technology  
Universiti Tunku Abdul Rahman**

**January 2022**

## DECLARATION

I hereby declare that this project report is based on my original work except for citations and quotations which have been duly acknowledged. I also declare that it has not been previously and concurrently submitted for any other degree or award at UTAR or other institutions.

Signature : *Joyee*

Name : Joyee Yap Chun Ting


ID No. : 19AGB00406


Date : 7<sup>th</sup> September 2022

**APPROVAL FOR SUBMISSION**

I certify that this project report entitled **“UV/OXIDANT DEGRADATION OF PRE-TREATED PALM OIL MILL EFFLUENT IN A PHOTOCATALYTIC FUEL CELL”** was prepared by **JOYEE YAP CHUN TING** has met the required standard for submission in partial fulfilment of the requirements for the award of Bachelor of Engineering (Hons) Environmental Engineering at Universiti Tunku Abdul Rahman.

Approved by,

Signature :   
Supervisor : ChM. Ts. Dr. Lam Sze Mun  
Date : 7<sup>th</sup> September 2022

Signature :   
Co-Supervisor : ChM. Ts. Dr. Sin Jin Chung  
Date : 7<sup>th</sup> September 2022

The copyright of this report belongs to the author under the terms of the copyright Act 1987 as qualified by Intellectual Property Policy of Universiti Tunku Abdul Rahman. Due acknowledgement shall always be made of the use of any material contained in, or derived from, this report.

© 2022, Joyee Yap Chun Ting. All right reserved.

## ACKNOWLEDGEMENTS

This thesis would not have come to fruition without the help of everyone in many ways. First and foremost, I would like to express my sincere gratitude to my research supervisor, ChM. Ts. Dr. Lam Sze Mun for her invaluable patience, guidance, advice and constant support throughout the entire final year project research process. My sincere appreciation also extends to my co-supervisor, ChM. Ts. Dr. Sin Jin Chung for his consistent support and guidance.

My heartfelt thankfulness goes toward to my seniors, specifically Yong Zi Jun and Warren Tong Meng Wei for their useful advices on providing me guidance in using the laboratory equipment and instruments. They have always been incredibly helpful and kind in assisting me throughout the whole journey of my research. A token of appreciation is also forwarded to the UTAR lab officers who diligently cater to my every request in the laboratory.

Lastly, I would like to thank my family for their love, unwavering physical and mental support in supporting me to complete the final year project research. This endeavor would not have been possible without their belief in me.

## UV/OXIDANT DEGRADATION OF PRE-TREATED PALM OIL MILL EFFLUENT IN A PHOTOCATALYTIC FUEL CELL

### ABSTRACT

Attributable to the prosperous palm oil production growth in Malaysia, the generated palm oil mill effluent (POME) poses a high threat owing to its highly polluted characteristic. As the disposal of this effluent raised public environmental concern, POME pollution abatement and potential energy recovery from the effluent are flagged up as a research topic of interest. In this study, a new photocatalytic fuel cell system with employment of ZnO/Zn nanorod array photoanode, CuO/Cu cathode and persulfate oxidant was successfully designed to improve the degradation of organic pollutant in POME and simultaneous energy production. The photoelectrodes were fabricated and characterized by Field emission scanning electron microscopy with energy, X-ray diffraction, UV–Vis diffuse reflectance spectroscopy and Mott–Schottky plot analysis. Owing to the properties of strong oxidant of persulfate, the proposed PFC system has exhibited exceptional performance, increasing the chemical oxygen demand (COD) removal efficiency from 39.6% to 96.2% and amount of electricity generated from 5.7 to 35.6 mW/cm<sup>2</sup> relative to the bare PFC system. The best PFC system performance was yielded under optimal conditions of 2.5mM of persulfate oxidant, POME dilution factor of 1:20 and natural solution pH of 8.51. Subsequently, a radical scavenging test was conducted, determining that the predominant radical species were sulfate radical (SO<sub>4</sub><sup>•-</sup>) and hydroxyl radical (•OH) contributed to effective removal of organics pollutant in POME and generation of electricity. The following recycling test affirmed the stability and durability photoanode after 4 continuous repetition usage and the cost analysis revealed the economic viability of PFC system serving as a post-treatment for degradation of POME. These findings contribute toward enhancing the sustainability criteria and economic viability of palm oil by adopting sustainable and efficient POME post-treatment technology.

## TABLE OF CONTENTS

<b>DECLARATION</b>	<b>ii</b>
<b>APPROVAL FOR SUBMISSION</b>	<b>iii</b>
<b>ACKNOWLEDGEMENTS</b>	<b>v</b>
<b>ABSTRACT</b>	<b>vi</b>
<b>TABLE OF CONTENTS</b>	<b>vii</b>
<b>LIST OF TABLES</b>	<b>x</b>
<b>LIST OF FIGURES</b>	<b>xi</b>
<b>LIST OF SYMBOLS / ABBREVIATIONS</b>	<b>xiv</b>

### CHAPTER

<b>1</b>	<b>INTRODUCTION</b>	<b>1</b>
	1.1 Advanced Oxidation Process for Treatment of Palm Oil Mill Effluent 1	
	1.2 Problem Statements	3
	1.3 Objectives of the study	5
	1.4 Scope of Study	5
<b>2</b>	<b>LITERATURE REVIEW</b>	<b>6</b>
	2.1 Palm Oil Mill Effluent Wastewater	6
	2.2 POME Treatment Methods	8
	2.2.1 Biological Treatment Methods	8
	2.2.2 Physicochemical Treatment Methods	10
	2.3 Advanced Oxidation Process	12
	2.3.1 Photocatalytic Fuel Cell	13
	2.4 Process Parameter Study	24

2.4.1	Types and concentration of oxidant	24
2.4.2	Initial pollutant concentration	26
2.4.3	Initial Solution pH	27
2.5	Detection of active species	30
2.6	Summary of literature review	31
<b>3</b>	<b>RESEARCH METHODOLOGY</b>	<b>32</b>
3.1	Materials and Chemicals	32
3.2	Apparatus and Equipment	35
3.2.1	Photocatalytic Fuel Cell (PFC) Experimental Apparatus	35
3.3	Analytic Procedure	37
3.3.1	Chemical Oxygen Demand (COD) Analysis	37
3.3.2	Biochemical Oxygen Demand (BOD) Analysis	37
3.3.3	Turbidity Analysis	38
3.3.4	Ammoniacal Nitrogen (NH <sub>3</sub> -N) Analysis	39
3.4	Preparation of Photoelectrodes	39
3.4.1	Preparation of Photoanode	39
3.4.2	Preparation of Cathode	42
3.5	Characterization of Photoelectrodes	43
3.5.1	Crystal Phase Analysis	43
3.5.2	Surface Morphology Analysis	43
3.5.3	Functional Group Analysis	43
3.6	PFC System Constructed Using ZnO/Zn Nanorod Array Structure Photoanode and CuO/Cu Cathode	44
3.7	Process Parameter Studies	45
3.7.1	Types and concentration of oxidant	46
3.7.2	Initial POME Concentration	46
3.7.3	Initial solution pH	46
3.8	Radical Scavenging Test	47
3.9	Reusability of the photoelectrodes	48
<b>4</b>	<b>RESULTS AND DISCUSSIONS</b>	<b>49</b>



4.1	Characterization of Photoelectrodes	50
4.1.1	Surface Morphology Analysis	50
4.1.2	Elemental Composition Analysis	52
4.1.3	Crystalline Phase Analysis	53
4.1.4	Band Gap Potential Measurement	55
4.1.5	Conduction Band (CB) Potential Measurement	56
4.2	Fundamental studies of PFC system	57
4.2.1	Effect of Open and Closed Circuit	61
4.3	Optimization of Operating Conditions for PFC System	63
4.3.1	Optimum concentration of oxidant	63
4.3.2	Optimum Initial Organic Matter Concentration	66
4.3.3	Optimum Initial pH condition	70
4.4	Roles of Different Radical Species in PFC system	75
4.5	Recycling Test	78
4.6	Cost Analysis	80
<b>5</b>	<b>CONCLUSION AND RECOMMENDATIONS</b>	<b>83</b>
5.1	Conclusion	83
5.2	Recommendations for Future Studies	85
	<b>REFERENCES</b>	<b>86</b>
	<b>AWARD</b>	<b>101</b>

## LIST OF TABLES

<b>TABLE</b>	<b>TITLE</b>	<b>PAGE</b>
Table 2.1:	General Characteristics of POME and Allowable Effluent Discharge	7
Table 2.2:	Oxidation potential of various oxidants (Mayyahi and Al-Asadi, 2018)	13
Table 2.3:	Summary of literature-reviewed fabrication methods for the photoelectrodes.	21
Table 2.4:	The effects of initial solution pH on the photocatalytic performance of PFC.	29
Table 3.1:	List of Materials and Chemicals Used.	34
Table 3.2:	List of Commonly Used Radical Scavengers (Li et al., 2019; Pelaez et al., 2016; Liang and Lei, 2015).	47
Table 4.1:	Summary of Measured Pre-treated POME Quality Parameters Pre- and Post-Photocatalytic Degradation Using PFC System of ZnO/Zn Nanorod Array Photoanode and CuO/Cu Cathode in the Presence of Persulfate Oxidant Under UVC light ([PS] = 2.5 mM; POME Dilution Ratio = 1:20; Solution pH = 8.51; UVC light Irradiation Time = 240 minutes).	75
Table 4.2:	Total Electricity Consumption and Cost for Fabrication of Photoanode and Cathode.	80

## LIST OF FIGURES

<b>FIGURE</b>	<b>TITLE</b>	<b>PAGE</b>
Figure 2.1:	Global production of palm oil from 2016/17 to *2021/22 (USDA, 2022)	7
Figure 2.2:	A simple set-up of PFC system with photoanode and photocathode.	14
Figure 2.3:	Photocatalytic Mechanism of a PFC System for Wastewater Treatment (Kemacheevakul and Chuangchote, 2021)	15
Figure 2.4:	The most commonly produced 0D, 1D and 2D nanostructures (nanoparticles, nanowires, nanotubes, nanorods and nanosheets) in the form of building blocks, hierarchical assembly and arrays (Concina, Ibupoto and Vomiero, 2017).	18
Figure 2.5:	Schematic Diagram of 0D, 1D and 2D nanostructured material (Li and Wang, 2019).	18
Figure 3.1:	The flow of Experimental Work Conducted in this Research.	33
Figure 3.2:	Schematic Diagram of PFC System	36
Figure 3.3:	Experimental Setup of PFC System	36
Figure 3.4:	Schematic Flow Chart for the Synthesis of ZnO/Zn Nanorod Array Photoanode.	41
Figure 3.5:	Schematic Flow Chart for the Synthesis of CuO/Cu Cathode.	42
Figure 4.1:	FESEM images of synthesized ZnO/Zn nanorod array photoanode under magnifications of (a) x 5,000 and (b) x 10,000.	51
Figure 4.2:	FESEM images of synthesized CuO/Cu cathode under magnifications of (a) x 20,000 and (b) x 40,000.	51

Figure 4.3: EDX Spectra of ZnO/Zn Photoanode	52
Figure 4.4: EDX Spectra of ZnO/Zn Photoanode	53
Figure 4.5: XRD pattern of ZnO/Zn nanorod array photoanode	54
Figure 4.6: XRD pattern of CuO/Cu cathode	55
Figure 4.7: UV-Vis Spectra of ZnO NRA	56
Figure 4.8: MS Plots of ZnO NRA.	57
Figure 4.9: Photocatalytic Degradation of POME Using PFC System Using Photolysis, Without addition of oxidant and With 0.5mM of Na <sub>2</sub> S <sub>2</sub> O <sub>8</sub> oxidant (POME dilution ratio = 1:20; Solution pH = 8.51).	58
Figure 4.10: The Difference Between Bare PFC System with Addition of Persulfate Oxidant on Electricity Generation by the PFC system (POME dilution ratio = 1:20; Solution pH = 8.51).	60
Figure 4.11: Photocatalytic Degradation of POME Using PFC System Under Open and Closed Circuit Condition (POME dilution ratio = 1:20; Solution pH = 8.51).	62
Figure 4.12: The effect of Na <sub>2</sub> S <sub>2</sub> O <sub>8</sub> Oxidant Loading on The COD Removal Efficiency Using PFC System (POME Dilution Ratio = 1:20; Solution pH = 8.51).	64
Figure 4.13: The effect of Na <sub>2</sub> S <sub>2</sub> O <sub>8</sub> Oxidant Loading on Electricity Generation Efficiency Using PFC System (POME Dilution Ratio = 1:20; Solution pH = 8.51).	65
Figure 4.14: The Effect of Initial Organic Matter Concentration on the Photocatalytic Degradation of COD Using PFC System ([PS] = 2.5 mM; Solution pH = 8.51).	67
Figure 4.15: The Effect of Initial POME Dilution Ratio on Electricity Generation Efficiency Using PFC System ([PS] = 2.5 mM; Solution pH = 8.51).	68
Figure 4.16: The Effect of pH on the COD Removal Efficiency of POME Solution Using PFC System ([PS] = 2.5 mM; POME Dilution Ratio = 1:20).	71
Figure 4.17: The Effect of pH of POME Solution on the Electricity Generation Efficiency Using PFC System ([PS] = 2.5 mM; POME Dilution Ratio = 1:20).	72

- Figure 4.18: COD Removal Rate of POME Using Developed PFC System in Existence of Various Radical Capturing Agents (POME Dilution Factor = 1:20; [PS] = 2.5 mM; Solution pH = 8.51; [Radical Scavenging Agent] = 2 mM). 76
- Figure 4.19: Schematic Diagram of photocatalytic mechanism of ZnO/Zn NRA photocatalyst, proposed persulfate activation, radicals' generation and POME degradation pathway in the PFC system. 77
- Figure 4.20: COD Removal Rate of POME Using Developed PFC System for Four Consecutive Cycles (POME Dilution Factor = 1:20; [PS] = 2.5 mM; Solution pH = 8.51). 79

## LIST OF SYMBOLS / ABBREVIATIONS

$^{\circ}\text{C}$	Degree Celsius
$\lambda$	Wavelength
$\theta$	Angle Between Incident X-Ray and Reflecting Plane
$2\theta$	Angle Between Incident X-Ray and Reflected Beam
$\Omega$	Ohm
A	Ampere
eV	Electron Volt
I	Circuit Current, A
$J_{sc}$	Short Circuit Current Density, mA/cm <sup>2</sup>
kWh	Kilowatt-Hour
$l$	Length of Light Transport Path
mM	Millimolar
nm	Nanometer
$P_{max}$	Maximum Power Density, mW/cm <sup>2</sup>
RM	Malaysian Ringgit
rpm	Revolutions Per Minute
V	Voltage
$V_{oc}$	Open Circuit Voltage, mV
W	Watt
$C_0$	Initial Dye Concentration Value
$C_f$	Final Dye Concentration Value
$DO_0$	Initial Dissolved Oxygen Value
$DO_5$	Final Dissolved Oxygen Value After 5 Days Incubation
$E_g$	Energy Band Gap
$E_{CB}$	Conduction Band (CB) Potential
$E_{VB}$	Valence Band (CB) Potential
$h\nu$	Light Energy

$R^2$	Coefficient of Linear Correlation
$Cl^-$	Chlorite Ion
$H^+$	Hydrogen Ion
$HO_2\cdot$	Hydroperoxyl Radical (or Hydrogen Superoxide)
$Na^+$	Sodium Ion
$NH_4^+$	Ammonium Ion
$NO_3^-$	Nitrate
$NO_2^-$	Nitrite
$OH^-$	Hydroxide Ion
$\cdot OH$	Hydroxyl Radical
$\cdot O_2^-$	Superoxide Anion
$SO_4^{2-}$	Sulfate Ion
$SO_4\cdot^-$	Sulfate Radical
$e_{CB}^-$	Electrons at Conduction Band
$e_{CB}^- - h_{VB}^+$	Electron-Hole Pair
$h_{VB}^+$	Positive Holes at Valence Band
1,4-BQ	1,4-Benzoquinone
AgCl	Silver Chloride
AgNO <sub>3</sub>	Silver Nitrate
C <sub>2</sub> H <sub>5</sub> OH	Ethanol
C <sub>6</sub> H <sub>12</sub> N <sub>4</sub>	Hexamethylenetetramine
C <sub>3</sub> H <sub>8</sub> O	Isopropyl Alcohol
CO <sub>2</sub>	Carbon Dioxide
Cu	Copper
CuO	Copper Oxide
H <sub>2</sub> O	Water Molecule
H <sub>2</sub> O <sub>2</sub>	Hydrogen Peroxide
H <sub>2</sub> SO <sub>4</sub>	Sulfuric Acid
HCl	Hydrochloric Acid
KOH	Potassium Hydroxide
NaCl	Sodium Chloride

NaOH	Sodium Hydroxide
Na <sub>2</sub> SO <sub>4</sub>	Sodium Sulfate
Na <sub>2</sub> S <sub>2</sub> O <sub>8</sub>	Sodium Persulfate
Pt	Platinum
Sn <sub>3</sub> O <sub>4</sub>	Tin Oxide
TiO <sub>2</sub>	Titanium Dioxide
Zn	Zinc
Zn(CH <sub>3</sub> COO) <sub>2</sub> •2H <sub>2</sub> O	Zinc Acetate Dihydrate
Zn(NO <sub>3</sub> ) <sub>2</sub> •4H <sub>2</sub> O	Zinc Nitrate Tetrahydrate
Zn(NO <sub>3</sub> )•6H <sub>2</sub> O	Zinc Nitrate Hexahydrate
ZnO	Zinc Oxide
EtOH	Ethanol
EDTA-2Na	Ethylenediaminetetraacetic Acid Disodium Salt
FEGT	Faculty of Engineering and Green Technology
FESEM	Field Emission Scanning Electron Microscopy
FTIR	Fourier Transform Infrared
FTO	Fluorine-Doped Tin Oxide
MBBR	Moving Bed Biofilm Reactor
MS	Mott-Schottky
NHE	Normal Hydrogen Electrode
NTU	Nephelometric Turbidity Units
PFC	Photocatalytic Fuel Cell
pH <sub>zpc</sub>	Point of Zero Charge
RBC	Rotating Biological Contactor
TN	Total Nitrogen
TSS	Total Suspended Solids
UTAR	Universiti Tunku Abdul Rahman
UV	Ultraviolet
UV-Vis DRS	UV-Vis Diffuse Reflectance Spectroscopy
VB	Valence Band
VOC	Volatile Organic Compounds
XRD	X-Ray Diffraction



## CHAPTER 1

### INTRODUCTION

#### 1.1 Advanced Oxidation Process for Treatment of Palm Oil Mill Effluent

Owing to the predicted extinction of fossil fuel, the energy industry faces hurdles in acquiring other powerful, yet environmentally friendly and abundant in nature to compete on the global energy platform. Research effort and interest in recent decades have been diverted to the employment of biofuels, notably palm oil, as a highly favourable sustainable alternative to renewable fuel resources that can create cheaper, cleaner and readily available energy resources (Kaniapan et al., 2021). According to Dashti et al. (2022), 75 million metric tonnes of palm oil were produced globally in 2020 and this figure was predicted to increase to cope with the ever-increasing energy demand and other human needs. While palm oil agribusiness has garnered global recognition for its contribution to Malaysia's and Indonesia's economy, it is also a major contributor to environmental pollution due to huge quantities of liquid waste produced, namely the palm oil mill effluent (POME) (Lim, Sethu and Selvarajoo, 2022).

POME is a brownish, foul-smelling and viscous waste with acidic properties (Syahin et al., 2020 and Isa, Bashir and Wong, 2022). This highly viscous waste is produced from sterilization, hydro-cyclone waste, and separator sludge where sterilizer effluent and separator sludge are the two major sources of POME, contributing to the highly contaminated wastewater characteristics (Kamyab et al., 2018). Sia, Tan and Abdullah (2020) estimated that approximately 5 to 7.5 tonnes of

clean water are needed to generate one ton of crude palm oil, whereas more than half of this quantity is being discharged as POME, indicating that 187.5 million tonnes to 281.25 million tonnes of POME were generated during the palm oil milling process in 2020. Treating POME is thus necessary in order to recover the vast amount of water used for water-reusing purposes within industrial processes or even sustainable water consumption to ensure water sustainability.

Direct discharge of POME without proper treatment imposes adverse environmental degradation and poses significant threats to aquatic organisms due to its highly polluting characteristic (Mohamad et al, 2022). According to Environmental Quality (Prescribed Premises) (Crude Palm-Oil) Regulations 1977 in Malaysia, treatment of POME is mandatory prior to discharge to waterways. Therefore, numerous biological, physical, and chemical techniques have hitherto been widely adopted to treat POME (Sia, Tan and Abdullah, 2020). In recent years, the research effort and attention have been shifted towards achieving economical and environmentally practical wastewater treatment solutions, remarkably the advanced oxidation processes (AOPs). The AOPs acts as a pivotal solution to break down recalcitrant organic pollutants as it generates highly reactive free radicals, particularly hydroxyl radical ( $\bullet\text{OH}$ ) which are the dominant oxidizing agent that can alter the organic pollutants to less harmful or even innocuous substances (Solanki et al., 2020).

Among the AOPs, photocatalytic fuel cell (PFC) is an innovative treatment method that degrades POME and recovers chemical energy simultaneously to be converted into electricity (Kokkinos, Venieri and Mantzavinos, 2021). In PFC, the fabricated metal-oxide semiconductor carries photocatalyst generates electrons ( $e^-$ ) while the cathode receives the electrons ( $e^-$ ) to degrade organic pollutants and generate electrical power simultaneously when exposed to UV radiation from sunlight or artificial light (Vasseghian, 2020). In addition, with the introduction of persulfate (PS) as an oxidant in PFC, the photocatalytic reaction will be accelerated, thus the treatment time of POME will be significantly shortened (Tang et al., 2019). With better knowledge and understanding of PFC in combination with oxidant, PFC will be a potential POME treatment to be invested in for the palm oil industry in Malaysia and Indonesia.

## 1.2 Problem Statements

POME consists of oil and grease, a vast amount of solids, biochemical oxygen demand (BOD) and chemical oxygen demand (COD) in richness (Oyekanmi et al., 2021). It is noteworthy that POME is classified as a non-toxic effluent since no chemical is added when the palm oil is extracted (Kamyab et al., 2018). Nevertheless, in a study conducted by Akhbari et al. (2020), one tonne of palm fruit bunches is estimated to yield approximately 0.5–0.75 tonnes of POME which contain 5 kg/ton of organic matter. Thus, the presence of POME enriched with organic matter in the water environment poses a serious threat to aquatic life as degradation of organic pollutants depletes dissolved oxygen (DO) in the watercourse. Furthermore, Hashiguchi et al., (2020) and Hashiguchi et al., (2021) have revealed that POME reduces plankton diversity and induces lethality of fish embryos owing to POME's high COD and acidic properties. Nonetheless, the ample organic substances in POME are important sources of chemical energy which can be converted to electricity through PFC treatment (Tang et al., 2019). Instead of perceiving POME as a burden to be dealt with, POME itself is henceforth a valuable resource that can be utilized with the employment of appropriate wastewater treatment.

PFC as one of the AOPs that utilizes heterogenous photocatalysis has attained an excessive research interest for efficient tertiary treatment for organic substances degradation and solar energy conversion. In PFC, photoexcitation of electrons occurs when there is light irradiation on the semiconductor catalyst surface, causing the transportation of electrons ( $e^-$ ) to the cathode and generate electricity. Among all the photocatalyst metal-oxide semiconductors that have been extensively explored for the photocatalytic purification of wastewaters, titanium dioxide ( $\text{TiO}_2$ ) and zinc oxide ( $\text{ZnO}$ ) has received great attention attributable to its environmental stability and wide band-gap that enables  $\text{TiO}_2$  and  $\text{ZnO}$  to be active under UV light irradiation.  $\text{ZnO}$  is a more preferable material as the photocatalysts since it exhibits higher electron mobility and longer carrier diffusion length than  $\text{TiO}_2$  (Commandeur et al., 2019). However, Oluwole, Omotola and Olatunji (2020) and Gao et al., (2021) have found out that the conventional powdered  $\text{ZnO}$  photocatalyst was difficult to be removed from the aqueous suspension from the reactor system, resulting in low photocatalytic activity

efficiency and generation of secondary pollution. The aforementioned issue is suggested to be overcome by adopting one-dimensional (1D) ZnO nanorod structures, which enables the recovery and reuse of the photocatalysts in the PFC system (Mustapha et al., 2020). In addition, the ZnO nanorod array has shown significant enhancement in wastewater treatment as this structure offer a larger specific surface area, lower impurity and better orientation to ensure effective charge transport, consequently enhancing the efficiency of the PFC system to degrade organic pollutant and generate power (Commandeur et al., 2019 and Du, et al., 2019).

To further improve the 1D ZnO nanorod consisted-PFC, persulfate (PS) as oxidant was added to combine with PFC for acceleration of the photocatalytic redox reactions in the PFC system. PS ( $S_2O_8^{2-}$ ) is a strong oxidant, which has a high oxidation potential ( $E^0$ ) of 2.01V that allows PS to act as an electron acceptor for improvement of electron-holes separation on the photoanode (Tang et al., 2019). Furthermore, the PS forms a reactive radical, which is known as the sulphate free radical ( $SO_4^{\cdot-}$ ) under light irradiation. The  $SO_4^{\cdot-}$  is capable to oxidize almost all organic compounds efficiently since  $SO_4^{\cdot-}$  has a stronger  $E^0$  value of 3.1V than  $\cdot OH$  which has a  $E^0$  of 2.7V, as reported by Li, et al., (2019). In addition, PS has a wide-ranging operating at pH range, it is hence a stable oxidant to enthusiastically treat POME with acidic properties (Ushani, et al., 2020). Overall, the addition of  $SO_4^{\cdot-}$  can remarkably contribute to electron transfer reactions, leading to increased performance of the PFC system.

Therefore, this study aimed to provide a novel and feasible PFC technology for efficient POME treatment and environmentally-friendly power generation by using ZnO nanorod array as the photocatalysts with the addition of PS as the oxidant. The effectiveness of ZnO nanorod array photoanode and CuO/Cu cathode in treating POME from real-life industry and synchronous electricity generation under the UV/PS oxidant will be further evaluated.

### 1.3 Objectives of the study

The objectives of this research are shown as following:

- i) To develop a PFC system consisting of ZnO/Zn nanorods array as the photoanode and CuO/Cu as the cathode.
- ii) To examine the effects of process parameters, the concentration of oxidant and pH of the solution to treat POME in different concentrations over the developed PFC system under UV/PS oxidant condition.
- iii) To study the photocatalytic mechanism of PFC system in degrading organic pollutant and generating electricity

### 1.4 Scope of Study

This study is conducted to investigate the efficiency of the PFC system with the employment of one-dimensional (1D) ZnO/Zn nanorod array as photoanode, CuO/Cu as cathode under UV /PS oxidant in treating real industrial POME. Characterization of the photocatalysts will be conducted using a variety of techniques such as field emission scanning electron microscopy (FESEM), energy-dispersive X-ray spectroscopy (EDX), X-ray powder diffraction (XRD) and photo-electrochemical test (PEC). Prior to the PFC treatment of POME, the physiochemical properties of POME, such as BOD, COD, turbidity, ammoniacal nitrogen (NH<sub>3</sub>-N) and pH will be carried out as it serves as a beneficial piece of information to the study and the palm oil mill industry. Besides, the optimum process parameter, which includes the concentration of oxidant, pH of the solution and concentration of the POME will be determined to obtain the best PFC performance to break down POME. The reusability of the photocatalysts of the developed PFC system will also be examined in the study.

## CHAPTER 2

### LITERATURE REVIEW

#### 2.1 Palm Oil Mill Effluent Wastewater

Palm oil, which is a vegetable oil obtained from the mesocarp of the oil palm fruit (*Elaeis guineensis*), is gaining prominence as a promising viable source of energy to replace fossil fuels, making it one of the fastest expanding equatorial agricultural plantations (Yusoff et al., 2021). Based on Figure 2.1, which is the worldwide palm oil global production figures gathered from the United States Department of Agriculture (USDA), while the palm oil production has been escalating steadily from 2017 to 2022, Indonesia and Malaysia being the top two countries have supplied 59.6% and 24.5% of palm oil to the world in 2020/21 reportedly (USDA, 2022). However, the palm oil production along with the effluent, known as POME is predicted to continue to increase, in order to cater for the world palm oil demand.

POME is a combination of wastewater generated from a variety of process units in production of palm oil, including clarification process (60%), sterilization of condensate (36%), and hydro-cyclone drain-off (4%) (Alhaji et al., 2016). POME exists as a massive amount of thick, brownish slurry liquid waste with acidic properties (pH ranging from 3.5 to 4.2) that is discharged at a temperature between 80°C and 90°C. In spite of its non-toxic nature as a result of the non-chemical extraction technique, POME was reported by the Malaysian Palm Oil Board (MPOB) (2014) to have high oil and grease (O&G) varying from 150 to 18,000 mg/L, biological oxygen demand (BOD) ranging from 10,250 to 43,750 mg/L, chemical oxygen demand (COD)

of 100,000 mg/L and other characteristics that exceed the water quality threshold limits established by the Department of Environment (DOE) Malaysia. Table 2.1 summarises the general properties of untreated POME and the permissible discharge limits (DOE, 2015).

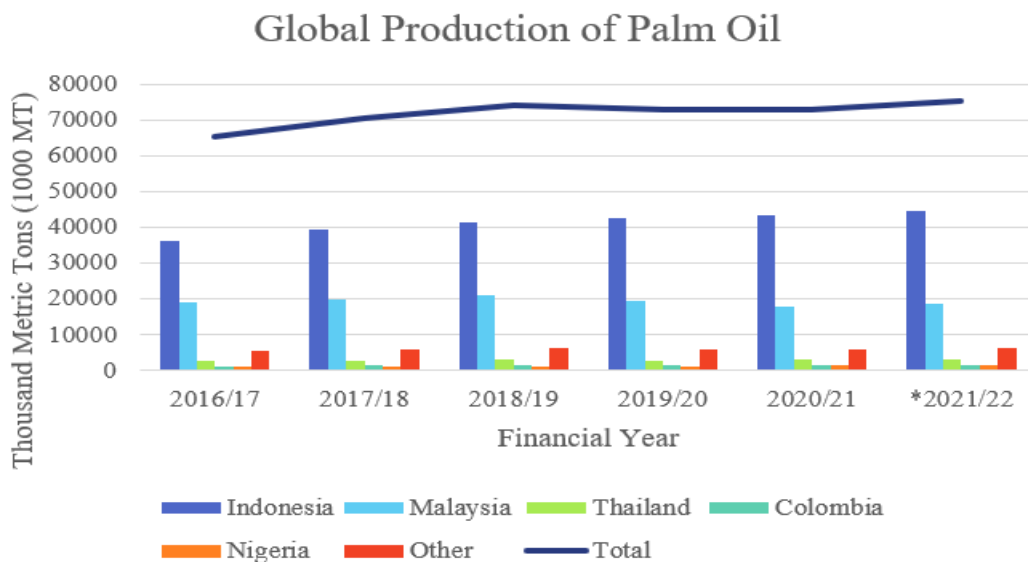


Figure 2.1: Global production of palm oil from 2016/17 to \*2021/22 (USDA, 2022)

**Table 2.1: General Characteristics of POME and Allowable Effluent Discharge**

Parameter	Concentration Range	Effluent Discharge Standard****	Units
Temperature**	80 – 90	45	°C
pH*	3.4 – 5.2	5 – 9	
Oil and Grease (O&G)*	150 – 18,000	50	mg/L
Biological Oxygen Demand (BOD; 3 days, 30°C)*	10,000 – 44,000	100	mg/L
Chemical Oxygen Demand (COD)*	15,000 – 100,000	-	mg/L
Total Suspended Solids (TSS)*	5,000 – 54,000	400	mg/L
Total Volatile Solids (TVS)	9,000 – 72,000	-	mg/L
Ammoniacal Nitrogen (AN)*	4 – 80	150	mg/L
Total Nitrogen (TN)*	180 – 1,400	200	mg/L
Turbidity***	11,000	-	NTU

\*MOBR (2014); \*\* Tan and Lim (2019); \*\*\*Ahmad et al. (2006); \*\*\*\* DOE (2015)

## **2.2 POME Treatment Methods**

Since oil palm takes 6.5 times lesser land area for cultivation compared to typical crops, it is one of the most economical and valuable sources of lignocellulosic biomass (Sadhukhan et al., 2018). It is thus essential to tackle the oil palm sustainability issue with considerable attention. However, in opinion of Lee et al., (2019), POME is regarded as one of the problematic wastes to manage owing to its enormous production and high polluting loads of organic matter in the form of BOD and COD. Up-to-date, various POME treatment technologies have been established, which can be classified into two main segments: biological, and physicochemical. This section will review the strength and limitations of each technology to determine the most technically and economically feasible POME treatment.

### **2.2.1 Biological Treatment Methods**

It is a common practice to use biological treatment in treating POME in the palm oil millers in Malaysia due to its affordability, simplicity, and environmentally friendly properties (Abdulsalam et al., 2018). In biological treatment, organisms such as bacteria, protozoan, aquatic plants, marshland plants and algae carry out biodegradation, breaking down unwanted organic and inorganic particles into harmless byproducts in order to consume and increase their population and size (Abdulsalam et al., 2018). Biodegradation of POME can be easily achieved either through an anaerobic or aerobic process.

The anaerobic system is carried out without the presence of oxygen,  $O_2$  to stabilize organic materials through conversion to  $CH_4$ , which may be used as an energy source, and inorganic end-products such as  $CO_2$  and  $NH_3$  to treat POME. At present, there are several anaerobic treatment systems have been developed to treat POME, such as anaerobic sequencing batch reactor (ASBR) and the up-flow anaerobic sludge blanket (UASB) bioreactor for instance. The treatment efficiency of POME using UASB bioreactor with hollow centred packed bed (UASB-HCPB), which was studied by Poh and her co-worker (2014) has shown a high removal percentage of both BOD and COD more than 90% from POME with the production of 60% of  $CH_4$  at  $55^\circ C$ .



Furthermore, Anakhu and Suleiman (2021) study has revealed a satisfactory removal efficiency of COD, BOD<sub>3</sub> and TSS over 60% in treating POME using the ASBR at a temperature between 37°C to 55°C.

On the other hand, an aerobic system can be defined as the process by which POME pollutants are biodegraded by microorganisms under aerobic circumstances (Al-Amshawee et al., 2020). Bala et al., (2018) reported that the aerobic treatment of POME with a combination of bacteria (*Micrococcus luteus*, *Stenotrophomonas maltophilia*, *Bacillus cereus*, and *Bacillus subtilis*) and fungi (*Aspergillus fumigatus* and *Aspergillus niger*) have produced a BOD reduction efficiency of 90.23%, COD reduction efficiency of 91.06%, and TSS removal efficiency of 92.23% at ambient room temperature. Various aerobic biological processes have been employed in conventional wastewater treatment to degrade POME, including aerobic lagoons, trickling filters, sequencing batch reactor (SBR) and rotating biological contactors (RBC) (Al-Amshawee et al., 2020). Recent studies have explored coupling aerobic processes in an anaerobic system to increase treatment efficiency, reduce energy consumption, and produce lesser sludge, such as the anaerobic-aerobic batch (IAAB) reactors which may remove up to 99% of BOD and COD (Chong et al., 2021) and hybrid membrane bioreactor (MBR) which is capable to deteriorate COD by 94 to 97% efficiency (Abdulsalam, et al., 2018).

In addition, Zulfahmi, et al., (2021) have experimented using phytoremediation to degrade POME via water spinach (*Ipomoea aquatica*). Phytoremediation is defined as a plant-based approach that utilizes plants to eliminate contaminants from the environment or to limit their bioavailability in the soil (Yan, et al., 2020). Zulfahmi, et al., (2021) observed that 86.3% of COD, 21.5% of nitrate and 91% of phosphate have been removed from POME using phytoremediation after 15 days. Several types of plants, such as *Vetiveria zizanioides* and *Spirogyra* sp have been examined as POME phytoremediation agents, which were also reported for successful reduction of the COD up to 94% and 63.1%, within 14 days and 20 days respectively (Darajeh et al., 2014; Baihaqi et al., 2017).

Biological treatment of POME offers various advantages in terms of cost-effectiveness, simplicity and high efficiency in degrading POME. Nonetheless, biological treatment is a time-consuming process since the bacteria need a long hydraulic retention time (HRT) to acclimate to the new environment and stabilise their decomposition performance to treat POME (Abdulsalam, et al., 2018). Additionally, parameters in terms of feed flowrate, upflow velocity, temperature and pH of biological treatment require careful manipulation as these parameters have a significant impact on the alkalinity and total volatile fatty acids of the wastewater, hence affecting the biological treatment efficiency (Saad, Wirzal and Putra, 2021).

### **2.2.2 Physicochemical Treatment Methods**

The physicochemical method incorporates physical process or chemical process or a combination of both the processes to remove the pollutants by modifying the physical state of the pollutant to a more stable and more coagulable form, such as coagulation and flocculation process, electrocoagulation process, and adsorption (Hu and Xu, 2020).

Coagulation–flocculation process refers to the inclusion of natural or chemical-based coagulants to separate the dissolved and/or suspended solids from the liquid phase to allow the removal of pollutants by sedimentation, which is one of the popular physicochemical treatment technologies used in treating POME (Karimifard and Moghaddam, 2018; Chung et al., 2018; Lee et al., 2019). It is an excellent treatment method for POME owing to its ease of design and operation and low usage of energy but require high capital cost (Lee et al., 2019; Lanan et al., 2021). Lanan et al. (2021) have utilised fenugreek (*Trigonella foenum-graecum*) coagulant and okra (*Abelmoschus esculentus*) flocculant to achieve removal efficiencies of turbidity for 94.97%, TSS for 92.7% and COD for 63.11% from POME respectively.

The electrocoagulation process entails a series of treatments, including coagulation, precipitation, and flotation to treat the wastewater (Mohammad et al., 2021). Instead of using chemical coagulant additives, hydrolysis reaction on aluminium or iron anodes are used to form flocs of aluminium or iron hydroxide, thus

improving the subsequent treatment of POME (Mohammad et al., 2021). Nasrullah, et al., (2019) have successfully decreased the COD (95%), BOD (94%) and TSS (96%) of the POME within 50 minutes via the electrocoagulation process that employed high current intensity (20A). Furthermore, treating POME with electrocoagulation process have resulted in 94% of colour removal within 60 minutes as per the research conducted by Saad et al. (2020).

Adsorption technologies is another favourable treatment that has been widely researched in the past due to their ease of implementation and the production of quality-treated effluent (Hamzah, et al., 2019; Oyekanmi, et al., 2019; Hayawin et al., 2020). Adsorption is a mass transfer mechanism in which the molecules are attracted to the surface of the adsorbents as a result of intermolecular forces of attraction (Hu and Xu, 2020). Hayawin et al. (2020) explored the treatment of POME using palm-keener-shell-based activated carbon. The authors observed that the bio-adsorbent have successfully reduced the amount of TSS from 240 mg/L to 18 mg/L (92% removal efficiency), COD from 604 mg/L to 189 mg/L (68% removal efficiency), colour from 3140 ADMI unit to 80 ADMI unit (97% removal efficiency) and BOD from 100 mg/L to 5.1 mg/L (95% removal efficiency) within 12 hours.

Although the aforementioned physicochemical treatment promises high efficiency in degrading POME, these methods require higher operational costs due to high sludge production, handling and disposal, elimination of adsorbents and high intensity of electricity required (Nasrullah, et al., 2019; Crini and Lichtfouse, 2019; Li and Yang, 2018). Therefore, the following section will introduce a cutting-edge technology in wastewater treatment, which is PFC, one of the AOPs technology that is potential to improve the current wastewater treatment technology used to degrade POME.

### 2.3 Advanced Oxidation Process

With the ever-growing environmental issues, AOPs have emerged as a novel and potential technology for wastewater treatment. The fundamental principle of AOPs entails the formation of hydroxyl radicals ( $\bullet\text{OH}$ ), which are highly reactive oxidants to mineralize the contaminants to carbon dioxide or other harmless and/or beneficial by-products (Pandis, et al., 2021). The most notable advantage of AOPs over other conventional remediation techniques is that the target molecule is able to be completely degraded to a mineralized and non-toxic form without any secondary pollutants (Rayaroth, Escobedo and Chang, 2019). AOPs, are classified into either homogenous or heterogeneous photocatalysis. While the former refers to the process that degrades compounds by absorbing UV radiation, the latter uses semiconductor (such as ZnO) catalysts in the solid phase to carry out the compound's degradation, which results in the acceleration of chemical reaction due to the existence of electron-hole pairs (Mayyahi and Al-Asadi, 2018).

$\bullet\text{OH}$  produced from AOPs is capable of oxidising organic compounds which cannot be oxidised by conventional oxidants, for instance, ozone, oxygen and chlorine (Mayyahi and Al-Asadi, 2018). Based on Table 2.2,  $\bullet\text{OH}$  has the second-highest oxidation potential (2.8V), it is thus capable to exhibit a faster a rate of oxidation reactions than conventional oxidations. With a higher reaction rate to break down the contaminants, elimination of sludge production using AOPs, AOPS is thus a highly favourable wastewater treatment method with a high removal efficiency of contaminant, cost-effective and sustainable compared to conventional technologies. Al-Amshawee et al. (2021) reported that treating POME with one of the AOPs technology, the ozone oxidation at ozone dosage of 30 mg/L exhibited 83% of COD removal rate within 24 to 96 hours.

**Table 2.2: Oxidation potential of various oxidants (Mayyahi and Al-Asadi, 2018)**

Oxidant	Oxidation Potential
Fluorine	3.03
Hydroxyl radical ( $\bullet\text{OH}$ )	2.80
Oxygen (Atomic)	2.42
Ozone	2.08
Hydrogen Peroxide	1.78
Hypochlorite	1.49
Chlorine	1.36
Chlorine Dioxide	1.27
Molecular Oxygen	1.23

### 2.3.1 Photocatalytic Fuel Cell

With the advent of AOPs, PFC has made a mark in the field of photocatalytic technology to treat wastewater and synchronous recovery of chemical energy from the wastewater into electricity upon light activation. The strong oxidation ability of PFC can remove most of the persistent organic pollutants, which prevents the fuel type limitation in conventional fuel cell while the elimination of the requirement for extra external energy through the generation of electricity decreases the cost of the treatment (Parvizi and Parsa, 2021). Since PFC does not generate secondary pollutants, this design may serve as an alternative to the energy and environmental crisis, allowing PFC to have a promising prospect in wastewater treatment technology. A general PFC system is composed of a photoanode that carries a semiconductor photocatalyst (e.g., ZnO/Zn), a cathode (e.g., CuO/Cu), liquid electrolytes, and an external circuit connecting the photoanode and photocathode as displayed in Figure 2.2.

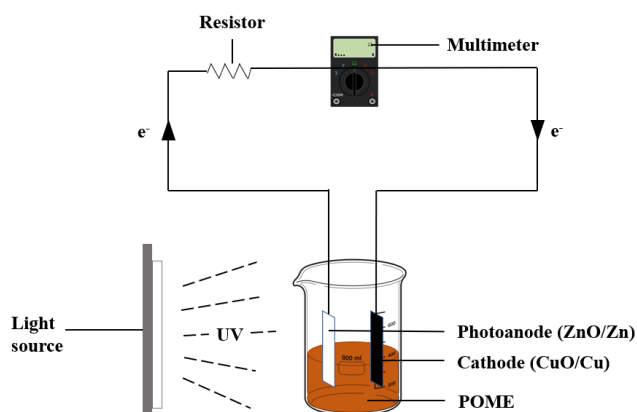
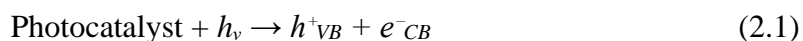


Figure 2.2: A simple set-up of PFC system with photoanode and photocathode.

As the light activates the semiconductor photocatalyst on photoanode, charges ( $e_{CB}^-$ ) are photoexcited and transported from the valence band (VB) to the conduction band (CB). An electron-hole ( $e_{CB}^- - h_{VB}^+$ ) pair was left in the VB as shown in Equation (2.1) (Moksin, et al., 2021). The  $h_{VB}^+$  will be produced at the VB of the photoanode. It is notably that the light irradiation used ought to be higher or equal to the photocatalyst energy band gap to ensure the photoexcitation of the photoanode (Singh and Pal, 2021).

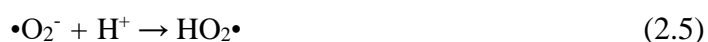


Hydroxyl radicals ( $\bullet\text{OH}$ ) is then produced by the photogenerated electron-hole ( $e_{CB}^- - h_{VB}^+$ ) pairs, which is extremely vital in organic matter degradation (Lui, et al., 2021). While the  $h_{VB}^+$  was utilised to produce hydroxyl radicals ( $\bullet\text{OH}$ ) by reacting with hydroxide ions ( $\text{OH}^-$ ) or water molecules ( $\text{H}_2\text{O}$ ) as represented in Equation (2.2) and Equation (2.3), electricity is produced via the transfer of  $e_{CB}^-$  from the photoanode to the cathode through the external circuit, as a result of the potential difference between the photoanode and cathode (Moksin, et al., 2021).



In the photocatalytic oxidation, molecular oxygen serves as a prevalent electron acceptor in photocatalytic oxidation (Rioja-Cabanillas, et al., 2021).

Superoxide radical anion ( $\bullet\text{O}_2^-$ ) and hydrogen superoxide (or hydroperoxyl radicals) ( $\text{HO}_2\bullet$ ) are formed when the oxygen is reduced by the  $e^-_{CB}$  that has reached the cathode as shown in Equation (2.4) and Equation (2.5). The subsequent reactions lead to hydrogen peroxide ( $\text{H}_2\text{O}_2$ ), which can be eventually converted into  $\bullet\text{OH}$ , as presented in Equation (2.6) and Equation (2.7) (Xiao, Xie and Cao, 2015).



The generated radicals, including  $\bullet\text{OH}$ ,  $\text{HO}_2^-$  and  $\bullet\text{O}_2^-$  in solution are effective non-selective oxidizers that lead to oxidation and increased degree mineralization of organic pollutants into carbon dioxide ( $\text{CO}_2$ ) and water ( $\text{H}_2\text{O}$ ) (Xiao, Xie and Cao, 2015). Equations (2.8) and (2.9) exhibits the reactions of  $\bullet\text{OH}$  and  $\bullet\text{O}_2^-$  participating in the degradation processes (Medel et al., 2020). On the other hand, Figure 2.3 depicts the photocatalyst mechanism involved in a PFC system.

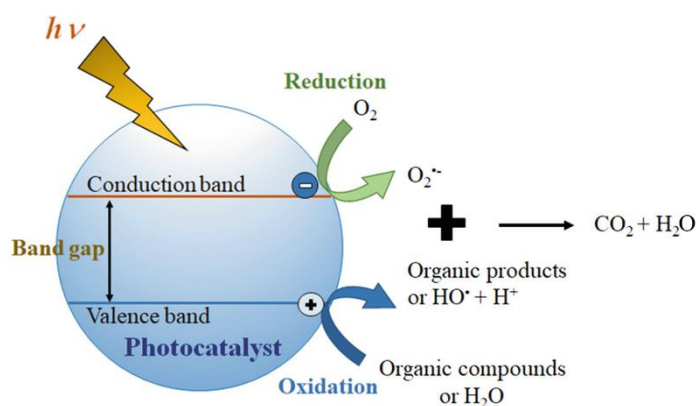
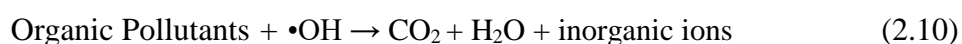
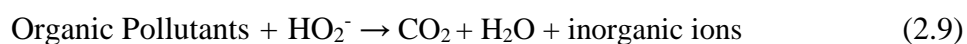
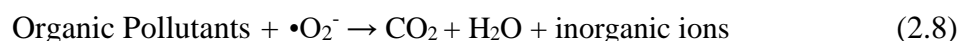


Figure 2.3: Photocatalytic Mechanism of a PFC System for Wastewater Treatment (Kemacheevakul and Chuangchote, 2021)

Appropriate selection of electrolyte as a reaction medium is pivotal in the PFC system in order to improve the transmission of ion and decrease the resistance within the system, thus producing more radicals to degrade the organic pollutants (Li, et al., 2019). According to Wang et al. (2014) and Liao et al. (2015), a moderate concentration of electrolyte concentration improves the conductivity in the solution, accelerate the movement of ions, and therefore increases the electricity produced by PFC systems. Several electrolytes are commonly in the PFC system, including phosphate, nitrates, sulphates, or alkali (for example: KOH and NaOH). Among these electrolytes, sodium sulfate ( $\text{Na}_2\text{SO}_4$ ) is often applied owing to its chemically inert and more stable properties compared to other electrolytes (Li et al., 2019).

The PFC system can be conducted under sunlight or ultraviolet light. While direct solar harnessing for photoactivation of photocatalysts is the most preferable method, sunlight fluctuation complicates continuous research (Cheng et al., 2021). In contrast to the majority of researchers that uses visible light or UV light to perform their POME photooxidation studies, Kanakaraju et al. (2017), obtained 88% COD removal from diluted POME through photooxidation employing a  $\text{TiO}_2$  system for 5 hours of solar exposure. As per the research conducted by Moxsin, et al. (2021), the PFC system which is constructed using  $\text{ZnO}/\text{Zn}$  photoanode and Pt wire cathode attained a COD removal efficiency of 74% and a maximum power density ( $P_{\text{max}}$ ) of  $38.88 \mu\text{W}/\text{cm}^2$  under a light intensity of 1300 lx. However, upon further increase of the light intensity to 1723 lx, the authors found out that the  $P_{\text{max}}$  had depleted to  $16.28 \mu\text{W}/\text{cm}^2$  in spite of having the maximum COD elimination efficiency of 94%. It is hypothesised by Moxsin, et al. (2021) that the photoexcitation will be more active at stronger light intensity, resulting in a higher percentage of organic matter removal efficiency.

Merely a few studies have investigated PFC in conjunction with the treatment of real industrial POME wastewater and more studies are needed to evaluate the use of PFC to treat industrial POME in the real application. It is immensely arduous to compare the performance from the very few published studies.



### 2.3.1.1 Methods of Synthesising Photoelectrodes

In PFC, the photoelectrodes are a key part that determines the overall photocatalytic activity of the PFC system to degrade organic pollutants and generate electricity. Hence, it necessitates the synthesis of photoelectrode in the best selection of material and structure, particularly ZnO in the nanostructure. ZnO, which is an n-type semiconductor, is an outstanding material for the synthesis of photoanode owing to its wide direct bandgap (3.37eV), nontoxicity, cost-effectiveness and high thermal conductivity (Masuda et al., 2020; Han and Liu, 2021).

In terms of the nanostructures, Figure 2.4 illustrates the most commonly produced 0D to 2D structures (nanoparticles, nanowires, nanotubes, nanorods and nanosheets). Generally, 1D and 2D nanostructures exhibit better electrochemical properties than 0D nanostructures since 1D and 2D nanostructures have a larger specific surface area (shown in Figure 2.5), orientated ionic transport channel and lesser impedance (Li and Wang, 2019). Nevertheless, although 2D nanostructures have a higher potential surface area, 1D nanostructures are relatively stable than 2D nanostructures, and cylindrical and/or tubular configurations of 1D nanostructures are easier to enhance the specific surface area while maintaining the overall geometric surface (Li and Wang, 2019; Hernández et al., 2015). Nanostructure-based photoanodes may be synthesised through several fabrication methods, such as chemical precipitation method, sol-gel method, heat attachment method, hydrothermal method, template synthesis method, physical pulverization method, physical coacervation method, and spray method (Bokov, et al., 2021; Lee et al., 2017; Xie et al., 2016)

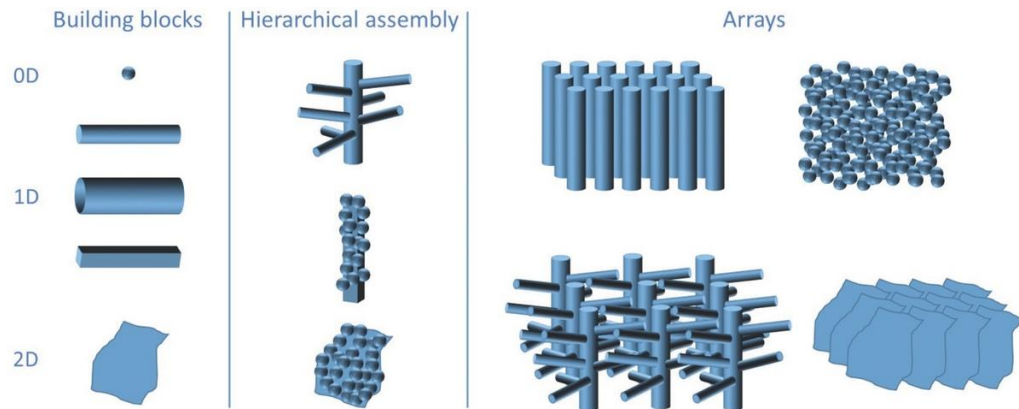


Figure 2.4: The most commonly produced 0D, 1D and 2D nanostructures (nanoparticles, nanowires, nanotubes, nanorods and nanosheets) in the form of building blocks, hierarchical assembly and arrays (Concina, Iupoto and Vomiero, 2017).

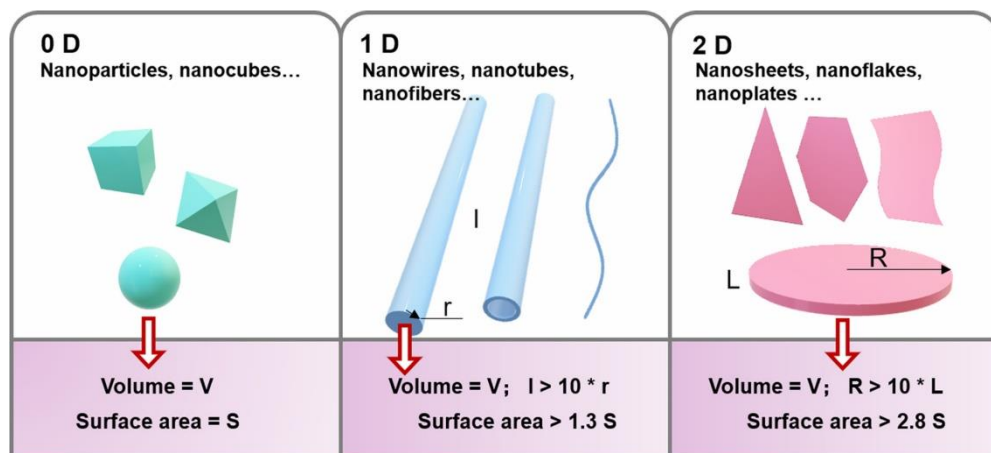


Figure 2.5: Schematic Diagram of 0D, 1D and 2D nanostructured material (Li and Wang, 2019).

Kee, Lam and Sin (2019) have studied the effectiveness of PFC utilizing ZnO/Zn photoanode in uniform nanorods and CuO/Cu cathode in uniform nanoflakes structure to break down organic pollutants in POME. The synthesis of the photoanode was carried out using the hydrothermal process by submerging an ultrasonic-cleaned Zn foil in hexamethylenetetramine ( $C_6H_{12}N_4$ ) and zinc nitrate hexahydrate solution ( $Zn(NO_3)_2 \cdot 6H_2O$ ) solution. The mixture was dehydrated at  $90^\circ C$  and calcined at  $300^\circ C$  to obtain ZnO/Zn photoanode. Meanwhile, the CuO/Cu cathode was immersed in a combination of sodium persulphate ( $Na_2S_2O_8$ ) and sodium hydroxide (NaOH) after

being sonicated by ethanol and deionized water. The authors reported that the PFC system has displayed a high COD and colour removal, which is 71% and 58 % respectively upon 240 minutes of UV light radiation, which is higher than commercial ZnO/Zn photoanode that merely achieved 53% COD and 42% colour removal. In addition, the employment of the ZnO/Zn nanorod arrays as photoanode in the PFC system has successfully generated a maximum power density,  $P_{\max}$  of 0.0121 mW/cm<sup>2</sup>. It has been deduced that the synthesized ZnO nanorods could generate more electron-hole ( $e_{CB}^- - h_{VB}^+$ ) pairs, which result in increased generation of  $h^+$  to degrade the POME and  $e^-$  to be transported to the cathode, thus producing more electricity.

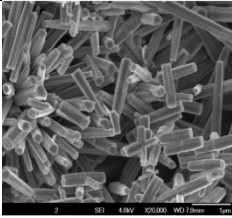
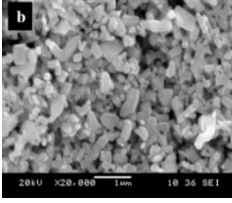
Aside from using ZnO/Zn photoanode treating POME, it is also a promising alternative in treating other wastewater such as dye. According to Lee et al., (2017), the PFC system with the utilisation of ZnO/Zn as photoanode achieved approximately 100% decolourization in 8 h in degrading Reactive Green 19. The ZnO/Zn photoanode is synthesized using the heat attachment method. Firstly, an ultrasonically-cleaned Zn film was immersed in 100mL distilled water with 1.0g of commercial ZnO powders for an hour. The Zn foil was subsequently dried at 90°C for 24h and was annealed at 300°C for 2 h. With the synthesized ZnO/Zn photoanode, the PFC system was able to produce maximum power density,  $P_{\max}$  of 0.0102 mW/ cm<sup>2</sup> as well. The authors have suggested that the structural characteristic of the photoanode, such as the active surface area and the thickness of the photoanode may impact the capability of photoanode to harvest light and the resistance of the photogenerated  $e^-$  to transport to cathode.

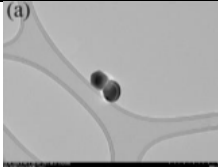
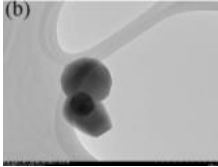
Moreover, Zainuri et al. (2018) investigated the reusability of ZnO nanoparticles for POME photocatalytic degradation. The ZnO nanoparticles were fabricated using the chemical precipitation method. The mixture of oxalic acid dihydrate solution and zinc acetate dihydrate solution was stirred for 12 hours at 25°C and subsequently were dried at 100°C for an hour and calcined at 550°C for 3 hours. The authors have fabricated two form of ZnO nanoparticles, including ZnO encapsulating with polyvinylpyrrolidone (PVP) and ZnO with polyethylene glycol (PEG). The authors have observed a POME turbidity reduction percentage of 45.75% and 37.25% respectively for ZnO-PEG and ZnO-PVP; and 33.12% and 31.18% for reused ZnO-PEG and ZnO-PVP in nanoparticles structure. Furthermore, the ZnO-PEG nanoparticles have exhibited

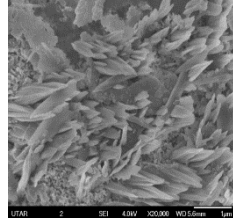
approximately 70% and 40% of colour removal percentage in the first cycle and the second cycle respectively; while ZnO-PVP nanoparticles have removed 60% and 40% of colour in the first cycle and the second cycle, which has portrayed the reusability of ZnO nanoparticles in photocatalytic degradation of POME.

Through reviewing reported past works, it is observed that there is little research studied on the employment of ZnO/Zn nanorod array as a practical photoanode to treat POME in a PFC system. However, as per these aforementioned research, ZnO/Zn nanorod array structure is a promising selection of photoelectrode not only to treat POME in this study but other types of wastewaters, with the capability to be reused as well. A suitable fabrication method is thereby vital to improving the structure of the photoelectrodes and ultimately enhancing the performance of the PFC system in treating real industrial POME wastewater and increasing the electricity generation rate. Table 2.3 summarises the reported fabrication methods of the photoelectrodes.

**Table 2.3: Summary of literature-reviewed fabrication methods for the photoelectrodes.**

Photoanode								
Type of Photoelectrodes	Nanostructures	Synthesis Methods	Precursors	Synthesis Conditions	Particle Size (nm)	Morphologies	PFC efficiency	References
ZnO/Zn (photoanode) CuO/Cu (cathode)	ZnO nanorod	Hydrothermal method, annealing	0.1 M of Zn(NO <sub>3</sub> ) <sub>2</sub> •6H <sub>2</sub> O solution and 0.1 M of C <sub>6</sub> H <sub>12</sub> N <sub>4</sub> solution	Reaction: 90 °C; calcination: 300°C	1000 – 1200		Removal rates of 71% of COD and 58% of colour.	Kee, Lam and Sin (2019)
ZnO/Zn (photoanode) Pt/C (cathode)	Rod and Tetragonal	Heat attachment	Ethanol, ZnO Suspension	Ultrasonication: 1 h; drying: 90 °C, 24h; annealing: 300 °C, 2 h	100 - 1000		Removal rate of 90.4 % for oxytetracycline hydrochloride.	Lee et al., (2017)

ZnO (no mentioning of photoanode and photocathode)	ZnO nanoparticles	Chemical Precipitation method	0.1M $C_2H_2O_4 \cdot 2H_2O$ and 0.1 M of $Zn(CH_3CO_2)_2 \cdot 2H_2O$	Reaction: stirred for 12 hours; drying: 100 °C, 1 h calcination: 550 °C, 3 h	60 – 150 for ZnO-PEG; 80 -150 for ZnO-PVP	 	<p>(a) ZnO-PEG and (b) ZnO-PVP</p>	<p>Turbidity reduction of 45.75% and 37.25% for ZnO-PEG and ZnO-PVP in 1<sup>st</sup> cycle and 33.12% and 31.18% for 2<sup>nd</sup> cycle; Colour removal of 70% and 60% for ZnO-PEG and ZnO-PVP in 1<sup>st</sup> cycle and 40% for both ZnO nanoparticles in 2<sup>nd</sup> cycle.</p>	Zainuri et al. (2018)
---	-------------------	-------------------------------	--	--	---	--	--	---	-----------------------

<b>Cathode</b>								
<b>Type of Photoelectrodes</b>	<b>Nanostructures</b>	<b>Synthesis Methods</b>	<b>Precursors</b>	<b>Synthesis Conditions</b>	<b>Particle Size (nm)</b>	<b>Morphologies</b>	<b>PFC efficiency</b>	<b>References</b>
ZnO/Zn (photoanode) CuO/Cu (cathode)	CuO nanoflakes	Hydrothermal method, annealing	Na <sub>2</sub> S <sub>2</sub> O <sub>8</sub> solution and NaOH solution	Drying: 90 °C; Annealing: 450°C	1000 – 1200		Removal rates of 71% of COD and 58% of colour.	Kee, Lam and Sin (2019)

## 2.4 Process Parameter Study

When constructing the PFC system, the photocatalytic degradation efficiency was governed by various operating parameters, including the initial concentration of the oxidant, the initial concentration of pollutant, and the initial solution pH (Li et al., 2019; Moksini et al., 2021; Kee et al., 2020; Li et al., 2018; Saha et al., 2018; Alhaji et al., 2018). These process parameters were thoroughly studied in this section to examine the influence of these parameters on the photocatalytic process of organic pollutants and electricity generation.

### 2.4.1 Types and concentration of oxidant

Many studies suggested that the addition of external oxidant such as hydrogen peroxide ( $\text{H}_2\text{O}_2$ ), potassium persulfate ( $\text{K}_2\text{S}_2\text{O}_8$ ) and sodium persulfate ( $\text{Na}_2\text{S}_2\text{O}_8$ ) enhanced the photocatalytic activity of the photocatalyst by preventing the electron-hole ( $e_{CB^-}-h_{VB^+}$ ) pairs from recombining at the photoanode (Lebeau, et al., 2020; Lee, Gunten and Kim, 2020; Tang et al., 2019; Li, et al., 2019; Li et al., 2018). Since the recombination of electron-hole ( $e_{CB^-}-h_{VB^+}$ ) pairs causes energy losses, the addition of external oxidant aids in increasing the generation of  $\bullet\text{OH}$  and other potential radicals to improve the photodegradation efficiency of the organic pollutants.

Li et al. (2018) demonstrated the effect of the addition of potassium persulfate on a PFC system which utilized  $\text{TiO}_2$  nanotube arrays as the photoanode to decolourise methyl orange and synchronous generation of electricity. The introduction of potassium persulfate as the oxidant exhibits a dual function, which was extending the reaction of active species from the photoelectrodes to the entire electrolyte through the formation of sulfate radical ( $\text{SO}_4^{\bullet-}$ ) and hydroxyl radical ( $\bullet\text{OH}$ ), and inhibiting the electron-hole ( $e_{CB^-}-h_{VB^+}$ ) pairs from recombining at the surface of photoanode. Therefore, with the addition of the oxidant, the decomposition of methyl orange dye and electricity generation was increased by 40.36% and 44.97% at a concentration of 1.0 mM compared to the PFC system without the addition of oxidant.



Another investigation conducted by Saha et al. (2018), the incorporation of hydrogen peroxide ( $\text{H}_2\text{O}_2$ ) as oxidant in photocatalytic decomposition of methylene blue dye wastewater has significantly increased the efficiency of photodegradation of methylene blue dye. The authors observed that the addition of hydrogen peroxide upon visible light irradiation enhanced the photodegradation of organic molecules in wastewater through the prevention of holes and electrons of the photocatalyst and increases of the amount of hydroxyl radical ( $\bullet\text{OH}$ ) to treat the organic pollutant. The results showed 46.5% of methylene blue degradation with 5.0 mM of hydrogen peroxide, which exhibited better performance of degradation than treatment without the oxidant (27.6% of methylene blue degradation).

Li et al. (2019) analysed the performance of PFC system to degrade norfloxacin and simultaneous electricity generation with the addition of potassium persulfate under UV light irradiation. It was noteworthy that the photocatalytic degradation rate of norfloxacin was significantly improved from 52.77% to 98.10% with the increasing of concentration of oxidant from 0.1 mM to 3.0 mM. According to Li et al. (2019), low concentration of oxidant (0.1 M) in PFC system resulted in insufficient amount of sulfate radical ( $\text{SO}_4\bullet^-$ ), which was not conducive to contribute to photocatalytic degradation of norfloxacin. However, no remarkable change was attained when the concentration of oxidant increased to 4.0 mM as the excessive sulfate radical ( $\text{SO}_4\bullet^-$ ) was able to react with itself and produced less-reactive of radicals, known as the peroxydisulfate ( $\text{S}_2\text{O}_8\bullet^-$ ), which reduced the number of strong radicals available in the PFC system and thus inhibited the photocatalytic degradation of norfloxacin.

As observed from the literature reviews, addition of oxidant in optimum concentration drastically enhanced the performance of PFC system to degrade various types of wastewaters. Therefore, it was anticipated that the addition of oxidant in this study will improve the photocatalytic degradation of POME and simultaneous electricity generation.

#### 2.4.2 Initial pollutant concentration

Industrial wastewater containing a vast amount of suspended solids and organic matter content have high turbidity and exhibit as a dark-coloured solution. The high turbidity and intense dark colour of the wastewater solution reduce the penetration of light into the PFC system. As the photocatalytic process of the PFC system requires light activation to produce  $\bullet\text{OH}$  radicals, an increment in the initial concentration of wastewater with high amount of organic pollutant concentration significantly decreases the efficiency of the photocatalyst in the PFC system (Agustina et al, 2021).

Li et al. (2019) experimented the performance of photocatalytic activity to treat norfloxacin under varied concentration of initial norfloxacin concentration ranging from  $10 \text{ mgL}^{-1}$  to  $200 \text{ mgL}^{-1}$ . The authors have discovered that the removal efficiency of norfloxacin was inversely proportional to the initial norfloxacin concentration as the degradation rate of norfloxacin drastically reduced from 98.10% to 12.92% when the initial norfloxacin concentration from  $10 \text{ mgL}^{-1}$  to  $200 \text{ mgL}^{-1}$ . The excessive initial pollutant concentration causes competition of sulfate radical ( $\text{SO}_4\bullet^-$ ) and hydroxyl radical ( $\bullet\text{OH}$ ) for limited active sites on the photoanode, thus reducing the photocatalytic degradation efficiency of norfloxacin in the PFC system. The optimal initial pollutant concentration obtained by the authors was  $10 \text{ mgL}^{-1}$ .

In a research conducted by Rabé, Liu and Nahyoon (2020), the degradation efficiency of tetracycline hydrochloride in a PFC system was analysed under varied initial concentration of tetracycline hydrochloride solution in  $10 \text{ mgL}^{-1}$ ,  $30 \text{ mgL}^{-1}$  and  $60 \text{ mgL}^{-1}$ . The authors have observed that  $10 \text{ mgL}^{-1}$  of initial tetracycline hydrochloride concentration have exhibited the best degradation efficiency of 97.3% tetracycline hydrochloride removal. A reduction in photocatalytic degradation rate was observed as the tetracycline hydrochloride removal achieved was 89.2 and 73.6% using concentration of  $30 \text{ mgL}^{-1}$  and  $60 \text{ mgL}^{-1}$  respectively. It was deduced that the high concentration of the tetracycline hydrochloride limited the accessibility of photons for generation of hydroxyl radical ( $\bullet\text{OH}$ ).

Samanta, Sahu and Roy (2020) demonstrated the impact of initial pollutant concentration in photocatalytic degradation of Malachite Green dye using a PFC system. Different initial concentrations of the dye have been tested in the authors' research, ranging from  $100 \text{ mgL}^{-1}$  to  $200 \text{ mgL}^{-1}$ . The overall result showed a high removal efficiency at lower initial concentration of the dye, which was 90% of removal rate at an initial concentration of dye of  $100 \text{ mgL}^{-1}$ . As the concentration of dye increased, the colour of the solution became more intense, thus reducing the path length of the photons to reach the photoanode surface.

In short, the initial concentration of pollutant is a crucial parameter in the photocatalytic degradation of pollutant in a PFC system. Based on these literature reviews, the increase of initial concentration of pollutant generally decreases the degradation efficiency of pollutants. The effect of initial concentration of POME will be analysed in this paper.

### **2.4.3 Initial Solution pH**

The photocatalytic performance of PFC is influenced by the initial solution pH as it regulates the surface charge of the photocatalyst. The variation in pH values impacts the photocatalytic degradation of the organic pollutant molecules, as well as the oxidation potential of the valence band and the formation of charged radicals during the photocatalytic oxidation process (Thor, et al., 2020; Kee, et al., 2018; Yin, et al., 2018). Table 2.4 summarizes the recent published research of the impact of pH of the initial solution on the photocatalytic efficiency of the PFC system.

Moksin et al., (2021) researched the effect of solution pH in the range of 4 – 8 on the efficiency of PFC system to treat organic pollutant wastewater using ZnO/Zn as the photoanode and Pt wire as the cathode under a visible light illumination. It was observed that 50% of photocatalytic degradation efficiency and  $7.398 \mu\text{W}/\text{cm}^2$  of maximum power density value were attained at optimum pH of 7.0. It was reported that more power was obtained at a higher pH since lesser electrons were required to reduce the  $\text{H}^+$  at the surface of photoanode, resulting in a higher transfer rate of

electrons from the ZnO/Zn nanorod array photoanode to the CuO/Cu cathode, leading to higher generation of electricity. Furthermore, the presence of OH<sup>-</sup> in a higher pH solution ensures efficient hole scavenging between electrons ( $e_{CB}^-$ ) and holes ( $h_{VB}^+$ ), and active production of •OH radicals in the PFC system. However, the increase of pH 4 to pH 8 has decreased the COD removal efficiency to 34% with a maximum power output of 6.912  $\mu\text{W}/\text{cm}^2$  owing to the high OH<sup>-</sup> concentration in the solution, which caused the electrostatic repulsion force to replace electrostatic attraction as the dominant force. The oxidation process has thus been obstructed, and the combination of the electron-hole ( $e_{CB}^-$ - $h_{VB}^+$ ) pairs was increased.

In addition, Kee et al. (2020) analysed the impact of initial solution pH on the photocatalytic activity of the PFC system to degrade organic pollutant. Kee et al. (2020) controlled the pH of the initial solution by using HNO<sub>3</sub> and NaOH in a range of pH of 3 to pH of 11. The results presented that the degradation of COD improved along with the increment of initial solution pH, yielding the best COD removal efficiency (90%) and maximum power density (0.0743  $\text{mW}/\text{cm}^2$ ) under a pH of 8.35. Under natural pH condition, the absence of H<sup>+</sup> or OH<sup>-</sup> from pH adjustors prevented the adsorption of organic pollutant on the photoanode and scavenging of the OH<sup>-</sup> ions, hence resulting in better COD removal efficiency and generation of electricity.

Alhaji et al. (2018) analysed the performance of photocatalytic degradation of pre-treated POME by varying pH as 3, 5, 7 and 9 under UV light radiation. According to Alhaji et al. (2018), when the pH values are closer to the point zero charge (pzc), the efficiency of photodegradation of organic contaminant increased dramatically. In contrast to the research conducted by Moxsin et al. (2021) and Kee et al. (2020), the highest photodegradation efficiency which was 98.5% has been obtained at a pH of 3. It was deduced that the non-dissociation of hydrated TiO<sub>2</sub> enhanced higher photocatalytic activity as the electron band shifting to more negative values, leading to a reduction of the oxidation potential of H<sup>+</sup>.

**Table 2.4: The effects of initial solution pH on the photocatalytic performance of PFC.**

<b>Pollutant type</b>	<b>Light source</b>	<b>Photocatalyst</b>	<b>pH range</b>	<b>Optimum pH</b>	<b>Degradation efficiency (%)</b>	<b>Maximum power density (<math>P_{max}</math>, mW/cm<sup>2</sup>)</b>	<b>References</b>
POME	Visible light	ZnO/Zn (photoanode) Pt/C (cathode)	4 - 8	7.0	50	$7.398 \times 10^{-3}$	Moksin et al., (2021)
POME	UV light	TiO <sub>2</sub> /ZnO/Zn (photoanode) TiO <sub>2</sub> /CuO/Cu (cathode)	3 - 11	8.35	98.5	0.0743	Kee et al. (2019)
Pre-treated POME	UV light	TiO <sub>2</sub> (photoanode)	3 - 9	3.0	98.5	NA	Alhaji et al. (2018)
Norfloxacin	UV light	TiO <sub>2</sub> Nanorods (photoanode)	3 - 11	3.0	97.19	NA	Li et al., (2019)
Methyl green	UV light	ZnO/Zn (photoanode) CuO/Cu (cathode)	3 - 10	5.2	92	0.0844	Kee et al. (2018)
Reactive Black 5 (RB5)	UV light	ZnO/Carbon felt (photoanode) Pt/C (cathode)	2 - 12	9.0	49.19	24.4803	Khalik et al. (2017)

## 2.5 Detection of active species

The degradation of organic pollutants during the photocatalytic and activated oxidant oxidation process is completed by generation of various reactive radical species, such as hydroxyl radical ( $\bullet\text{OH}$ ) as discussed in Section 2.3.1. In order to better elucidate the mechanism of the dominant active species during the treatment of POME in enhanced PFC system with addition of oxidant in this work, radical scavenging test was conducted as reported by several authors.

Li et al. (2019) have reported that the roles of different reactive species in a PFC/PS system was determined through a variety of scavenger agents, including ethanol as a scavenger of sulfate radicals ( $\text{SO}_4^{\bullet-}$ ) and hydroxyl radicals ( $\bullet\text{OH}$ ), isopropanol as specific  $\bullet\text{OH}$  scavenger and EDTA-2Na as a typical quenching agent for hole ( $h^+$ ). All scavenger agents were added in a concentration of 0.3 M.

In a comparative study of persulfate oxidants promoted PFC system conducted by Tang et al. (2019), the mechanism of dominant active substances during the decomposition of dye was analysed through addition of 1 mM Tert-butanol (scavenger for  $\bullet\text{OH}$  radicals), 1 mM ethanol (scavenger for both  $\bullet\text{OH}$  and  $\text{SO}_4^{\bullet-}$ ), 20  $\mu\text{M}$  *p*-benzoquinone (scavenger for  $\text{O}_2^{\bullet-}$ ), 50 mM phenol (scavenger of singlet oxygen  $^1\text{O}_2$ ) and 50 mM *L*-histidine which has a scavenging effect on  $\text{O}^*$ ,  $\text{SO}_4^{\bullet-}$  and  $^1\text{O}_2$ .

In addition, Lam et al. (2020) have detailed a list of capture agents used to scavenge the specific active species in the developed PFC system. The capture agents employed included isopropanol (IPA), ethylenediaminetetraacetate (EDTA) as well as *p*-benzoquinone (BQ) to quench  $\bullet\text{OH}$  radicals, hole ( $h^+$ ), and superoxide anion ( $\text{O}_2^{\bullet-}$ ) radicals, respectively. All scavenger agents were added in a concentration of 2 mM in this study.

## 2.6 Summary of literature review

The properties of POME wastewater and various spectrums of conventional treatment methods that have been employed to degrade organic pollutants have been investigated in depth in the section of the literature review. Each type of POME wastewater treatment method has varying degrees of effectiveness in treating the POME since each of the treatment methods exhibits its limitation. Upon extensive research, photocatalytic fuel cell (PFC) was one of the promising AOPs technology to overcome the constraint commonly associated with other traditional treatment methods. The principle and mechanisms of PFC system were discussed in detail to enhance the understanding of the PFC process. As a key component of a PFC system, several fabrication methods to synthesise nanostructure-based photoelectrodes, have been discussed in this section. Due to the benefit of having larger effective surface-to-volume ratio and higher available active sites on the surface, the ZnO photoanode was modified into 1D nanorod array structures is opted owing to its. In addition, in order to ensure better pollutants degradation efficiency and generation of electricity, the role of the process parameters of PFC such as types and initial concentration of oxidants, the initial concentration of pollutants in terms of POME dilution factor, initial solution pH have been scrutinized in this research.

There was scarce literature highlighting the photocatalytic degradation of POME obtained from real-life industry utilising a PFC system built with ZnO/Zn nanorod array structure photoanode and CuO/Cu cathode, particularly with the addition of oxidant. Hence, this study intends to examine the photocatalytic performance of a novel PFC system to treat POME using ZnO/Zn nanorod array structure photoanode and CuO/Cu cathode with the addition of persulfate oxidant.

## **CHAPTER 3**

### **RESEARCH METHODOLOGY**

This chapter focused on the experiment design and methods used in this research work. The flowchart depicted in Figure 3.1 summarised the progression of this study.

#### **3.1 Materials and Chemicals**

The materials and chemicals that were utilised in the research are tabulated in Figure 3.1. All chemicals were analytical grade and used as-purchased without further purification prior to their use in experiments.



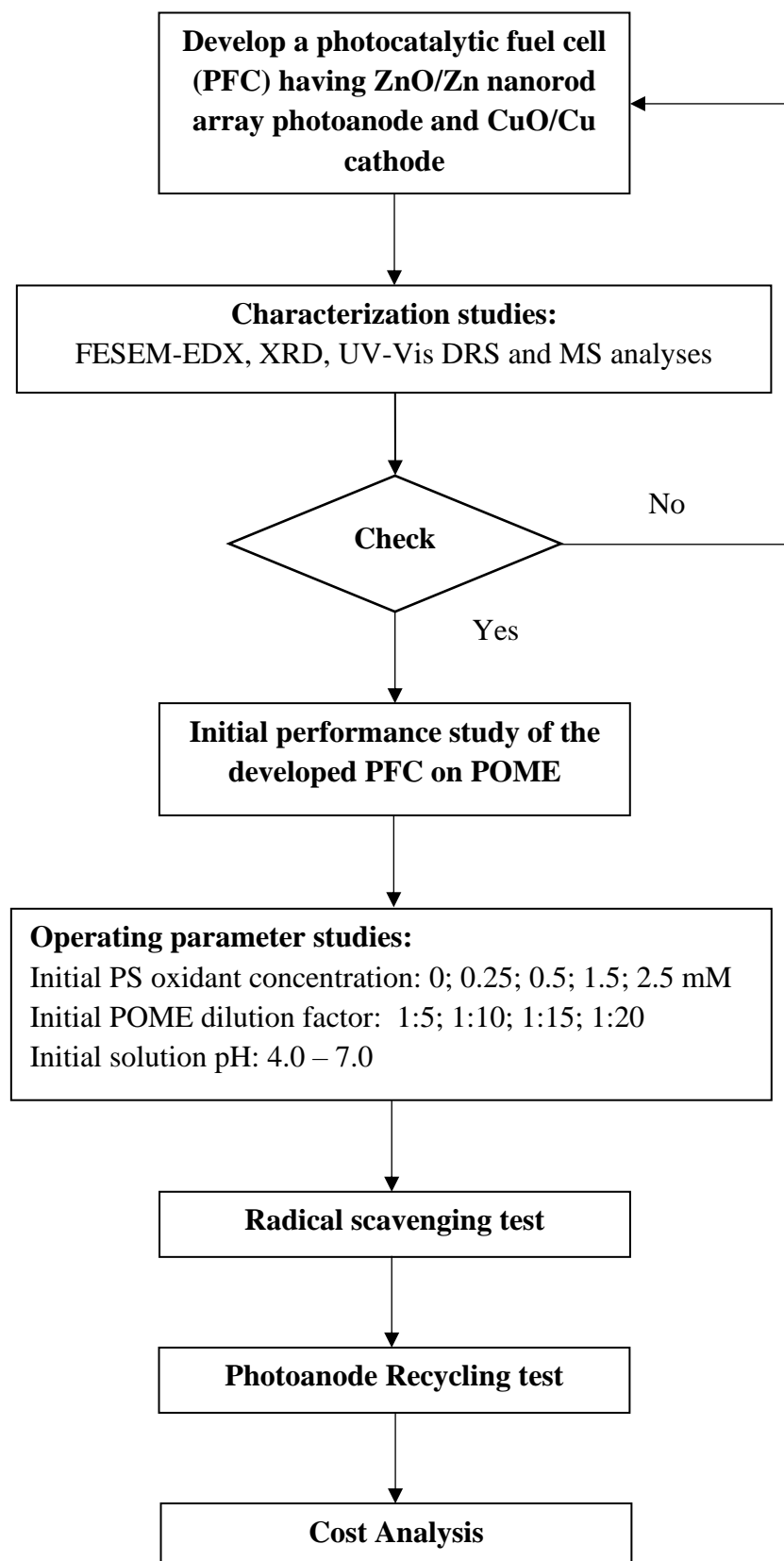


Figure 3.1: The flow of Experimental Work Conducted in this Research.

**Table 3.1: List of Materials and Chemicals Used.**

<b>Chemical / Reagent</b>	<b>Purity (%)</b>	<b>Supplier</b>	<b>Function</b>
Distilled water	N/A	Favorit	Used in the preparation of photoelectrodes and cleaning purposes.
Ethanol (C <sub>2</sub> H <sub>5</sub> OH)	95	ChemAR	Used for pre-cleaning of materials during photoelectrodes preparation and radical scavenging test.
Zinc Foil			Used for photoanode preparation.
Zinc Nitrate Tetrahydrate [Zn(NO <sub>3</sub> ) <sub>2</sub> •4H <sub>2</sub> O]	98	Chem Solution	Used for photoanode preparation.
Zinc Acetate [(CH <sub>3</sub> COO) <sub>2</sub> Zn•2H <sub>2</sub> O]	98	ARCOS Organics	Used for photoanode preparation.
Copper Foil			Used for cathode preparation.
Sodium Persulfate (Na <sub>2</sub> S <sub>2</sub> O <sub>8</sub> )	99	BDH Laboratory Supplies	Used for cathode preparation and as an oxidant.
Sodium Sulfate (Na <sub>2</sub> SO <sub>4</sub> )	99	Bendosen	Used as a supporting electrolyte.
Hydrochloric Acid (HCl)	99	R&M Chemicals	Used as a pH adjuster.
Sodium Hydroxide (NaOH)	99	R&M Chemicals	Used as a pH adjuster.
Ethylenediaminetetraacetic acid disodium salt (C <sub>10</sub> H <sub>14</sub> N <sub>2</sub> Na <sub>2</sub> O <sub>8</sub> )	99	System	Used for radical scavenging test.
2-Methyl-2-Propanol ((CH <sub>3</sub> ) <sub>3</sub> COH)	99	Bendosen Laboratory	Used for radical scavenging test.
1,4-Benzoquinone (C <sub>6</sub> H <sub>4</sub> O <sub>2</sub> )	98	ARCOS Organics	Used for radical scavenging test.
Silver nitrate (C <sub>3</sub> H <sub>8</sub> O)	99	GENE Chemicals	Used for radical scavenging test.
High Range (HR) COD Digestion Reagent	-	HACH	Used for COD analysis.
Real Industrial POME Wastewater			Used to evaluate the effectiveness of the developed PFC system in real POME wastewater treatment.

## **3.2 Apparatus and Equipment**

### **3.2.1 Photocatalytic Fuel Cell (PFC) Experimental Apparatus**

In this study, a PFC system has been devised to degrade pre-treated POME and produce power output concurrently under UVC light irradiation. Figure 3.2 and Figure 3.3 illustrate the schematic diagram and actual configuration of a complete PFC.

The PFC system was encased in an acrylic black box throughout the research work, which acted as a confinement area for the UVC light emitted within the box in order to ensure the reaction was entirely mediated by the inner UVC light source without interference from external light sources. A multimeter was linked through an external circuit to a variable resistor that served as a voltage regulator to measure the capacity of generated electricity in the PFC system during the photocatalytic process. While the photoanode and cathode were placed 4 cm apart, the photoanode and light source were separated by a fixed distance of 2 cm for photoanode to be photoexcited (Kee, Lam and Sin., 2019). An UVC lamp was used as light source to irradiate ultraviolet C (UVC) to power PFC system. Throughout the experiment, a quartz tube was employed to contain the UVC lamp, keeping it from coming into direct contact with the test solution and causing electric shock. The effectiveness of the PFC system was investigated in a 100 mL beaker consisting of the test solution and was the solution was ensured to be evenly mixed by being placed above a magnetic stirrer with a stirring rate of 150 rpm. In addition, an air pump was applied in the PFC, purging air into the PFC system to aerate the photocathode compartment. Using an air flow meter with control valve, the aeration process was maintained at a constant rate of 2 L/min. Two cooling fans were designated at the side of the acrylic black box in order to provide ventilation and regulate the temperature of PFC system inside the acrylic black box.

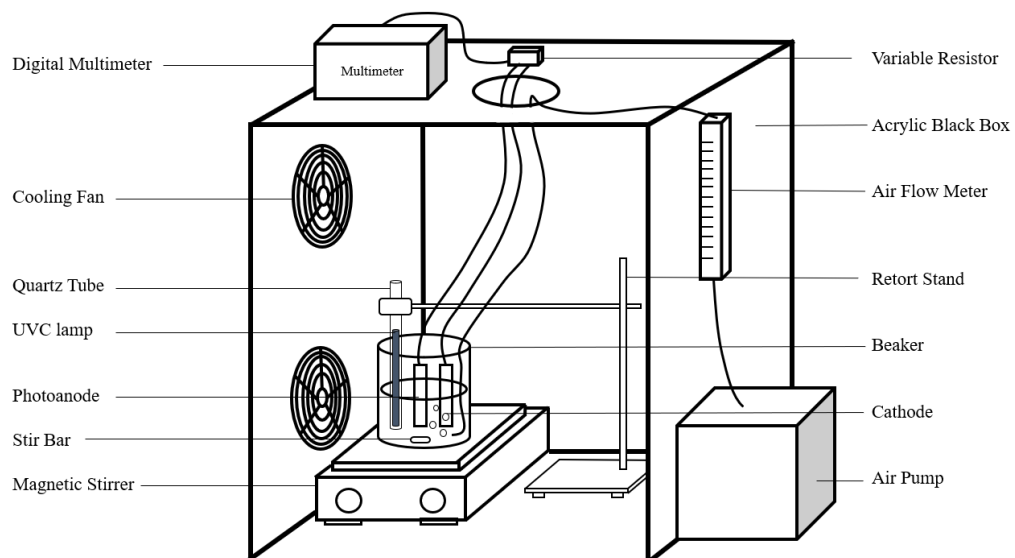


Figure 3.2: Schematic Diagram of PFC System

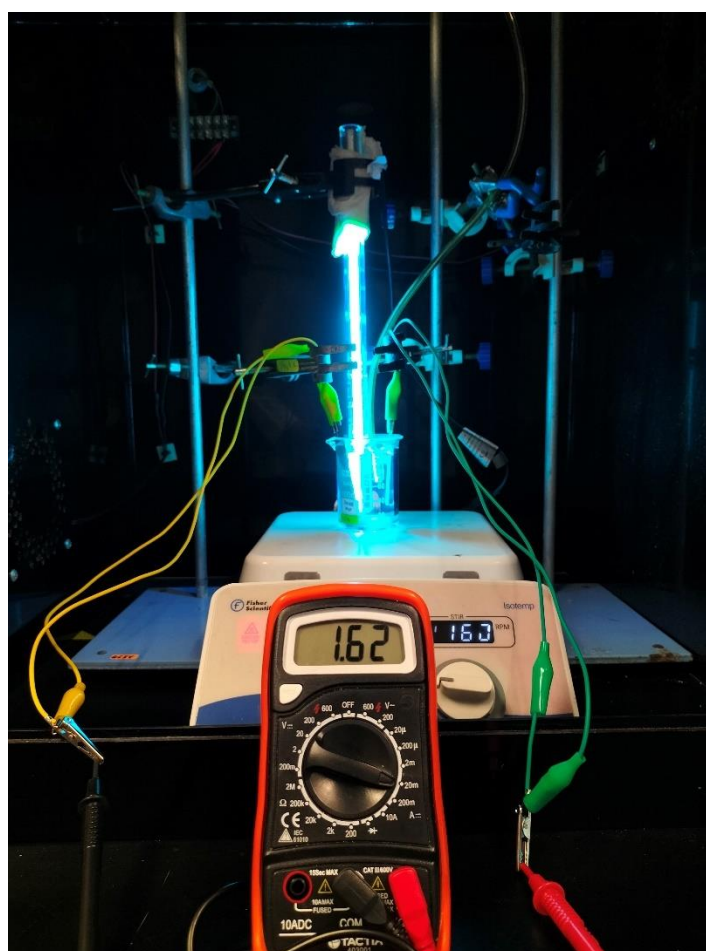


Figure 3.3: Experimental Setup of PFC System

### **3.3 Analytic Procedure**

#### **3.3.1 Chemical Oxygen Demand (COD) Analysis**

Chemical oxygen demand (COD) is a unit of measurement for the amount of oxygen a chemical consumed to oxidize organic pollutant in wastewater samples and a critical indicator of the contamination level of the wastewater samples (Islam et al., 2019; Hassan et al., 2018). To measure the mineralization extent of POME samples during photocatalysis, the COD analysis was carried out on the POME test solution using a COD analyzer (*HACH DRB 200*). In this research study, the COD Hach Method 8000 was applied to perform the COD analysis (HACH, 2021). Initially, the COD reactor was preheated to 150 °C prior to placing the vial. 2 mL of distilled water as blank sample was prepared to reset the reading of the COD analyzer to zero before the measurement of COD value of other test vials, and 2 mL of the POME sample were pipetted into high range (HR) COD digestion reagent vial and shaken gently to mix the solution evenly. After the test samples were digested in the COD reactor for continuous 2 hours, the vials were cooled to room temperature and preceded for UV-Vis spectroscopy test using *HACH DR6000* UV-Vis spectrophotometer. By using UV absorption, the concentration of organic matter in terms of COD was detected as most organic compounds have absorption characteristics in the ultraviolet region (Zhao et al., 2011). Multiple COD analysis was performed to obtain the average reading in order to improve the accuracy of the readings.

#### **3.3.2 Biochemical Oxygen Demand (BOD) Analysis**

Biochemical oxygen demand (BOD) implies the amount of oxygen that aerobic microorganisms consume to degrade organic matter in wastewater at a particular temperature with a given time period (Shmeis, 2018). In this research work, BOD analysis was performed in accordance with international standards ISO 5815-1:2003 and ISO 5815-2:2003 by determining the difference of dissolved oxygen in the test samples before and after the incubation period (Jouanneau et al., 2014). To carry out BOD analysis, the diluted POME test samples with pertinent dilution factor were stored in 300 mL BOD bottles. Secondly, the *EUTECH DO 2700* dissolved oxygen

(DO) meter was used to attain the initial dissolved oxygen value,  $DO_0$  of the test sample in the BOD bottle. In order to prevent evaporation and dissolve of atmospheric oxygen into the solution, the BOD bottle was sealed and no air bubble should present in the sample (Okpashi, et al, 2019). It was then incubated inside *VELP SCIENTIFICA FOC 225E* incubator at  $20\text{ }^\circ\text{C} \pm 1\text{ }^\circ\text{C}$  for continuous five days according to the APHA standard methods 5220D and 5210B (Baird, Eaton and Rice, 2017). The  $DO_5$  in the solution in the BOD bottle was measured upon the completion of 5-days incubation period. Equation (3.1) presents the calculation to obtain the value of  $BOD_5$  (Patel and Vashi, 2015).

$$BOD_5 = (DO_0 - DO_5) / \text{Dilution Factor} \quad (3.1)$$

where

$DO_0$  = the initial DO value, mg/L,

$DO_5$  = the final DO value measured after 5-days incubation period, mg/L.

### 3.3.3 Turbidity Analysis

By applying light-scattering principle and possible absorption effects caused by the suspended particles in the test sample, the turbidity analysis is able to identify the presence of suspended particles in the test sample (Wei et al., 2021). The turbidity of the test samples was obtained using a *Lovibond Turbichack* turbidimeter based on the instruction manual of the equipment. The turbidimeter was initially calibrated using the standard solution. The turbidity vial was then filled to the marked line on the side of the vial with well-mixed test solution. In order to attain accurate readings, the vial had to be dry and devoid of air bubbles and fingerprints. Turbidity measurements were recorded in Nephelometric Turbidity Units (NTU). An average reading was obtained through taking multiple readings in the turbidity analysis.

### 3.3.4 Ammoniacal Nitrogen (NH<sub>3</sub>-N) Analysis

The concentration of NH<sub>3</sub> and NH<sub>4</sub><sup>+</sup>, which is a crucial water quality parameter in POME solution is quantified by using the ammoniacal nitrogen analysis. The analysis was conducted according to HACH Method 8038 in Hach Water Analysis Handbook, which is known the Nessler method (HACH, 2017). Firstly, 25 mL of deionized water as a blank sample and test solution were prepared separately. It was notably that the test solutions were filtered using a filter paper to remove any sediment in the test samples to avoid error in spectrophotometer reading (Nazri, Chong and Nithyanandam, 2018). Next, 3 drops of mineral stabilizer were added into each of the blank samples and test solution. Once the solutions were well-mixed, 3 drops of polyvinyl alcohol dispersing agent were added to each of them and the solution were mixed thoroughly. 1 mL of Nessler reagent was pipetted into each of the test samples and the test samples were once again mixed evenly. By altering the response timer on the *HACH DR6000* UV-Vis spectrophotometer, the reaction time was then adjusted to one minute. In order to achieve zero calibration, a vial containing 10 mL of the blank sample was inserted into the UV-Vis spectrophotometer after one minute. The test samples were then measured several times to ensure accuracy of the readings in the unit of mg/L.

## 3.4 Preparation of Photoelectrodes

### 3.4.1 Preparation of Photoanode

The method used for synthesise of ZnO/Zn nanorod array photoanode was adapted from the research work done by Meng, Lin and Lin (2014) and Yong et al. (2021). Firstly, the Zn plate were ultrasonically cleaned by using ethanol (C<sub>2</sub>H<sub>5</sub>OH) and was then rinsed with distilled water to remove any impurities on the surface of Zn plate in order to obtain uniform deposition of ZnO nanorods array structure (Patella et al., 2022). Next, by mixing 20 mM of zinc acetate ([ (CH<sub>3</sub>COO)<sub>2</sub>Zn•2H<sub>2</sub>O ]) together with 10 mM of sodium hydroxide (NaOH) in 50 mL ethanol solution, ZnO seed solution was prepared. After the ZnO seed solution was heated at 100 °C for 1 hour under constant stirring, the ZnO seed solution was casted onto the Zn plate and calcined in a

furnace at 300 °C for 1 h. After the calcination of Zn plate, the casting of ZnO seed solution was repeated to coat 2 layers of ZnO onto the Zn plate and calcined at 300 °C for 1 h in order to improve the deposition of ZnO nanorods array structure on the Zn plate.

Next, electrodeposition was conducted by using the casted Zn plate as the working electrode and a plain Zn plate as the counter electrode in an electrolyte solution prepared by dissolving 0.15 g of zinc nitrate ( $[\text{Zn}(\text{NO}_3)_2 \cdot 4\text{H}_2\text{O}]$ ) in 100 mL of distilled water. After heating the electrolyte solution to 80 °C, electric current of 0.01 A and voltage of 1.1 V were applied for a duration of 2 h. During the electrodeposition process, it was critical to remove microbubbles adhering to surface of Zn plate in every 20 minutes. Then, the ZnO/Zn photoanode was dried in oven and followed by calcination in a furnace at 400 °C for 1 h. The flow of the preparation of ZnO/Zn nanorod array photoanode was illustrated in the following Figure 3.4.



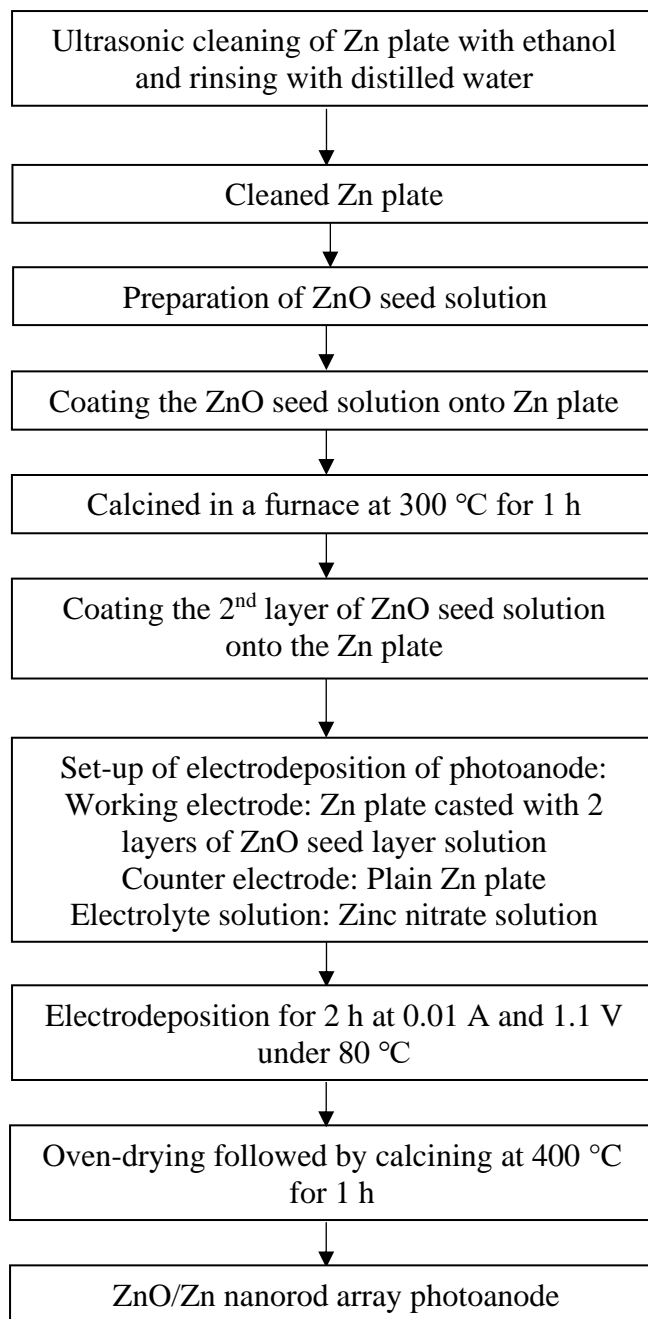


Figure 3.4: Schematic Flow Chart for the Synthesis of ZnO/Zn Nanorod Array Photoanode.

### 3.4.2 Preparation of Cathode

To synthesize CuO/Cu cathode, wet chemical method was used to prepare CuO/Cu cathode as reported by Gawande et al. (2016); Kee et al. (2018); Priya, Nesaraj and Selvakumar (2021). Firstly, the Cu plate was ultrasonically cleaned by using ethanol and rinsed with distilled water. Upon drying under room temperature, it was then immersed in a mixture of 2.5 M NaOH and 0.125 M Na<sub>2</sub>S<sub>2</sub>O<sub>8</sub> for 30 minutes. The Cu plate was rinsed with distilled water to remove any remaining residue. After a drying treatment at 90 °C for 24 h in an oven, the Cu plate was calcined at 450 °C for 1 h. Figure 3.5 depicts the summarized flow for synthesis process of CuO/Cu cathode.

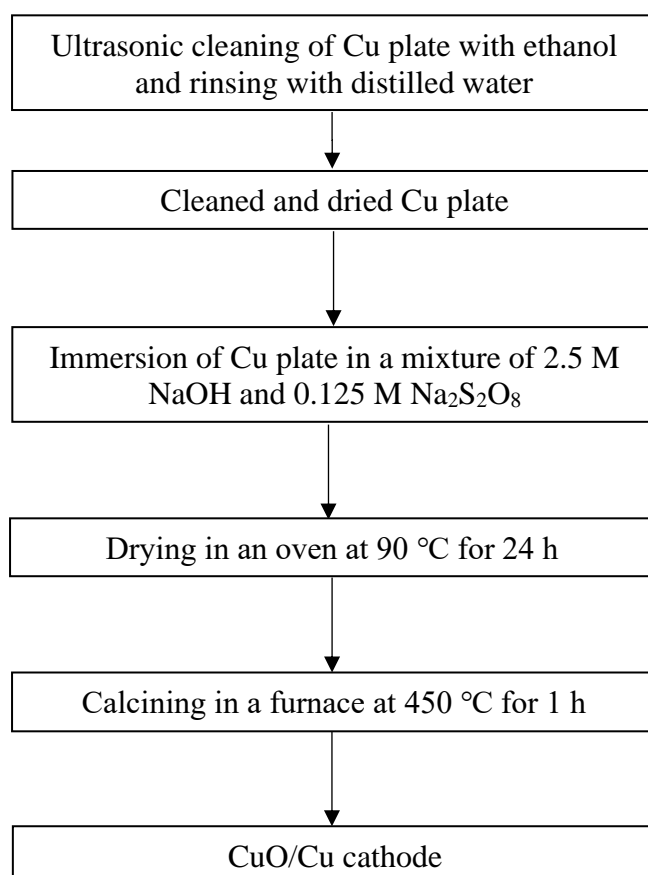


Figure 3.5: Schematic Flow Chart for the Synthesis of CuO/Cu Cathode.

## **3.5 Characterization of Photoelectrodes**

### **3.5.1 Crystal Phase Analysis**

X-ray diffraction (XRD) is a non-destructive analysis used to identify detailed crystallographic size, structure and orientation of the ZnO/Zn nanorod array photoanode (Vilar, 2016; Gonon, 2021). This analysis was performed using a *Philips PW1820* diffractometer equipped with Cu K $\alpha$  radiation ( $\lambda = 1.5406 \text{ \AA}$ ) at scanning rate of  $2^\circ \text{ min}^{-1}$  in the range of  $2\theta$ , which was set to  $20 - 70^\circ$ . The analysis was conducted in the laboratory of Faculty of Science, Universiti Tunku Abdul Rahman (UTAR), Kampar Campus.

### **3.5.2 Surface Morphology Analysis**

The surface morphology of the photoelectrodes was studied using field emission scanning electron microscopy combined with energy dispersive X-ray spectroscopy (FESEM-EDX) analysis by using a *JEOL JSM-6701F* FESEM. Prior to the analysis, the samples were cleaned to ensure the accuracy of the readings and was coated with a thin layer of platinum as a conductive material using *JEOL JFC-1600* auto fine coater. Carbon tape was then used to secure the samples on a sample holder. In addition, EDX analysis was conducted to determine the chemical composition of the electrodes by using the same equipment. FESEM-EDX analysis was carried out at the laboratory of Faculty of Science, UTAR, Kampar Campus.

### **3.5.3 Functional Group Analysis**

Fourier transform infrared spectroscopy (FTIR) identifies the morphology and functional group of the nanostructure-based photoelectrode samples by applying the infrared spectrum of absorption frequency and photoconductivity of the photoelectrodes (Pandey et al, 2015; Azad and Rasul, 2019). In this research work, *Perkin Elmer Spectrum RX-1* FTIR Spectrometer was used to perform the FTIR analysis. The photoelectrode samples were first crushed to a fine powder form. After

addition of powdered potassium bromide (KBr), the sample were thoroughly mixed and was once again grounded to powder form. The mixture was then compressed into an evacuable die set to form a pellet-shaped test sample. Prior to analysis, FTIR accessories kit including FTIR sample holder, evacuable die set and grinder was cleaned with absolute ethanol to remove the impurities. FTIR analysis was performed at the laboratory of Faculty of Science, UTAR, Perak Campus.

### **3.6 PFC System Constructed Using ZnO/Zn Nanorod Array Structure Photoanode and CuO/Cu Cathode**

The photocatalytic performance of developed PFC system using ZnO/Zn photoanode and CuO/Cu cathode in aspects of organic pollutant removal efficiency from POME and power generation in the presence of UVC light irradiation was aimed to investigate in this study. The experiments were conducted in a 100 mL glass beaker which contained 100 mL of the POME solution, 0.1 M of Na<sub>2</sub>SO<sub>4</sub> as electrolyte which is proposed by Ong and his co-workers (2021), a given mass of oxidant and two-thirds of submerging photoelectrodes in the test solution, located inside an acrylic black box. Air was bubbled to the CuO/Cu cathode via a tube at a constant aeration rate of 2 L/min. With the aid of a hot plate stirrer, the test solutions were continuously agitated. Prior to the experiment, the test solution was mixed in the dark for 30 minutes before it was exposed for the irradiation of light to ensure the adsorption-desorption equilibrium between the POME compound and the photocatalyst was achieved (Saputera, et al., 2021; Nawaz, et al, 2019). After the elapse of 30 minutes of PFC system in the acrylic black box, the UV-light source was placed 2 cm apart from the photoanode above the reaction solution to photoexcite the photoanode. During the photocatalytic degradation of POME, 5 mL of the solution was withdrawn from the system, centrifuged and filtered with 0.45 µm polytetrafluoroethylene (PTFE) membrane filter-equipped syringe before being subjected to analysis and subsequently analyzed using COD analyzer and a UV-vis spectrophotometer. Equation (3.2) was applied to determine the organic pollutants degradation efficiency of the PFC system (Mohamed and Harraz, 2020).

$$\text{Degradation efficiency (\%)} = ((COD_0 - COD_f) / COD_0) \times 100\% \quad (3.2)$$

where

$COD_0$  = the initial COD value, mg/L,

$COD_f$  = the final COD value, mg/L.

In order to determine the electricity generated, a *NJTY T-33* mini digital multimeter was used. The voltage and electric current produced across the circuit coupled to a 1 k $\Omega$  variable resistor was measured and recorded as well. The power density output per unit area of photoanode of the PFC system was calculated based on the following Equation (3.3) (Momoh and Naeyor, 2016).

$$P = (I \times V) / A \quad (3.3)$$

Where

P = power density output, W

I = current, A

V = voltage, V

A = surface area of the photoanode, m<sup>2</sup>.

### 3.7 Process Parameter Studies

The photocatalytic activity of the developed PFC system in degrading POME wastewater and producing electricity were governed by varying operating parameters such as concentration of POME wastewater, concentration of oxidant and initial solution pH. In this study, these process parameters were adjusted sequentially at a time while the other process parameters remain constant.

### **3.7.1 Types and concentration of oxidant**

The addition of an oxidant in the PFC system enhances the effectiveness of the PFC system to degrade the organic pollutant as it promotes the formation of oxidative radicals (Li et al., 2018). It was noteworthy that the addition of an oxidant was performed prior to the start of the reaction in the PFC system under UV light illumination (Tang et al., 2019). A comparison of the performance of the PFC system with the addition of oxidant and without the addition of oxidant was performed in this study. Different  $\text{Na}_2\text{S}_2\text{O}_8$  oxidant concentrations were used, such as 0.25 mM, 0.5 mM, 1.5 mM and 2.5 mM. The selection of the concentration of oxidant was designated according to the research study conducted by Xu and Liu (2022) and Sun, Liu and Yang (2022). In this study, the PFC experiment was conducted at an initial concentration of the POME wastewater at a dilution factor of 1:20 with a natural pH level of 8.51.

### **3.7.2 Initial POME Concentration**

The effect of initial POME concentration on the effectiveness of PFC system was studied using 100 mL of mixture of POME at different dilution factor. The initial POME concentration was varied by dilution with water in factor of 1:5; 1:10; 1:15 and 1:20 to determine the optimum concentration for the best organic pollutant degradation efficiency. The selection of initial POME concentration range was based on the research studied by Kee et al. (2020). In this research work, the experiments were carried out with optimum concentration of oxidant and natural POME pH level of 8.51.

### **3.7.3 Initial solution pH**

The initial solution pH is another crucial factor that influences the performance of PFC system to degrade organic pollutant as the pH dictates the surface charge of the photocatalyst due to differences of electron distribution and transfer in the PFC system as reported by Li et al. (2018). Four different pH of solutions were adjusted by addition of dilute 1.0 M HCl solution or 1.0 M NaOH solution prior to initiation of the

experiment. The values of solution pH were selected based on the different conditions such as acidic, natural, neutral, and alkaline media by employing *HANNA Instruments HI 2550 pH/ORP/EC/TDS/NACL* benchtop meter. The experiments were carried out with optimum concentration of oxidant and initial POME concentration which were obtained from aforementioned process parameter studies.

### 3.8 Radical Scavenging Test

Aside from hydroxyl radicals ( $\bullet\text{OH}$ ), there are other radical species, such as superoxide ion radicals ( $\text{O}_2\bullet^-$ ) and sulfate radical ( $\text{SO}_4\bullet^-$ ) contribute to the photocatalytic activity in a PFC system (Schneider, et al., 2020). In order to identify the most effective radical species for photocatalytic degradation of organic pollutants in POME, a radical scavenging test was conducted. Once the test samples were extracted and filtered, which eliminated the impurities, the initial COD concentration of the test samples was analyzed using a COD analysis at regular intervals. After addition of scavenger species to the test sample, the final COD concentration was obtained and the degradation efficiency was attained by using Equation (3.2). The effect of a corresponding radical species responsible for the degradation efficiency of organic pollutant was then able to be identified. The selected scavenger compounds and corresponding targeted radical species was listed in Table 3.2. In this research work, 2mM of all scavenger species will be used to identify the radical species (Chen et al., 2022; Lam et al., 2020).

**Table 3.2: List of Commonly Used Radical Scavengers (Li et al., 2019; Pelaez et al., 2016; Liang and Lei, 2015).**

Radical Scavengers	Targeted Radical Species
Ethylenediaminetetraacetic acid disodium salt (EDTA-2Na)	$h_{\nu B}^+$
Silver nitrate	$e_{CB}^-$
1,4-benzoquinone	$\bullet\text{O}_2^-$
Tertiary butanol (Tert-butanol)	$\bullet\text{OH}$
Ethanol (EtOH)	$\text{SO}_4\bullet^-$

### **3.9 Reusability of the photoelectrodes**

Recycling test is conducted to evaluate the reusability of ZnO/Zn nanorod array photoanode and CuO/Cu cathode in the PFC system for repetitive uses. The selection of number of cycles was based on the research work conducted by Kee et al. (2018). The recycling experiments were performed under natural pH solution with optimum initial concentration of POME and concentration of oxidant for each run. For the succeeding cycles, the photoelectrodes were soaked in deionised water 30 minutes, rinsed with deionised water and dried in an oven at 90 °C.



## CHAPTER 4

### RESULTS AND DISCUSSIONS

This chapter outlined the experimental findings of the research study. The characterization studies of the ZnO/Zn nanorod array photoanode and CuO/Cu cathode that were utilized in the PFC system through two analysis techniques was addressed in the first section of this chapter. The preliminary studies were explained in the following section. Subsequently, the performance of the PFC system through photodegradation rate of pre-treated POME and amount of power produced under various process parameters such as concentration of oxidant, initial concentration of POME solution and initial solution pH were focused in the third section. The succeeding section focused on the radical scavenging test of the PFC system under optimal conditions which were identified previously. Recycling tests will be conducted to determine the stability of the developed ZnO/Zn nanorod array photoanode against continuous use. In order to study the economic viability of the ZnO/Zn nanorod array photoanode and CuO/Cu cathode in real-world applications, a cost analysis of fabrication of the photoelectrodes was performed.

## 4.1 Characterization of Photoelectrodes

Both photoelectrodes employed in the constructed PFC system were characterized to examine the physiochemical characteristics, enabling better understanding in terms of the effectiveness of the PFC system developed in this study in COD removal and electricity yield. The FESEM technique accompanied by EDX analyses were performed to identify the surface morphology and elemental composition of the photoelectrodes. In addition, through XRD analysis, the crystallinity and phase purity degree of ZnO/Zn nanorod array photoanode and CuO/Cu cathode were verified prior to conducting the experiment. In addition, the band gap energy of the ZnO/Zn nanorod array photoanode was ascertained by utilising the UV-Vis spectra analysis.

### 4.1.1 Surface Morphology Analysis

Figures 4.1a and b portray the morphological characterisation of ZnO/Zn nanorod array photoanode obtained through FESEM analysis at various magnifications. The ZnO adhered on the surface of Zn film by using an electrodeposition method exhibited rod-like shapes, as evidenced from the figures. Upon higher magnification in Figure 4.1b, it was indicated that the ZnO nanoparticles were densely packed on top of the Zn film. It was anticipated that 1D nanostructures would offer substantial advantages, including increasing the surface area which led to increase of reaction sites and promoting chemical accessibility of electrolytes to deeper part of the photoelectrodes (Li and Wang, 2019; García-Betancourt, et al., 2020; Castillo-Blas, et al., 2020). The ZnO particles were found with ranging in an approximate size from 263 nm to 882 nm.

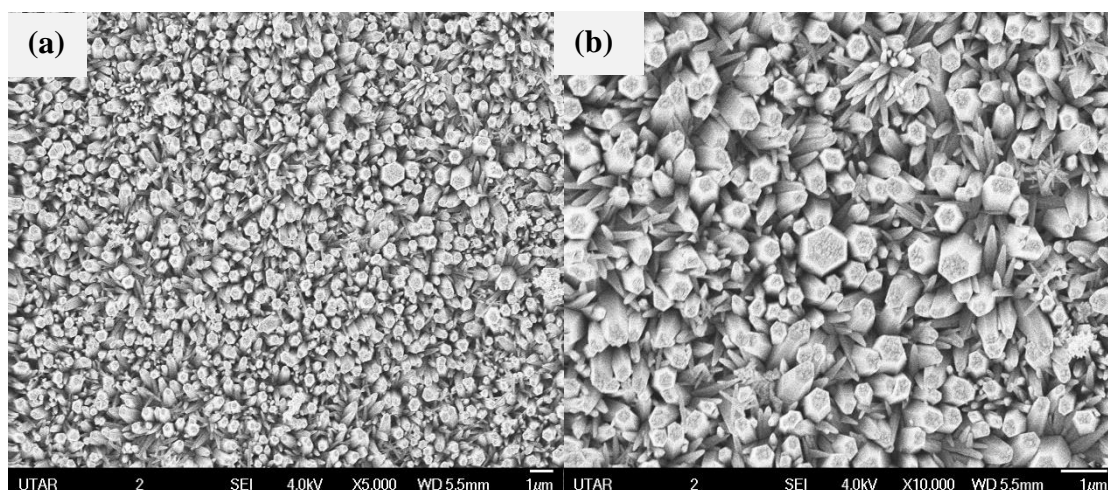


Figure 4.1: FESEM images of synthesized ZnO/Zn nanorod array photoanode under magnifications of (a) x 5,000 and (b) x 10,000.

On the other hand, Figures 4.2a and b depict the morphology of CuO/Cu cathode under various FESEM magnifications. It was observed from these figures that the CuO nanoparticles were dispensed homogeneously on the Cu plate. The observed range of particle size for the CuO was ranging from 91 nm to 392 nm.

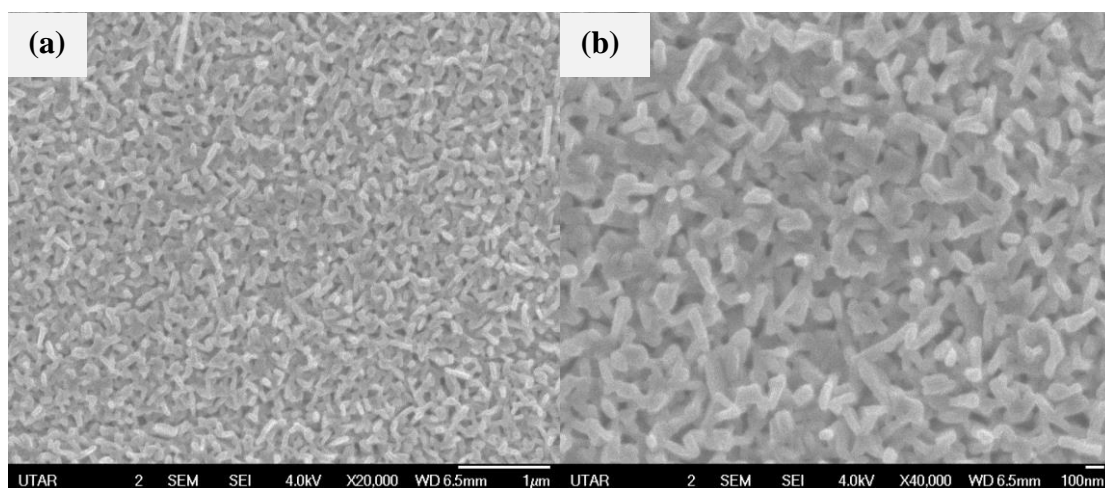


Figure 4.2: FESEM images of synthesized CuO/Cu cathode under magnifications of (a) x 20,000 and (b) x 40,000.

### 4.1.2 Elemental Composition Analysis

EDX measurements were conducted to identify the elemental composition of ZnO/Zn nanorod array photoanode and CuO/Cu cathode. Figure 4.3 demonstrates the EDX spectrum for the ZnO/Zn nanorod array photoanode. It was verified that the ZnO/Zn nanorod array were predominantly composed of Zn and O based on atomic percentage. As shown in Figure 4.3, there was 71.10% of Zn and 28.90% of O weightage in the elemental composition of the synthesized ZnO/Zn nanorod array photoanode. Hence, it was assured that Zn and O elements exhibited on the ZnO/Zn nanorod array photoanode.

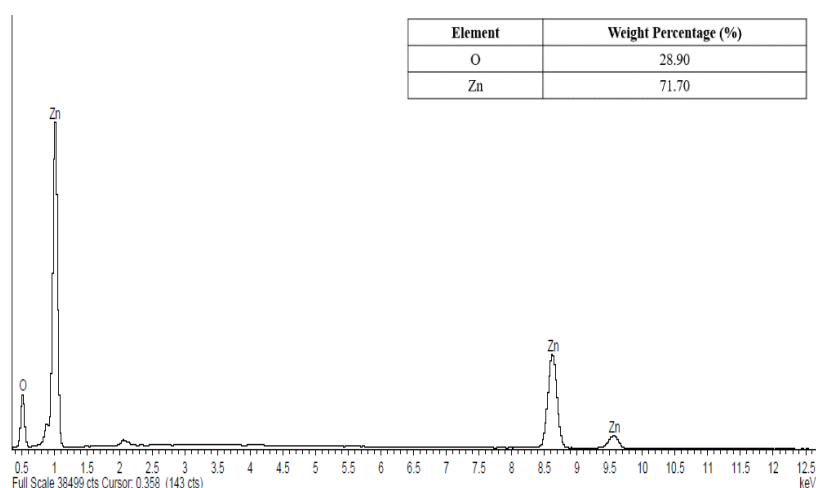


Figure 4.3: EDX Spectra of ZnO/Zn Photoanode

On the other hand, Figure 4.4 revealed the EDX spectrum for the CuO/Cu cathode. It was affirmed that the CuO/Cu cathode constituted of Cu and O elements, with weight percentages of 61.86% and 38.14%. It was confirmed that the merely Cu and O elements exhibited on the CuO/Cu cathode according to the EDX spectrum.

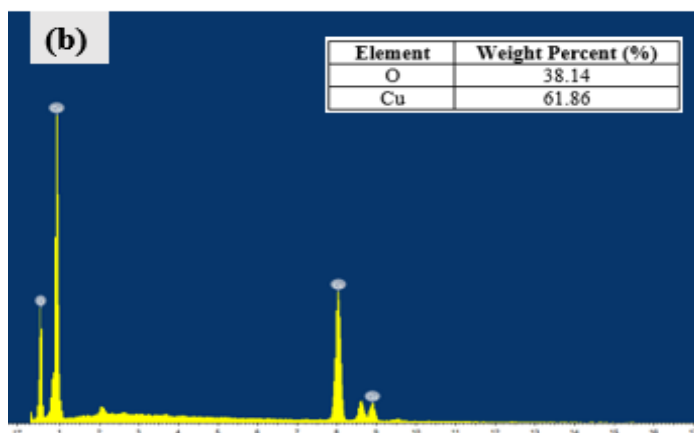


Figure 4.4: EDX Spectra of ZnO/Zn Photoanode

### 4.1.3 Crystalline Phase Analysis

The XRD analysis identified the crystalline structure of the ZnO/Zn nanorod array photoanode and CuO/Cu cathode. Figure 4.5 depicts the XRD pattern of ZnO/Zn nanorod array photoanode. All of the samples displayed well-crystallized samples, as verified by the sharp, narrow and intense peaks in Figure 4.5. The ZnO/Zn nanorod array exhibited diffraction peaks at  $31.08^\circ$  (100),  $34.50^\circ$  (002),  $36.32^\circ$  (101),  $42.74^\circ$  (102),  $56.30^\circ$  (110),  $62.94^\circ$  (103),  $68.04^\circ$  (112),  $69.16^\circ$  (201), and  $72.68^\circ$  (004), which were indexed with ICCD card no.00-036-1451. Furthermore, the identified ZnO/Zn peaks in this study were also consistent with those reported by Jabeen et al. (2014), Yunus et al. (2017) and Carmen et al. (2022), validating the phase purity of the photoanode employed in this study.

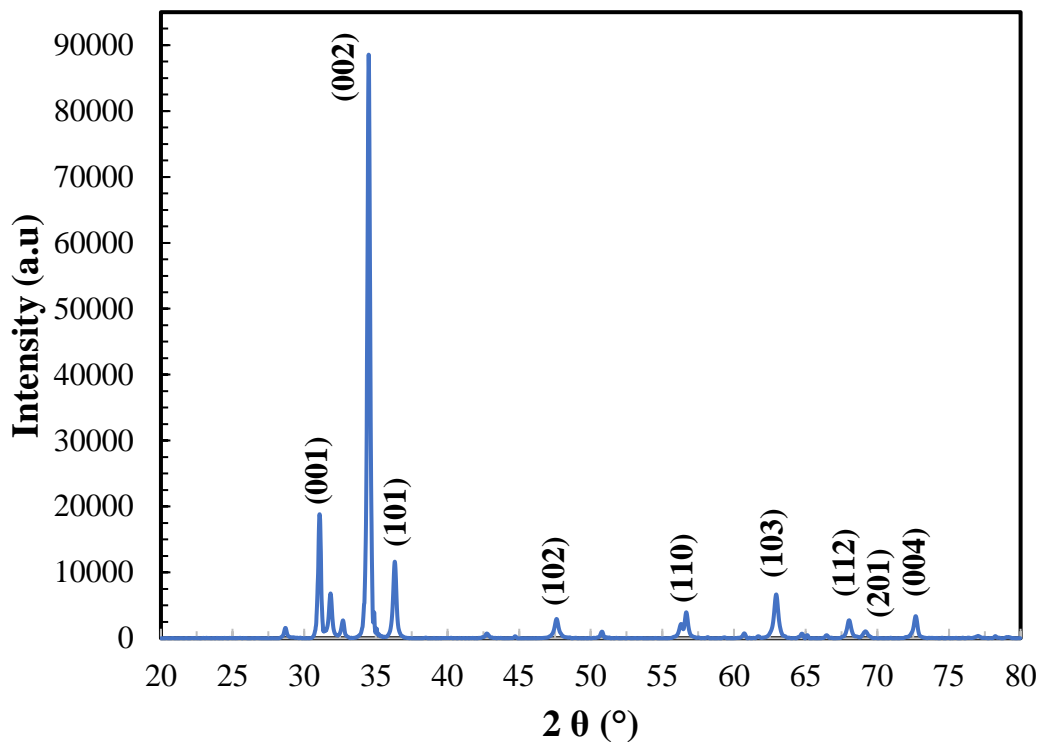


Figure 4.5: XRD pattern of ZnO/Zn nanorod array photoanode

The XRD pattern of CuO/Cu cathode was displayed in Figure 4.6. The diffraction peaks observed for CuO/Cu were at 31.89 ° (110), 35.79 ° (111), 38.99 ° (111), 42.69 ° (200), 49.69 ° (202) and 72.67 ° (221). The identified Cu peaks were assigned to the Cu substrate. The identified CuO/Cu peaks in this research work were in line with the characterization reported by Kee et al. (2018). The phase purity of CuO/Cu was validated as there was no other peaks detected.

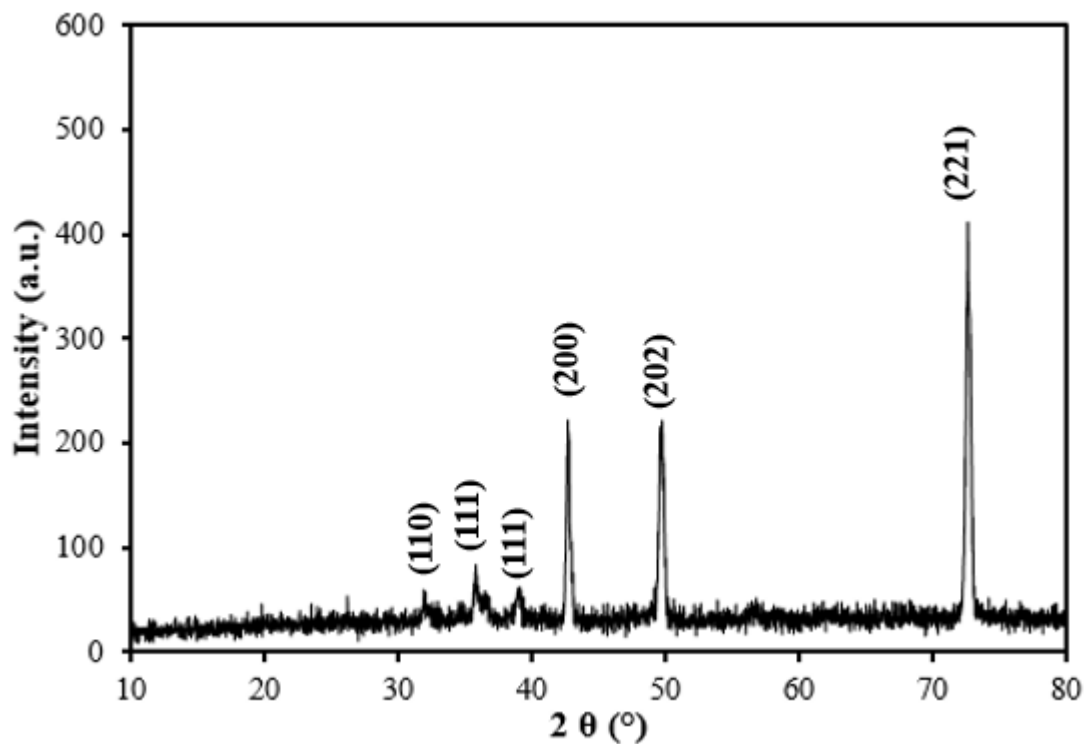


Figure 4.6: XRD pattern of CuO/Cu cathode

#### 4.1.4 Band Gap Potential Measurement

Figure 4.7 delineates the UV-Vis spectra of ZnO NRA. By using the Kubelka–Munk method, the red dotted line indicated the band gap of ZnO NRA which was measured through extrapolation of the linear portion of the plot of  $[F(R)hv]^2$  versus photon energy to the photon energy axis. It was ascertained that the band gap of ZnO NRA as 3.05 eV, which is in accordance with the published values in the literature (Yu et al., 2019, Yu et al., 2021, Albiss and Dalo, 2021).

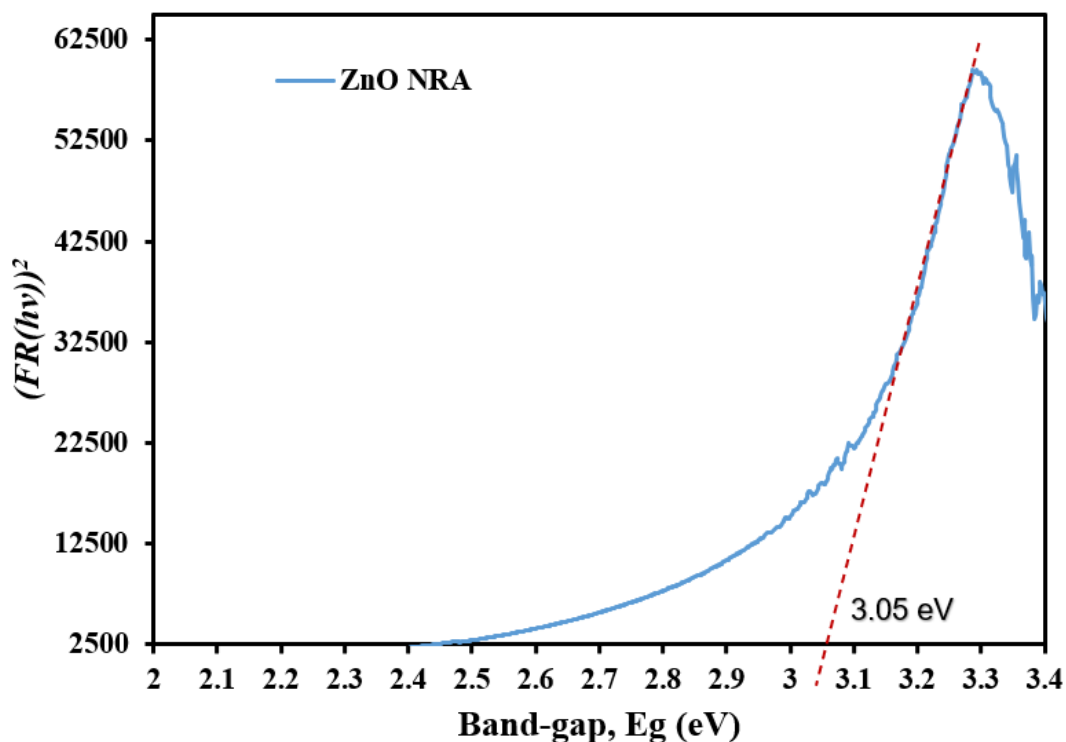


Figure 4.7: UV-Vis Spectra of ZnO NRA

#### 4.1.5 Conduction Band (CB) Potential Measurement

The conduction band (CB) potential,  $E_{CB}$  of ZnO was determined through Mott-Schottky measurement, which is illustrated in Figure 4.8. In order to obtain the  $E_{CB}$  values, x-intercept was determined for the plot through interpolation of line tangent to the graph. The  $E_{CB}$  values for ZnO NRA as shown in Figure 4.8 was -0.42 eV. The CB values determined in this research work coincided with the literature reported by Yong et al. (2022) and, Irshad and Munichandraiah (2015). As the band gap potential,  $E_g$  of ZnO NRA was previously determined to be 3.05 eV through UV-Vis DRS spectra, the valence band (VB) potential,  $E_{VB}$  for ZnO was computed to be 2.63 eV by using Equation (4.1) (Sim et al., 2018). Bhosale et al. (2019) stated that a *n*-type semiconductor correlated to a MS plot with a negative gradient, whereas *p*-type semiconductor corresponded to MS plot with positive gradient. Thus, the MS plots affirmed the *p*-type conductivity for ZnO NRA produced in this research work since the MS plots exhibited negative slopes.



$$E_{VB} = E_{CB} + E_g \quad (4.1)$$

where

$E_{VB}$  = the valence band (VB) potential, eV,

$E_{CB}$  = the conduction band (VB) potential, eV,

$E_g$  = the band gap potential, eV.

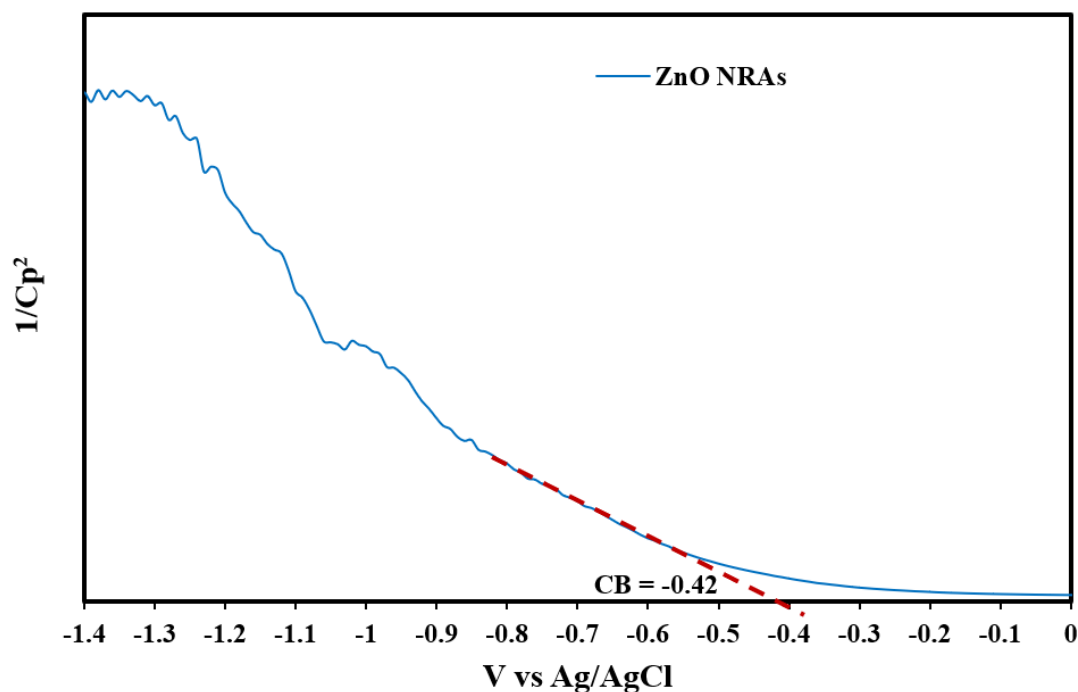


Figure 4.8: MS Plots of ZnO NRA.

## 4.2 Fundamental studies of PFC system

Photocatalytic activity of ZnO NRA photoanode in the constructed PFC system was studied by the degradation effectiveness of palm oil mill effluent (POME). Figure 4.9 depicts the photodegradation of POME subjected to various conditions. After 240 minutes of irradiation under UVC light, the photolysis process exhibited a mere degradation rate of 21.9 % without any photocatalyst, while COD degradation rate of POME of 39.6 % was achieved when using the PFC system was comprised of ZnO/Zn photoanode and CuO/Cu cathode. Subsequently, the effect of addition of 0.5mM of sodium persulfate ( $Na_2S_2O_8$ ) as oxidant was conducted in the presence of the

photoanode and cathode in degrading the organic pollutants. It was observed that 70.9% COD degradation rate was obtained with addition of persulfate oxidant, after similar irradiation time. The results indicated that addition of persulfate oxidant was more efficient than bare PFC system.

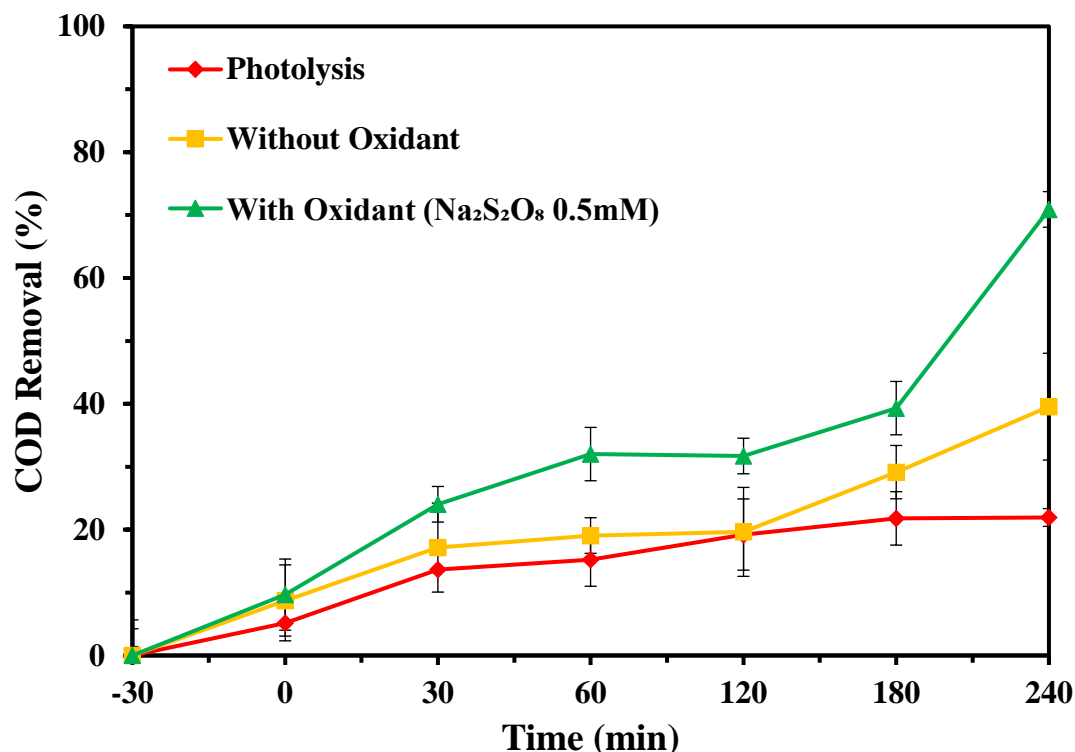
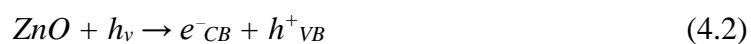


Figure 4.9: Photocatalytic Degradation of POME Using PFC System Using Photolysis, Without addition of oxidant and With 0.5mM of Na<sub>2</sub>S<sub>2</sub>O<sub>8</sub> oxidant (POME dilution ratio = 1:20; Solution pH = 8.51).

Based on Figure 4.9, removal of organic pollutants in POME solely due to the photolysis was negligible owing to the stable properties of POME under UVC light irradiation (Kee et al., 2020). The photolysis test demonstrated that POME showed minimal self-decomposition when it is exposed to UVC light irradiation. The obtained result was supported by Lee et al. (2017); Chin et al. (2018) and Chin et al. (2022).

The POME was degraded to different extents at substantially higher efficiencies with the application of PFC system involving ZnO/Zn NRA photoanode. The production of highly reactive  $\bullet\text{OH}$  and  $\bullet\text{O}_2^-$  radicals from oxidation of H<sub>2</sub>O and O<sub>2</sub> was primarily responsible for the increased rate of photodegradation of POME. Upon UVC light illumination, the photocatalyst-coated surface of the photoanode underwent

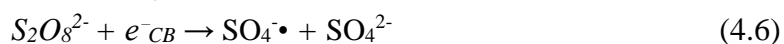
photoexcitation, which triggered the formation of  $e_{CB}^- - h_{VB}^+$  pair and simultaneously promoted the migration of  $e_{CB}^-$  to the cathode compartment via an external circuit and reduced the recombination of  $e_{CB}^- - h_{VB}^+$ . Meanwhile, the  $h^+$  that remained at the photoanode would react with  $H_2O$  to form  $\bullet OH$  radicals, while the  $e_{CB}^-$  would flow to the aerated cathode and react with  $O_2$  to generate  $\bullet O_2^-$  radicals, which were capable in the mineralization of the organic pollutants (Alhaji et al., 2018; Moxsin, et al., 2021). The production of these radicals is represented by following Equations (4.2) to (4.4).



However, according to Li et al. (2018), the vast majority of reactive species reactions of the PFC system predominantly occurred on the photoanode and cathode surfaces, but the superficial area of the electrodes could not be increased indefinitely, leading to limitation of the current efficiency of PFC in organic degradation and power generation. Thence, the introduction of oxidants such as sodium persulfate ( $Na_2S_2O_8$ ) in enhancing the performance of the PFC system were examined in this study.

Remarkably, the addition of persulfate oxidant has showed better COD degradation efficiency than virgin PFC system in terms of the COD removal rate. Li et al. (2018) and Tang et al. (2019) stated that the oxidation potential of sulfate radical ( $SO_4^{\bullet -}$ ), which is activated by UVC light as stated in Equation 4.4 or reacted directly with  $e_{CB}^-$  as stated in Equation 4.5, could reach 3.1 V, which is stronger than the potential of  $\bullet OH$  radicals (2.7 V), thus  $SO_4^{\bullet -}$  is able to react with organic compounds containing unsaturated bonds or aromatic  $\pi$ -electrons via electron transfer (Tan et al., 2019). Moreover, persulfate oxidant could act as an electron acceptor for ZnO/Zn NRA photoanode and an electron scavenger for cathode, increasing the separation effectiveness of  $e_{CB}^- - h_{VB}^+$ . Many studies also suggested that the activation product of persulfate oxidant, which is the highly activated  $SO_4^{\bullet -}$  radical is more superior to the  $\bullet OH$  radicals due to longer lifespan (30–40  $\mu s$ ) compared to  $\bullet OH$  radicals (20 ns), considerable pH range (2-8), free of secondary contaminants and lower costs of storage

and transportation owing to the availability of persulfate salts (Li et al., 2018; Tang et al., 2019; Lee, Gunten and Kim, 2020).



On the other hand, Figure 4.10 compares the electricity generation efficiency of the PFC system between without oxidant and with addition of two different type of oxidants in the constructed PFC system. It can be perceived that the addition of oxidant significantly improved the power generation of PFC system.

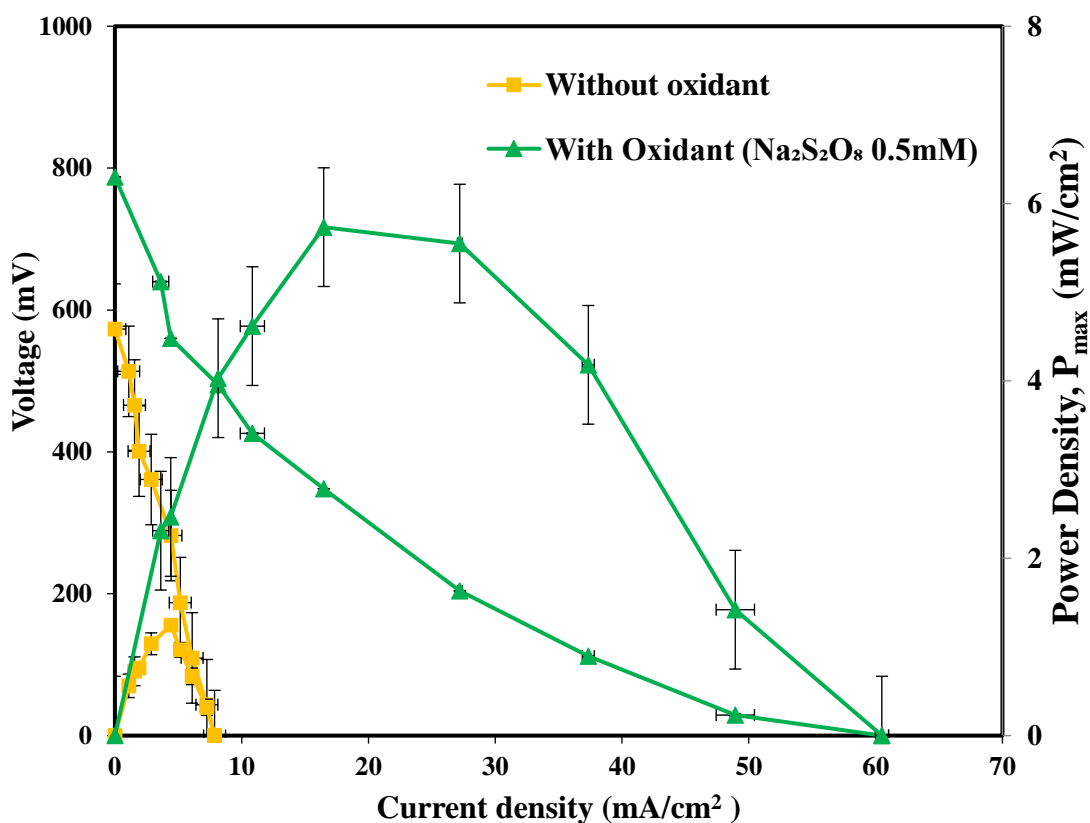


Figure 4.10: The Difference Between Bare PFC System with Addition of Persulfate Oxidant on Electricity Generation by the PFC system (POME dilution ratio = 1:20; Solution pH = 8.51).

The open-circuit voltage ( $V_{oc}$ ) of the virgin PFC system and PFC system with persulfate oxidant were 573.0 mV, 787.5 mV, respectively. In addition, the short

circuit current density ( $J_{sc}$ ) were 7.8 mA/cm<sup>2</sup> and 60.5 mA/cm<sup>2</sup>, respectively, while for maximum output power density ( $P_{max}$ ) were 1.3 mW/cm<sup>2</sup> and 5.7 mW/cm<sup>2</sup>.

The addition of persulfate oxidant in the PFC system has observed a notable improvement of electricity generation as the use of persulfate as an oxidant acted as an electron scavenger to remove the accumulated electrons on the cathode, hence accelerating the electricity generation in the PFC system (Li et al. 2018). Moreover, according to Li et al. (2019), the addition of PS oxidant would increase the amount of supporting electrolyte, leading to enhanced electrical conductivity and separation of photogenerated  $e_{CB}^- - h_{VB}^+$  pairs, thus suggesting better electricity generation with addition of persulfate oxidant in a PFC system.

Consistent findings also reported by other researchers. Zhou, Cheng and Liu. (2019) revealed that the addition of persulfate on the PFC system to degrade tetracycline exhibited better performance with 14 times higher kinetic rate constant than bare PFC system. In addition, Li et al. (2019) validated that the addition of persulfate oxidant in the PFC system successfully attained higher degradation rate of norfloxacin, implying a good synergistic effect between persulfate and PFC system. Furthermore, Crincoli and Huling (2021) have demonstrated that the Rhodamine B dye degradation was significantly better in the ultra-violet activation of persulfate oxidant. Due to aforementioned technical advantages of persulfate oxidant in a PFC system, addition of persulfate oxidant is employed in the following studies for better photocatalytic degradation performances.

#### 4.2.1 Effect of Open and Closed Circuit

In order to gain a deeper understanding of the mechanism of  $e_{CB}^-$  transfer in the PFC system, the PFC system was investigated in both open and closed circuit conditions. It was revealed that the degradation efficiency of POME was influenced by the external circuit connection of the PFC. For open circuit study, the photoanode and cathode were not connected. Meanwhile, closed circuit analysis was conducted by linking the photoanode and cathode via an external resistor of 1000  $\Omega$ . Figure 4.11 illustrates the COD removal rate of organic contaminants in POME of an open and closed circuit

PFC, respectively. In the open circuit PFC system, there was 70.9% of COD removal in within 240 minutes of irradiation time, while 28.7 % of COD removal was achieved for the closed circuit PFC system within the same time interval.

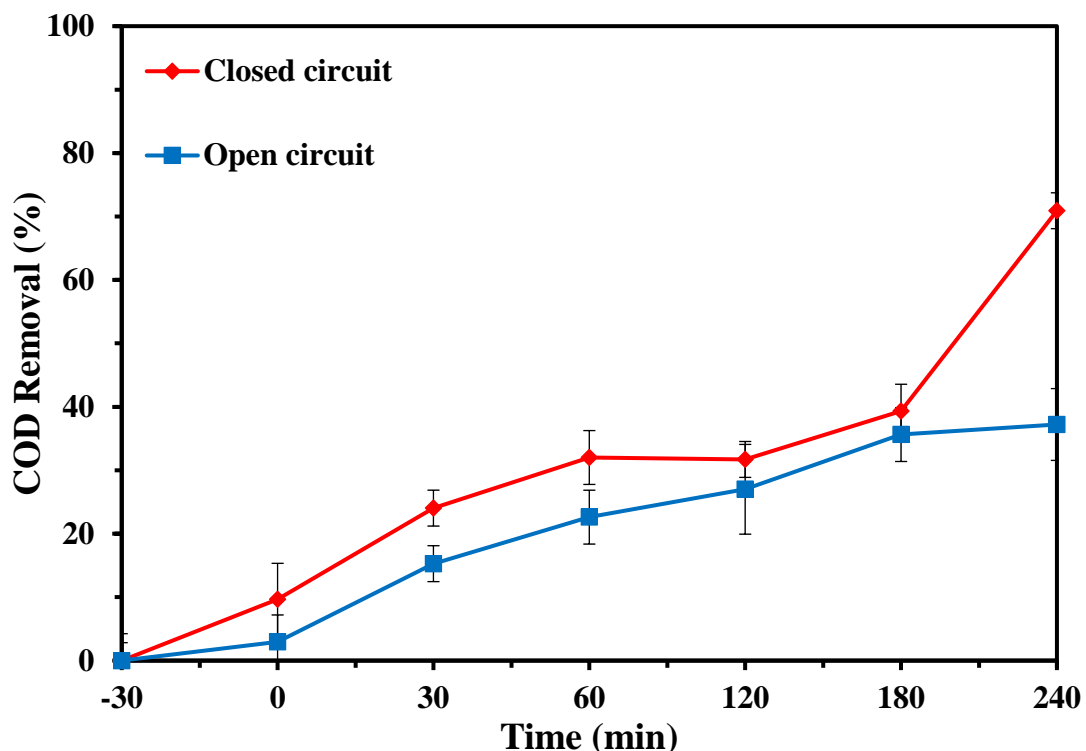


Figure 4.11: Photocatalytic Degradation of POME Using PFC System Under Open and Closed Circuit Condition (POME dilution ratio = 1:20; Solution pH = 8.51).

When the ZnO/Zn NRA was irradiated by UVC light irradiation,  $e_{CB}^- - h_{VB}^+$  pair was formed at the photoanode compartment in both open and closed circuit of PFC. The generated  $h_{VB}^+$  reacted with  $H_2O$  to form  $\bullet OH$  radicals and oxidize the organic pollutants directly and contributed to COD removal. However, higher COD removal rate was observed in closed circuit PFC system compared to open circuit condition. The better photocatalytic performance under closed circuit can be attributed to the promoted separation of  $e_{CB}^- - h_{VB}^+$  and limited recoupling rate of  $e_{CB}^- - h_{VB}^+$ , owing to the potential bias of photoanode and cathode (Lee et al., 2017). Furthermore, the  $e_{CB}^-$  arrived on the cathode from photoanode reacted with  $O_2$  to form  $\bullet O_2^-$  radicals, leading to further oxidation of POME organic pollutants in the closed circuit condition (Khalik et al., 2018). Counter-intuitively, in the condition of open circuit PFC system, the photoexcited  $e_{CB}^-$  were confined within the photoanode compartment, hence

aggravating the recombination rate of  $e_{CB}^- - h_{VB}^+$  and limiting the formation of  $\bullet\text{OH}$  radicals, which resulted in lower COD degradation efficiency of organic pollutants in open circuit PFC system.

### 4.3 Optimization of Operating Conditions for PFC System

#### 4.3.1 Optimum concentration of oxidant

The concentration of oxidant plays a major role in boosting the performance of the PFC system. As discussed in the preliminary studies, sodium persulfate ( $\text{Na}_2\text{S}_2\text{O}_8$ ) was chosen as the oxidant in view of its ability to generate sulfate radicals ( $\text{SO}_4^{\bullet-}$ ) which are capable of improving performance of PFC system (Lee et al., 2020). In this experiment, POME dilution ratio was 1:20 and had a natural pH of 8.51 under UVC lighting conditions with different concentrations of  $\text{Na}_2\text{S}_2\text{O}_8$  applied, specifically 0 M, 0.25 mM, 0.5 mM, 1.5 mM and 2.5 mM.

Figure 4.12 depicts the performance of the PFC system in degrading the organic pollutants in the absence of the oxidant and under various oxidant concentration added into the PFC system. Based on Figure 4.12, the COD removal and power production enhanced as the concentration of persulfate oxidant increased from 0 to 2.5 mM. The mineralization efficiency of organic pollutants in POME under 0 mM, 0.25 mM, 0.5 mM, 1.5 mM and 2.5 mM were 39.6 %, 50.0 %, 70.9%, 78.4% and 88.9%, respectively. The findings demonstrated that the COD removal efficiency of POME increased when the concentration of added persulfate oxidant increased. The substantially increased performance was mainly attributed to the higher catalytic activity and the more active species generated to participate in the degradation of pollutants (Zhou, Hou and Liu, 2019).

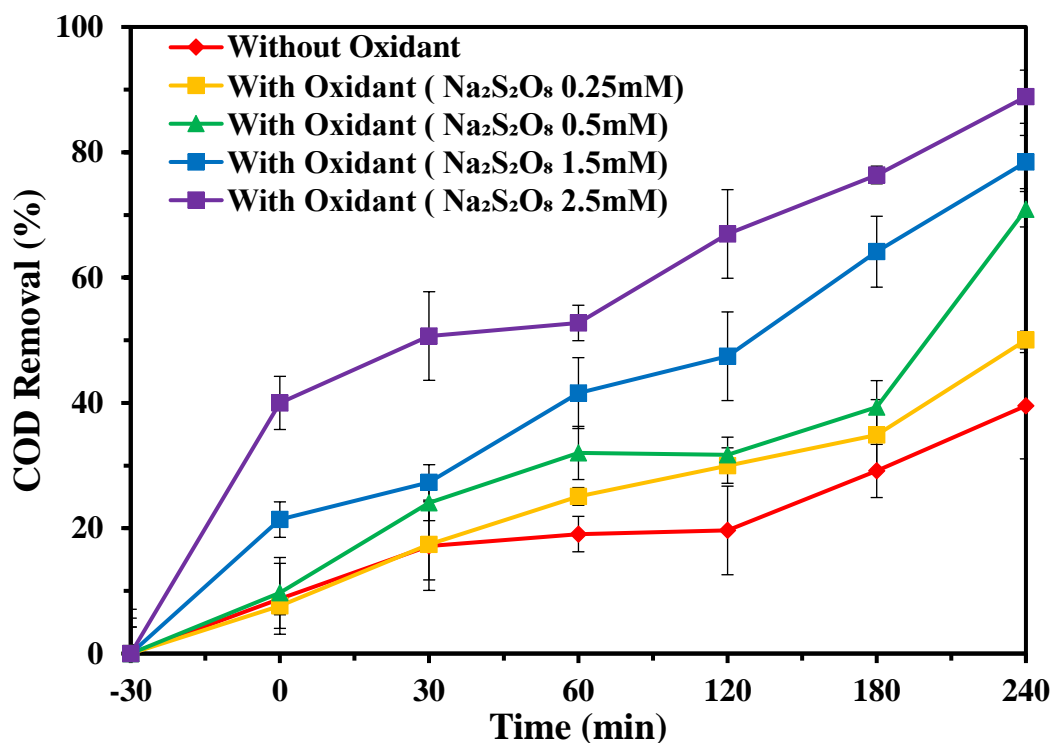


Figure 4.12: The effect of Na<sub>2</sub>S<sub>2</sub>O<sub>8</sub> Oxidant Loading on The COD Removal Efficiency Using PFC System (POME Dilution Ratio = 1:20; Solution pH = 8.51).

Figure 4.13 summarizes the influence of persulfate oxidant concentration on the electricity generation efficiency of the PFC system. It was noteworthy that the electricity performance of the PFC system improved notably in the presence of persulfate oxidant. The  $V_{oc}$  obtained for persulfate concentrations of 0 mM, 0.25 mM, 0.5 mM, 1.5mM and 2.5 mM were 573.0 mV, 787.5 mV, 790.5 mV, 797.0 mV and 850.0 mV, respectively. In addition, the  $J_{sc}$  achieved under persulfate oxidant concentrations of 0 mM, 0.25 mM, 0.5 mM, 1.5mM and 2.5 mM were 7.9 mA/cm<sup>2</sup>, 60.5 mA/cm<sup>2</sup>, 57.9 mA/cm<sup>2</sup>, 101.8 mA/cm<sup>2</sup> and 186.7 mA/cm<sup>2</sup>. Besides that, the  $P_{max}$  attained in the event of 0 mM, 0.25 mM, 0.5 mM, 1.5mM and 2.5 mM persulfate oxidant concentrations were 1.2 mW/cm<sup>2</sup>, 5.7 mW/cm<sup>2</sup>, 7.0 mW/cm<sup>2</sup>, 19.1 mW/cm<sup>2</sup> and 27.3 mW/cm<sup>2</sup>. The results deduced that the optimum persulfate oxidant dose was 0.25 mM as it facilitated the highest COD removal rate and electricity generation efficiency among the varied oxidant concentration.



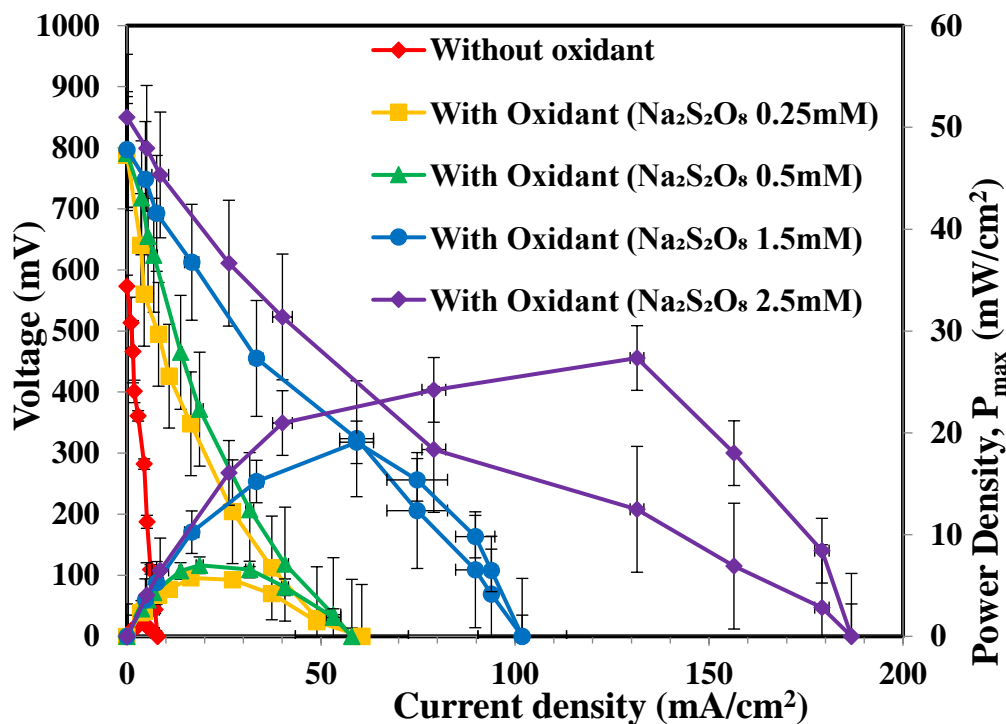


Figure 4.13: The effect of  $\text{Na}_2\text{S}_2\text{O}_8$  Oxidant Loading on Electricity Generation Efficiency Using PFC System (POME Dilution Ratio = 1:20; Solution pH = 8.51).

The enhancement in COD removal efficiency and electricity generation as persulfate oxidant varied from 0 to 2.5mM could be attributed to increased persulfate anion ( $\text{S}_2\text{O}_8^-$ ) and sulfate radicals ( $\text{SO}_4^{\bullet-}$ ) concentration in the solution. As discussed in the preliminary studies, the product of oxidized  $\text{S}_2\text{O}_8^-$ , which is  $\text{SO}_4^{\bullet-}$ , is a relatively strong sacrificial agent for effective separation of  $e_{CB^-} - h_{VB}^+$  on the photoanode to enhance photocatalytic reactions, while the  $\text{SO}_4^{\bullet-}$  also plays a scavenger role to consume reactive species from the cathode when the photogenerated electrons,  $e_{CB^-}$  transferred from the photoanode to the cathode as seen in Equations (4.4) to (4.7) (Sayed et al., 2017; Li et al., 2018; Zhou, Hou and Liu, 2019). In addition, the increased concentration of  $\text{SO}_4^{\bullet-}$  has surged the amount of active radicals and supporting electrolyte in the solution, leading to augmentation the range of reactions between active species and organic pollutants in POME from interface of photoelectrodes-electrolyte to the whole solution and accelerated electron transfer (Li et al., 2019). In general, the more persulfate oxidant added to the solution, the more active radicals participated in the photocatalytic activity in the PFC system, which effectively boosted the PFC performance in mineralization of POME and generation of electricity.

The findings from the present study were in agreement with some reported literature studies, including Li et al. (2018), Li et al. (2019) and Tang et al. (2019). Li et al. (2018) demonstrated that the increase of persulfate oxidant from 0.05 mM to 1.0 mM has led to higher methyl orange dye degradation efficiency from 49% to 80%. Similar research studied by Li et al. (2019) reported that the degradation of norfloxacin was enhanced from 52.77% to 98.10% with the increasing persulfate oxidant dose ranging from 0.5 mM to 3.0 mM as well. In another literature review, Tang et al. (2019) mentioned that the performance of PFC system with addition of persulfate oxidant on electricity generation was enhanced significantly as persulfate oxidant concentration further increased from 0.5mM to 2.0mM.

#### **4.3.2 Optimum Initial Organic Matter Concentration**

In a PFC system, the initial organic matter concentration is another pivotal factor impacting the COD degradation and maximum power generation, since organic matter can be degraded over time (Moksin et al., 2021). The effect of increasing organic matter substrates on performance of PFC system was evaluated at different dilution ratios of POME were employed in this study, including 1:5, 1:10, 1:15 and 1:20. The higher the dilution ratios, the lower the initial organic matter concentration. The experiments were conducted under fixed conditions of persulfate oxidant dosage of 2.5 mM and at natural solution pH of 8.51 in order to determine the optimum initial organic matter substrates.

Figure 4.14 illustrates the plot of COD removal rate as a function of time with respect to different initial POME dilution factors under UVC light irradiation. The COD removal rate were 28.1%, 56.0%, 77.0% and 89.0% in dilution ratio of POME of 1:5, 1:10, 1:15 and 1:20, respectively. It was observed that rising POME dilution ratio manifested a positive effect on the performance of PFC system on the removal of organics pollutants in POME.

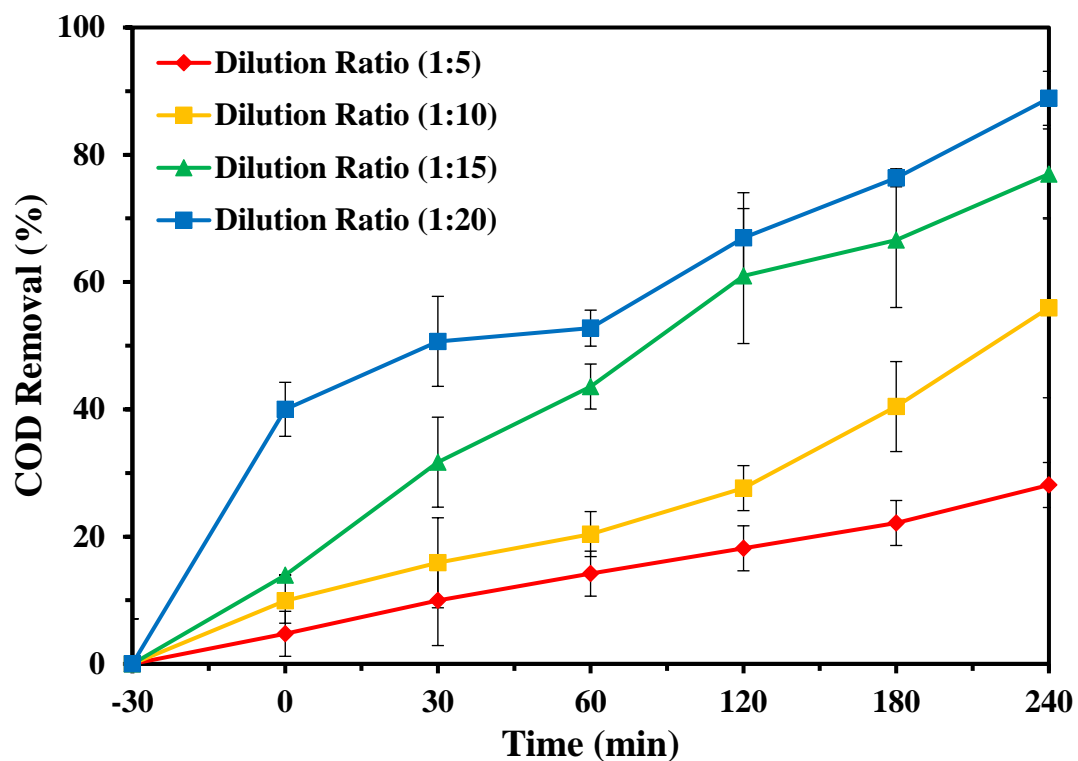


Figure 4.14: The Effect of Initial Organic Matter Concentration on the Photocatalytic Degradation of COD Using PFC System ( $[PS] = 2.5 \text{ mM}$ ; Solution pH = 8.51).

Figure 4.15 details investigation of initial POME concentration on power output through varied dilution ratios of 1:5, 1:10, 1:15 and 1:20. In contrast with the COD removal rate, the highest electricity output was recorded at dilution ratio of 1:10, in which the  $V_{oc}$ ,  $J_{sc}$ , and  $P_{max}$  were 893.0 mV, 282.7 mA/cm<sup>2</sup> and 30.2 mW/cm<sup>2</sup>, respectively. On the other hand, when subjected to dilution ratio of 1:5, the electricity performance of the PFC system was the weakest, where the  $V_{oc}$ ,  $J_{sc}$ , and  $P_{max}$  yielded were 564.0 mV, 88.6 mA/cm<sup>2</sup> and 10.8 mW/cm<sup>2</sup>. Subsequently, the  $V_{oc}$ ,  $J_{sc}$ , and  $P_{max}$  for dilution ratio of 1:15 and dilution ratio of 1:20 were 915.5 mV, 236.7 mA/cm<sup>2</sup>, 28.8 mW/cm<sup>2</sup> and 850.0 mV, 186.7 mA/cm<sup>2</sup>, 27.3 mW/cm<sup>2</sup>, respectively. The photoelectric data was not concordance with COD removal rate as dilution factor of 1:20 showed the best COD removal efficiencies while dilution 1:10 yielded the maximum power output.

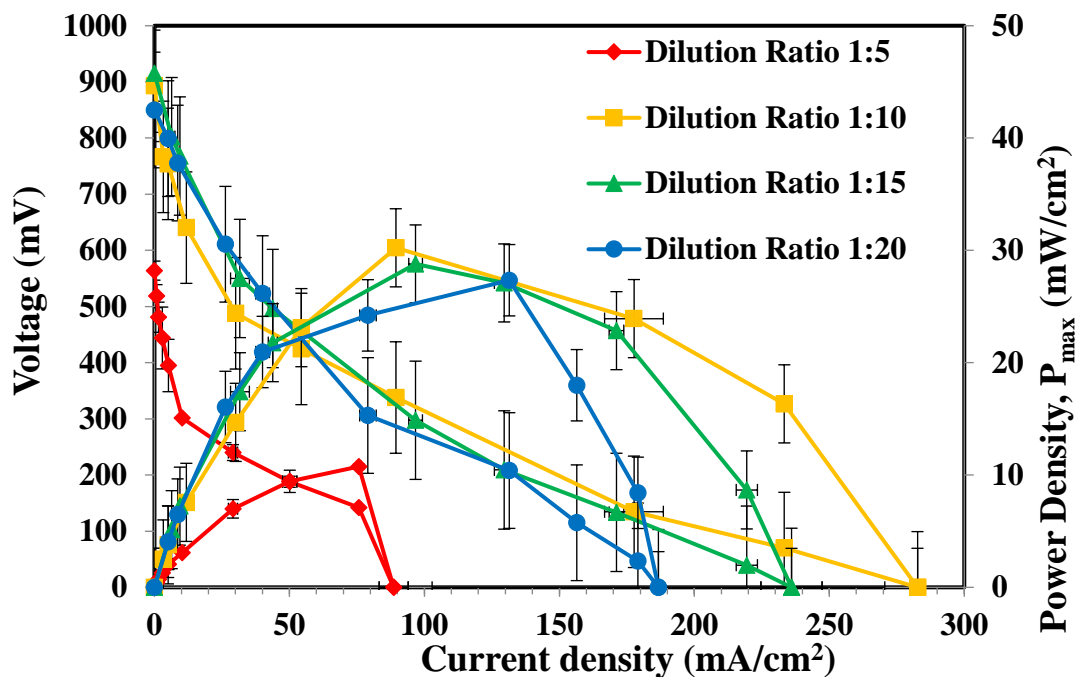


Figure 4.15: The Effect of Initial POME Dilution Ratio on Electricity Generation Efficiency Using PFC System ([PS] = 2.5 mM; Solution pH = 8.51).

The varying photodegradation efficiency and electric yielding of the PFC system observed with alteration of POME dilution factors could be explained using the concentration of organic substances and optical opaque of the solution. In terms of the COD removal rate, Kee et al., (2020) mentioned that the declination of COD removal along with the increase of initial dye concentration was caused by the increase of organic pollutants molecules that inhibits light penetration. As the initial organic matter concentration increases, the solution color intensifies and the path length of the photons entering the solution reduces, resulting in fewer photons reaching the surface of the photoanode to separate  $h_{VB}^+$  from  $e_{CB}^- - h_{VB}^+$  pairs. Therefore, it led to limited availability of  $h_{VB}^+$  for generation of  $\bullet\text{OH}$  to degrade organic pollutants at high initial COD concentration (Lee et al., 2016; Pan et al., 2019 and Kee et al., 2022). In addition, the excessive initial organic pollutants in POME solution would compete for the limited activated sites on the photoanode and active radicals such as  $\bullet\text{OH}$  and  $\text{SO}_4\bullet$  in the solution as other operational parameters such as surface area of the ZnO/Zn nanorod array photoanode, the concentration of persulfate oxidant and UVC light irradiation intensity were fixed (Li et al., 2019).

On the other hand, in terms of the electricity generation, POME dilution ratio of 1:10 has produced the maximum power output, followed by dilution ratio of 1:15, 1:20 and 1:5 as presented in Figure 4.16. In a general PFC system, the organic compounds represented as the source of energy as the oxidation of organic pollutants at the photoanode would produce and transmit  $e_{CB}^-$  to the cathode through the external circuit (Vasseghian et al., 2020). Theoretically, a higher organic matter concentration in the solution led to higher greater production of electricity since the oxidation of organic matter accelerated the consumption of  $\bullet\text{OH}$  and  $\text{SO}_4\bullet^-$  for more efficient scavenging of  $h_{VB}^+$ . Thus, the speed of transfer of electrons is increased, yielding more electricity as a result (Lee et al., 2017). Nevertheless, further increase in initial organic contaminants concentration to lower dilution ratio (1:5) led to lower power density. The declination in power generation may be ascribed to the optical opaque of the solution that reduced the and deposition of organic matter layer on the surface of the photoanode as observed during conducting the experiment owing to the high concentration of organic matter in the POME solution. Therefore, the diminishment of the accessibility of active sites on ZnO/Zn nanorod array photoanode limited the mass transfer photo-electric reactions, resulted in fewer  $e_{CB}^-$  flowing from the photoanode to the cathode and produced a lower voltage output (Kee et al., 2019; Pouramini, Ayati and Babapoor, 2022).

The experimental findings were in concurrence with the past studies. Samanta, Sahu and Roy (2020) justified that the treatment of Malachite Green Dye reduced as the initial concentration of the dye increased from 100 mg/L to 200 mg/L. It was also observed that near-complete removal was attainable using low concentration of dye. Another research studied by Moksini et al. (2021) reported that the increase of organic matter concentration in fresh POME dilution ratio from 1:200 to 1:100 resulted in an increase of  $J_{sc}$ , and  $P_{max}$ , while deterioration of electricity generation was recorded when the initial organic matter concentration was further increased to 1:50. Lee et al. (2017) pointed out that the optimal point for each predefined parameter was based on the overall performance of the PFC system in terms of COD degradation efficiency and electricity production performance, which was not solely based on merely one aspect. Since the maximum power density generated through POME dilution factor of 1:10, which was  $30.2 \text{ mW/cm}^2$  had insignificant contrast with the maximum power density generated through POME dilution factor of 1:20, which was  $27.3 \text{ mW/cm}^2$ ,

POME dilution factor of 1:20 was adopted as the optimum initial organic substrate concentration for the further research in this study.

### **4.3.3 Optimum Initial pH condition**

The effect of pH was crucial to be investigated on photocatalytic degradation and electricity transmission, as varied pH values can contribute to diverse outcomes in the POME treatment. In the study, different initial pH condition varying from pH 4 to pH 10 was studied, while employing the optimum concentration of persulfate oxidant (2.5 mM) and initial POME dilution factor (1:20). The measured natural pH of the POME solution was 8.51 and desired pH value of POME solution was adjusted using 1.0 M HCl solution and 1.0 M NaOH solution.

Figure 4.16 shows the role of pH on POME COD removal in the PFC system. The results indicated that PFC operated in natural condition (pH 8.51) without any pH adjustment achieved highest COD removal rate of 96.2%. The observed COD removal rate were obtained as 90.2%, 78.2% and 52.4% at neutral condition (pH 7), alkali condition (pH 10) and acid condition (pH 4), respectively.

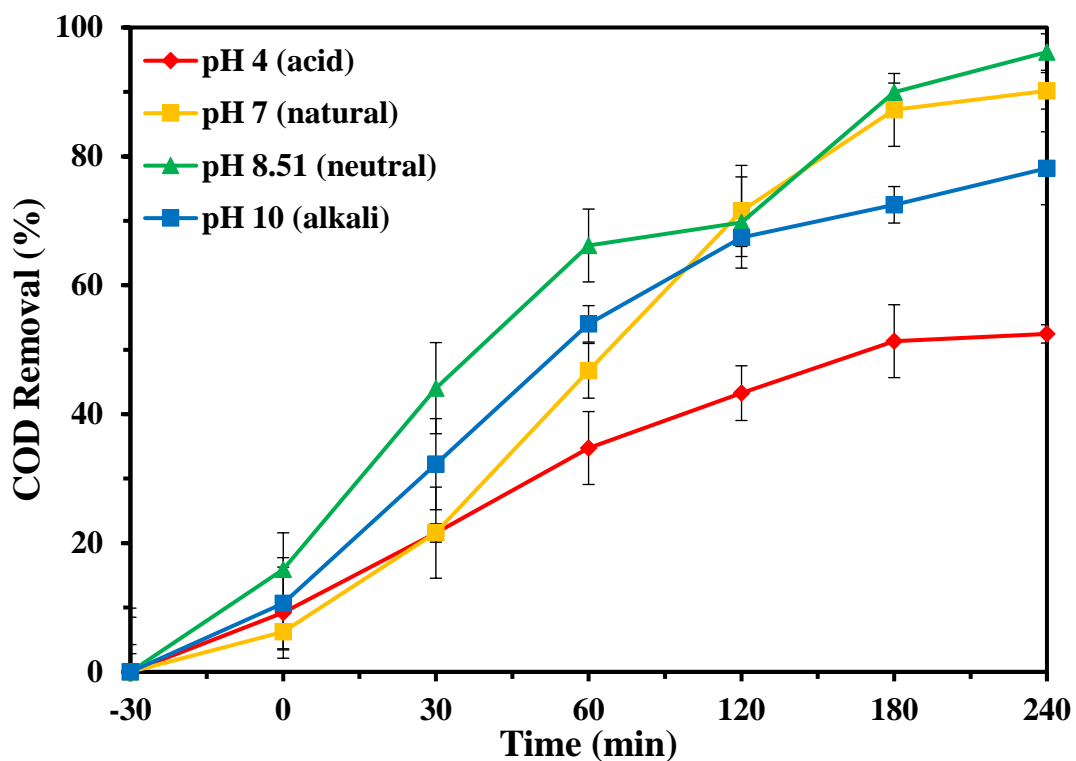


Figure 4.16: The Effect of pH on the COD Removal Efficiency of POME Solution Using PFC System ([PS] = 2.5 mM; POME Dilution Ratio = 1:20).

Figure 4.17 indicated the produced electricity by the PFC system under various pH conditions. The greatest amount of electricity produced was attained at natural pH of 8.51, producing  $V_{oc}$ ,  $J_{sc}$ , and  $P_{max}$  of 846.5 mV, 238.0 mA/cm<sup>2</sup> and 35.6 mW/cm<sup>2</sup>, respectively. Subsequently, the  $V_{oc}$  obtained under neutral pH of 7, alkali pH of 10 and acid pH of 4 were 850.0 mV, 765.0 mV and 861.0 mV, respectively. The  $J_{sc}$  gained in solution pH of 7, 10 and 4 were 237.0 mA/cm<sup>2</sup>, 341.8 mA/cm<sup>2</sup> and 114.3 mA/cm<sup>2</sup>, respectively whereas for  $P_{max}$  were 27.3 mW/cm<sup>2</sup>, 25.4 mW/cm<sup>2</sup> and 27.3 mW/cm<sup>2</sup>, respectively. It was observed that natural POME solution pH (pH 8.51) favoured the PFC performance in degrading organic pollutants and generating electricity as the trend of COD removal rate (Figure 4.16) was similar as the trend showed in electricity generation of PFC system (Figure 4.17).

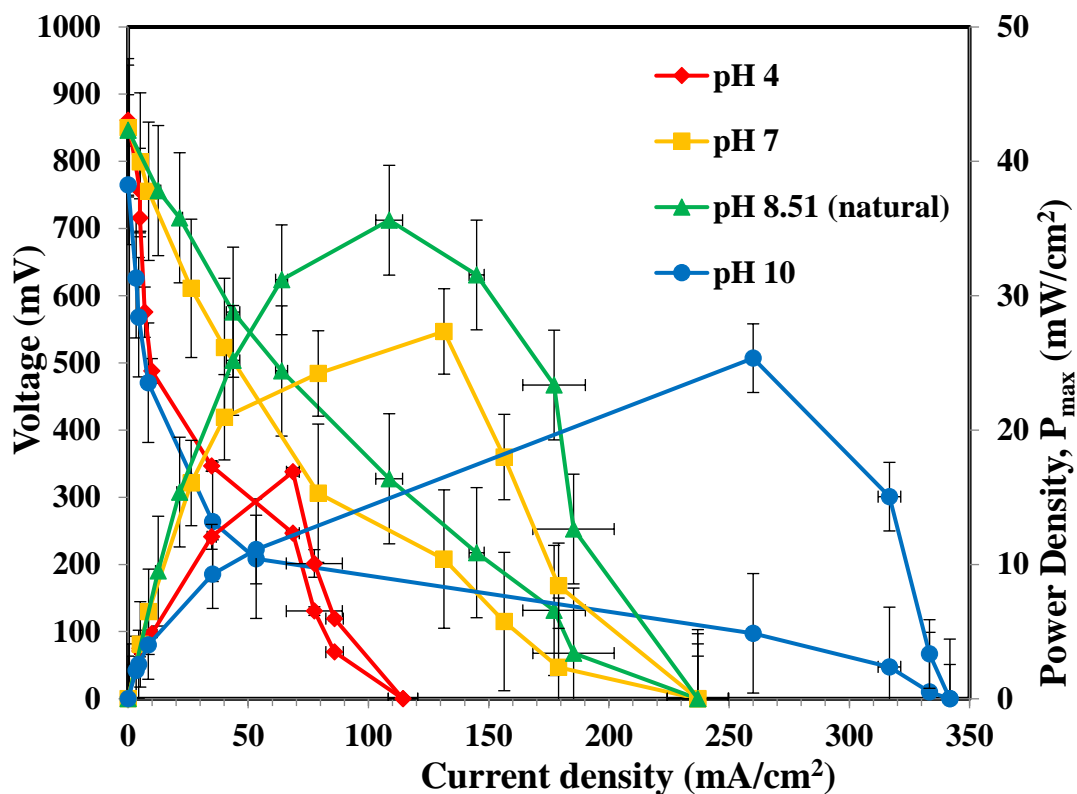


Figure 4.17: The Effect of pH of POME Solution on the Electricity Generation Efficiency Using PFC System ([PS] = 2.5 mM; POME Dilution Ratio = 1:20).

The theory of point of zero charge ( $\text{pH}_{\text{zpc}}$ ) was commonly applied to explain the effect of pH of solution on the photodegradation of organic matter (Aslam, et al., 2022; Kee et al., 2020 and Sidik et al., 2018).  $\text{pH}_{\text{zpc}}$  is generally identified as the pH at which a semiconductor will have zero surface charge. At pH levels lower or higher than the  $\text{pH}_{\text{zpc}}$ , the surface of the semiconductor will be positively-charged or negatively-charged by adsorbed  $\text{OH}^-$  ions, respectively (Abbas, 2021). Both Khatee et al. (2016) and Ali et al. (2018) have addressed that  $\text{pH}_{\text{zpc}}$  of ZnO nanoparticles is approximately  $9.0 \pm 0.3$ , thus justifying the high COD elimination effectiveness and electricity yield of PFC system under natural pH of 8.51 since best performance for photocatalytic removal of organic matter were generally attained when the pH values are near to the  $\text{pH}_{\text{zpc}}$  (Alhaji et al., 2018). According to Zahrim, Nasimah and Hilal (2014), POME are negatively-charged pollutants specifically after being treated in aerobic pond. As the ZnO surface become positively-charged at natural pH medium, resulting in an electrostatic attraction force towards negatively-charged organic molecules and thereby an increased adsorption of POME on the photoanode. In

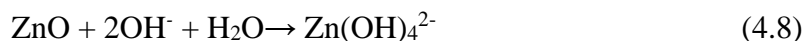


addition, the absence of pH adjustor, including HCl and NaOH, in neutral pH solution is another factor for the enhanced PFC performance. The introduction of  $H^+$  and  $OH^-$  by pH adjustor could increase the competition of surface adsorption on photoanode with POME. The lack of pH adjustment led to absence of  $H^+$  ions as  $\bullet OH$  scavenger, hence causing higher generation of  $\bullet OH$  species that involved in mineralization of organic pollutants and transmission of  $e_{CB}^-$  to the cathode at natural pH (Shibuya, Sekine and Mikami, 2015; Tang et al., 2019). Moreover, based on a research study reported by Liang and Su (2009), while  $SO_4^{\bullet -}$  was predominant radical at acidic condition and  $\bullet OH$  was the predominant radical at a more basic pH, both  $\bullet OH$  and  $SO_4^{\bullet -}$  were present at solution pH of 9, which suggested that more radical species participated in the photocatalytic reaction in natural pH condition in this study.

Lowest COD removal rate and power generation was recorded at solution pH of 3, which may be attributed to the reaction between ZnO and the acids in forming  $Zn^{2+}$  as stated in Equation (4.6) (Moksin et al.2021). Owing to the fact that ZnO was an amphoteric oxide which was soluble under acidic conditions (Greenwood and Earnshaw, 1997), Equation (4.7) resulted in dissociation of ZnO from the photoanode surface as observed during the experiment. Therefore, the photocatalytic properties of ZnO were suppressed in the acidic medium. Furthermore, owing to inadequate amount of  $OH^-$  ions in acidic condition, frequent recombination of  $e_{CB}^- - h_{VB}^+$  at photoanode led to reduction of  $\bullet OH$  generation and migration of  $e_{CB}^-$  to the cathode, eventuating in the poor COD removal and electricity production (Lee et al., 2017).



On the contrary, further increasing in solution pH value to pH 10 has recorded a deterioration of COD removal rate and power output as well. In 2020, Kee et al. mentioned that formation of complexes such as  $Zn(OH)_4^{2-}$  owing to dissolution of ZnO under alkaline condition as stated in Equation (4.8) would repel the negatively-charged POME organic molecules. The electrostatic repulsion caused the formation of surface hydroxyl radicals which were hardly desorbed, thus interfering the oxidation process at the photocatalyst and increasing the combination of  $e_{CB}^- - h_{VB}^+$  (Chen et al., 2020).



On the other hand, addition of acidic pH adjustor at pH of 7 have observed a declination in efficiency of COD removal and electricity production. The  $\text{Cl}^-$  ions dissociated from pH adjustor (HCl) reduced the collision rate between  $h_{\nu B}^+$  and  $\text{OH}^-$  ions, hindering the generation of  $\bullet\text{OH}$  radicals and thus decreasing the COD removal rate and electricity generation by the developed PFC system (Khalik et al., 2018).

Similar findings were published on account of the impact of pH conditions on effectiveness of PFC system. Kee et al. (2020) ascertained that solution pH of 8.35 without alteration of pH yielded the best degradation of POME and electrical output using anodic  $\text{TiO}_2/\text{ZnO}/\text{Zn}$  PFC system. In another literature review, Tang et al. (2019) reported that highest treatment efficiency of Reactive Brilliant Blue dye was observed in solution pH of 9 in persulfate oxidants promoted PFC, followed by pH 11, 3 and 6.3. Fu et al. (2018) also emphasized on the influence of zero point charge oh photocatalyst to generate higher amount of reactive oxygen species for enhanced COD removal efficiency and production of current density. Thus, natural solution pH of 8.51 was selected as the optimal initial solution pH for degradation of pre-treated POME using PFC system.

Generally, in the treatment of wastewater, the COD is a valuable test for analysis of organic and inorganic components, whereas the  $\text{BOD}_5$  is commonly used to determine the quantity of  $\text{O}_2$  required for biological oxidation of organic pollutants (Chin et al., 2022). In addition, it was crucial to evaluate the extent of photocatalytic process for other wastewater parameters, including the  $\text{BOD}_5$ , turbidity,  $\text{NH}_3\text{-N}$  and pH. As represented in Table 4.1, the tested pre-treated POME wastewater parameters were significantly reduced after 4 hours of PFC treatment. Notably, the quality parameter of treated POME wastewater by the developed PFC system used in this study were below the water quality threshold limits established by the Department of Environment (DOE) Malaysia as shown in Table 2.1. Therefore, the proposed PFC system offers promising potential for extensive application as an alternative green technique to degrade pre-treated POME wastewater and concurrently retrieving electricity.

**Table 4.1: Summary of Measured Pre-treated POME Quality Parameters Pre- and Post-Photocatalytic Degradation Using PFC System of ZnO/Zn Nanorod Array Photoanode and CuO/Cu Cathode in the Presence of Persulfate Oxidant Under UVC light ([PS] = 2.5 mM; POME Dilution Ratio = 1:20; Solution pH = 8.51; UVC light Irradiation Time = 240 minutes).**

Parameter	Before Treatment	After Treatment	Efficiency (%)
BOD <sub>5</sub> (mg/L)	250	9	96.4
COD (mg/L)	1206	46	96.2
NH <sub>3</sub> -N (mg/L)	32.5	23.3	28.3
Turbidity (NTU)	10.3	1.05	89.8
pH	8.51	7.42	-

#### 4.4 Roles of Different Radical Species in PFC system

In order to further elucidate the mechanism of enhanced POME degradation and identify the predominant active radical species in the PFC system, radical quenching test was conducted, with 1,4-benzoquinone (1,4-BQ), ethylenediaminetetraacetic acid disodium salt (EDTA-2Na), ethanol (EtOH), tertiary butanol (Tert-butanol) and silver nitrate, being selected to specifically quench  $\bullet\text{O}_2^-$ ,  $h_{VB}^+$ ,  $\text{SO}_4^{\bullet-}$ ,  $\bullet\text{OH}$ , and  $e_{CB}^-$ , respectively. The radical scavenging test was conducted under optimal condition in the PFC system and the results was provided in Figure 4.18.

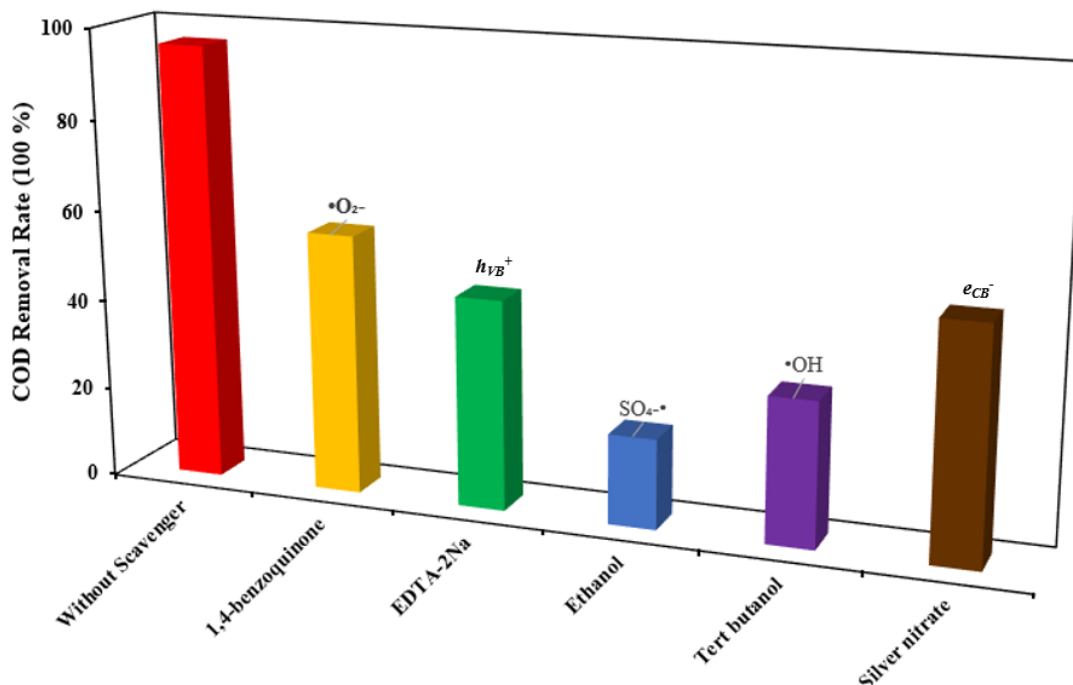


Figure 4.18: COD Removal Rate of POME Using Developed PFC System in Existence of Various Radical Capturing Agents (POME Dilution Factor = 1:20; [PS] = 2.5 mM; Solution pH = 8.51; [Radical Scavenging Agent] = 2 mM).

As depicted in Figure 4.18, 96.186% of COD removal rate was achieved after 4 hours without any scavenging agent added. Nevertheless, degradation of POME was clearly inhibited with the addition of EtOH and Tert-butanol, which were merely 19.8% and 31.9%, respectively. On the contrary, the COD removal efficiencies observed after photocatalytic reaction under the presence of EDTA-2Na, silver nitrate and 1,4-BQ were 46.3%, 51.4% and 57.4%, respectively. These results obtained in this study signified that  $\text{SO}_4^{\bullet-}$  and  $\bullet\text{OH}$  were the two dominant radical species influencing the photocatalytic degradation performance of the developed PFC system, while  $h_{\nu B}^+$ ,  $\bullet\text{O}_2^-$  and  $e_{CB}^-$  performed a marginal but positive contribution to the degradation of POME.

According to the aforementioned analysis, including radical scavenging test, UV-Vis DRS and Mott-Schottky analyses, a tentative mechanism for the degradation of POME in the PFC system was proposed as shown in Figure 4.19.

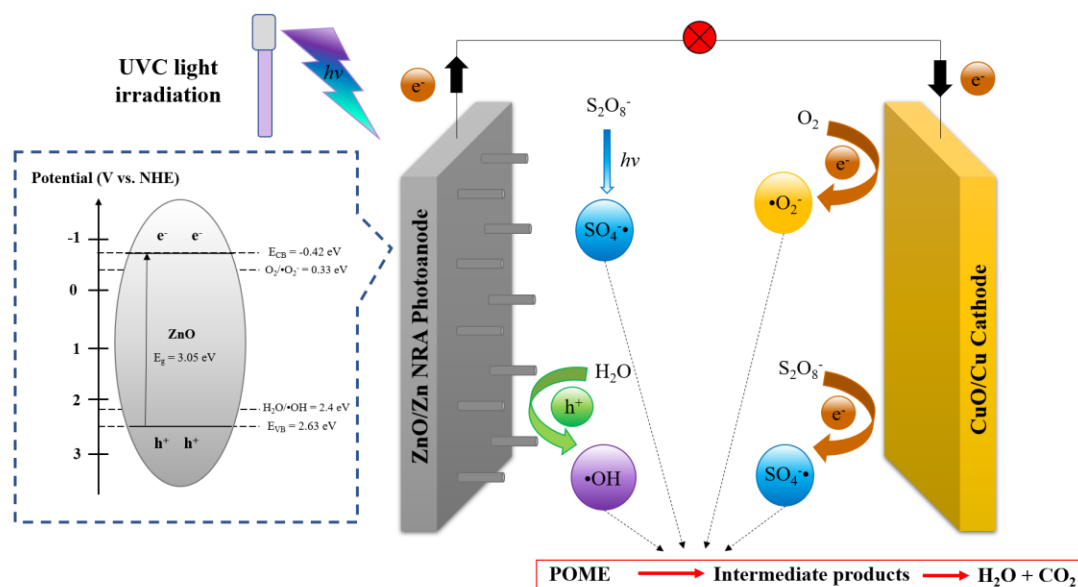
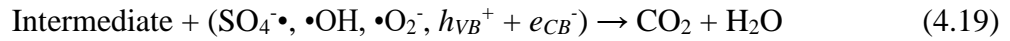
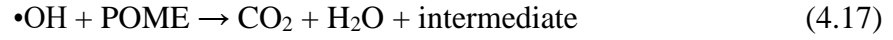
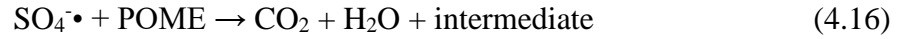
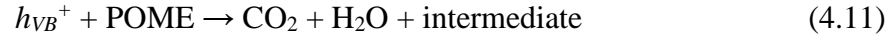


Figure 4.19: Schematic Diagram of photocatalytic mechanism of ZnO/Zn NRA photocatalyst, proposed persulfate activation, radicals' generation and POME degradation pathway in the PFC system.

When irradiated by UVC light, the ZnO nanorod array on the Zn film underwent photoexcitation, transferring the electron from valence band (VB) to conduction band (CB) and forming  $e_{CB}^- - h_{VB}^+$  pair as represented in Equation (4.9). According to Liu et al. (2017), the dissolved  $O_2$  in the solution was readily reduced into  $\cdot O_2^-$  by the  $e_{CB}^-$  in CB of ZnO due to less negative standard reduction potential of  $O_2/\cdot O_2^-$  (-0.33 eV) than the CB potential of ZnO (-0.42 eV). Subsequently, the less positive standard reduction potential of  $H_2O/\cdot OH$  (2.4 eV) than the VB potential of ZnO (2.63 eV) led to oxidation of  $H_2O$  by  $h_{VB}^+$  in VB of ZnO to form  $\cdot OH$  radicals as shown in Equation (4.10) while a limited portion of  $h_{VB}^+$  directly participated in degradation of POME as shown in Equation (11) (Yang et al., 2016). Subsequently, as shown in Equation (4.12), the  $e_{CB}^-$  excited the persulfate oxidant to decompose and form  $SO_4^{\cdot -}$  after it was transferred to the cathode via the external circuit. In addition, according to Tan et al. (2019),  $SO_4^{\cdot -}$  could be generated through UVC light activation of persulfate (Equation (4.13)). Furthermore, the oxygen provided at the cathode compartment would react with  $e_{CB}^-$  to form  $\cdot O_2^-$  as explained in Equation (4.14). According to radical quenching test and Equation (4.15), the generated  $\cdot O_2^-$  played a trivial role in degradation of POME by transforming into  $\cdot OH$  by reacting with water. Eventually, the degradation of POME in both the solution and on the ZnO/Zn nanorod

array surfaces through oxidation of reactive radical species ( $\text{SO}_4^{\bullet-}$ ,  $\bullet\text{OH}$  and  $\bullet\text{O}_2^-$ ),  $h_{VB}^+$  and  $e_{CB}^-$  as shown in Equation (4.16) to (4.19) (Guan et al., 2020; Tang et al., 2019 and Li et al., 2019).



## 4.5 Recycling Test

The repetitive use and stability of the photoelectrodes are significant considerations in determining the commercial potential and sustainability of the developed PFC system. Therefore, the reusability of the ZnO/Zn nanorod array photoanode, POME mineralization was conducted for four continuous cycles using the constructed PFC system under optimal conditions. The photodegradation performance of the PFC system decreased with each cycle, from 96.2% to 73.0% in the fourth cycle. As reflected in Figure 4.20, this result confirmed that the ZnO/Zn photoanode showed excellent stability for long-term application in the developed PFC system.

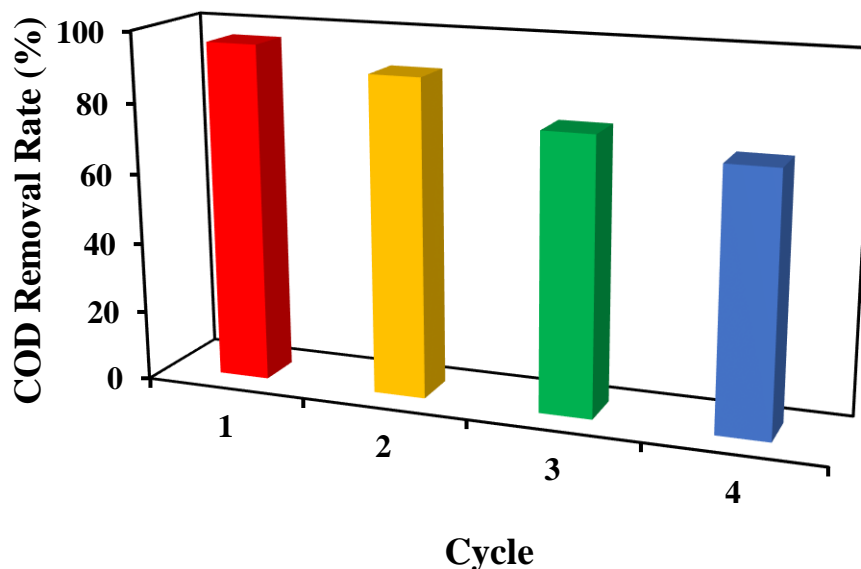


Figure 4.20: COD Removal Rate of POME Using Developed PFC System for Four Consecutive Cycles (POME Dilution Factor = 1:20; [PS] = 2.5 mM; Solution pH = 8.51).

The decrement of PFC system performance in terms of COD degradation efficiency of POME could be attributed by the inevitable loss of ZnO photocatalyst from the surface of the photoanode during repetitive action of rinsing and drying of photoanode (El-Bindary, Ismail and Eladi, 2019). The gradual depletion of photocatalyst decreased the amount of active sites available for photoexcitation, resulting in inefficient formation of  $e_{CB}^- - h_{VB}^+$ , which involved in generation of radical species. Consequently, fewer radical species contributed to the photodegradation process and led to deterioration of performance of the PFC system with each repetition.

Even after four successive cycles, the ZnO/Zn photoanode employed in the PFC system was able to maintain adequate photocatalytic performance as evidenced by the results in this section. Compared to photocatalyst in powder form, immobilization of the ZnO/Zn photocatalysts onto film-type photoanode owing to strong adhesion on surface of photoanode have eased in collection of photocatalysts during the recycling test (Ghosh and Mondal, 2015; Marcello et al., 2020). The findings of stability of ZnO photoanode was concurrence with studies by Lam et al. (2020), Kee et al. (2018) and Li et al, (2019). Lam et al. (2020) revealed that no substantial drop was observed in COD removal rate of semiconductor wastewater by

utilizing ZnO/Zn photoanode in a PFC system after three recycling runs. In 2018, Kee and his co-workers demonstrated that COD degradation efficiency of Methyl Green dye declined slightly from approximately 65% to 55% after four successive cycles. On the other hand, Li et al. (2019) revealed that there was no significant declination of performance of the PFC system with addition of persulfate oxidant in degrading norfloxacin by using TiO<sub>2</sub> nanorods photoanode after five times repetitions.

#### 4.6 Cost Analysis

In addition to the effectiveness of the developed PFC system in degrading the pre-treated POME solution, it is critical to consider the economical aspect of the PFC system. Therefore, in this section, the cost of preparation of photoelectrodes was studied. The bill preparation is accordance to the Low Voltage Industrial Tariff as introduced by Tenaga Nasional Berhad (TNB). Table 4.2 highlights the total electricity cost required for the synthesis of ZnO/Zn nanorod array photoanode and CuO/Cu cathode, whereas Table 4.2 details the total cost of materials used during the synthesis of electrodes. The electricity usage was calculated using Equation (4.20) reported by Martínez, Ebenhack and Wagner (2019):

$$\text{Electricity Consumption (kWh)} = \frac{\text{Power (W)} \times \text{Operation Hour (h)}}{1000} \quad (4.20)$$

**Table 4.2: Total Electricity Consumption and Cost for Fabrication of Photoanode and Cathode.**

<b>Equipment</b>	<b>Power (W)</b>	<b>Duration (h)</b>	<b>Total Consumption (kWh)</b>
<b>i. Photoanode</b>			
Ultrasonic Homogenizer	500	0.5	0.25
Muffle Furnace	4500	3	13.5
Oven	1000	2	2
DC Power Supply	420	3	1.26
Magnetic Stirrer	650	4	2.60
<b>Sub Total</b>			<b>19.61</b>



<b>ii. Cathode</b>			
Ultrasonic Homogenizer	500	0.5	0.25
Muffle Furnace	4500	1	4.5
Oven	1000	24	24
<b>Sub Total</b>			<b>28.75</b>
<b>Grand Total</b>			<b>48.36</b>

$$\begin{aligned} \text{Total Electricity Cost} &= 48.36 \text{ kWh} \times \text{RM } 0.38 / \text{kWh} \\ &= \text{RM } 18.38 \end{aligned}$$

**Table 4.3: Total Material Cost for Synthesizing of Photoanode and Cathode.**

<b>Material</b>	<b>Quantity</b>	<b>Unit</b>	<b>Unit Price (RM)</b>	<b>Price (RM)</b>
<b>i. Photoanode</b>				
Zn Foil	20	cm <sup>2</sup>	0.76	15.20
Zn(CH <sub>3</sub> COO) <sub>2</sub> •2H <sub>2</sub> O	0.22	g	0.08	0.02
Zn(NO <sub>3</sub> ) <sub>2</sub> •4H <sub>2</sub> O	0.16	g	0.15	0.02
NaOH	0.82	g	0.03	0.03
C <sub>2</sub> H <sub>5</sub> OH	0.010	L	12.00	0.12
<b>Sub Total</b>			<b>15.39</b>	
<b>ii. Cathode</b>				
Cu Foil	15	cm <sup>2</sup>	0.14	2.10
Na <sub>2</sub> S <sub>2</sub> O <sub>8</sub>	2	g	0.06	0.12
NaOH	8	g	0.03	0.24
C <sub>2</sub> H <sub>5</sub> OH	0.010	L	12.00	0.12
<b>Sub Total</b>			<b>2.58</b>	
<b>Grand Total</b>			<b>17.97</b>	

$$\begin{aligned} \text{Total Production Cost} &= \text{Total Electricity Cost} + \text{Total Material Cost} \\ &= \text{RM } 18.38 + \text{RM } 17.97 \\ &= \text{RM } 36.35 \end{aligned}$$

The overall production cost for the photoelectrodes employed in this study was RM 36.35. It was observed that approximately 51 % of the cost was attributed to the use of electricity throughout the synthesis of ZnO/Zn nanorod array photoanode and CuO/Cu cathode. However, PFC system is envisioned to be widely utilised as a green alternative to treat pre-treated POME wastewater and contemporaneously recovering energy. The photoanode that exhibited a significant ability for recycling and reuse for photocatalytic activity without diminishing photoreactivity served as a prerequisite to minimise the cost required for the constructed PFC system and further demonstrating the economic feasibility of the developed PFC system in this research.

## CHAPTER 5

### CONCLUSION AND RECOMMENDATIONS

#### 5.1 Conclusion

In the present research, a synergistic PFC system with ZnO/Zn nanorod array photoanode and CuO/Cu cathode was successfully refined in degrading the pre-treated POME and concurrently energy recovery. The FESEM and EDX analyses validated that the prepared photoanode contained high-level purity of ZnO nanorods with an approximate size varying from 263 nm to 882 nm while the prepared cathode contained pure CuO appeared in a rod shape as well with sizes ranging from 91 nm to 392 nm. Additionally, the phase purity of ZnO/Zn nanorod array photoanode and CuO/Cu cathode were successfully verified through the XRD analysis by detecting the corresponding diffraction peaks. The outcomes of M-S analysis showed that the CB potential and VB potential of ZnO was -0.42 eV and 2.63 eV, respectively, which affirmed the *p*-type conductivity for ZnO NRA produced in this research work.

The preliminary studies unveiled that the coupled PFC system with persulfate oxidant exhibited outstanding photocatalytic activity in aspects of COD removal efficiency and electricity yield compared to photolysis and sole PFC system when subjected to UVC light illumination. The COD removal rate with the magnitude of 70.9% compared to 39.6% experienced by the treated POME verified the effectiveness of persulfate oxidant in inducing the superior sulfate radicals ( $\text{SO}_4^{\cdot-}$ ) to the photodegradation activity in the PFC system. Correspondingly, the addition of persulfate oxidant has amplified the electricity generation as supported by the fact that the use of persulfate as an oxidant acted as an electron scavenger that further enhanced

the electrical conductivity and separation of photogenerated  $e_{CB}^- - h_{VB}^+$  pairs. On the other hand, the study on opened and closed circuit of PFC also revealed the closed circuit PFC system enhanced the removal of organic pollutants in POME. The presence of external circuit allowed the transfer of  $e_{CB}^-$  from photoanode to cathode, hence restricting the recombination of  $e_{CB}^- - h_{VB}^+$  pairs and resulting in ameliorated degradation of organic pollutants.

Subsequently, numerous operating parameters, specifically the concentration of persulfate oxidant, initial POME dilution factor and initial solution pH have demonstrated their distinct performances on COD removal efficiencies and electrical production of the developed PFC system. It was determined that the optimized PFC system under the conditions of 2.5mM of persulfate oxidant, initial POME dilution factor of 1:20 and natural condition of pH 8.51 was determined to be the most optimized condition in this study. This PFC system augmented the COD removal of pre-treated POME to 96.2% with  $V_{oc}$ ,  $J_{sc}$ , and  $P_{max}$  of 846.5 mV, 238.0 mA/cm<sup>2</sup> and 35.6 mW/cm<sup>2</sup>, respectively after 4 hours of UVC light irradiation. The enhanced PFC system performance was attributed by the increased formation of active radicals, expanded accessibility of activated site on the photoanode due to better optical opaque of the solution, and the absence of pH adjustor which led to higher generation of radical active species to mineralize the organic pollutants in the POME solution. Notably, the removal efficiencies of other wastewater parameters such as BOD<sub>5</sub> (96.4%), NH<sub>3</sub>-N (28.3%), turbidity (89.8%), and pH (7.42) was also obtained, which were attained below the water quality threshold limits established by the DOE Malaysia.

Consecutively, the radical quenching studies discovered that  $SO_4 \cdot^-$  was the most dominant radical, while  $\cdot OH$  was the second most dominant radical to drive the treatment of POME in the constructed PFC system.  $h_{VB}^+$ ,  $\cdot O_2^-$  and  $e_{CB}^-$  performed a marginal but also positive contribution to the degradation of POME simultaneously. A tentative mechanism was also proposed based on the analyses of radical scavenging studies to interpret the photodegradation process of the PFC system. The pronounced performance of COD removal in recycling using the same ZnO/Zn nanorod array photoanode after 4 cycles of repetition cycles also demonstrated the recyclability and stability of photoelectrodes for durable application. Lastly, the total production cost

was calculated in the cost analysis section was RM 36.35, which included the synthesis of ZnO/Zn nanorod array photoanode and CuO/Cu cathode. Nevertheless, with the ability of PFC system to generate electricity and stable properties of photoanode, the treatment cost could be further minimized. In summary, the research outcomes demonstrated the feasible and efficient performance of the proposed PFC system for organics elimination and contemporaneous energy recovery from the POME wastewater, prompting it promising to address environmental and energy concerns.

## **5.2 Recommendations for Future Studies**

Upon completion of the present study, several fundamental aspects were suggested to be taken into consideration in the future PFC studies:

1. The study should investigate the impact of other process parameters that were not analysed in current study, including the types of electrolytes, UV irradiation intensity and initial solution temperature for investigation in an effort to further improve the performance of the PFC system.
2. It is suggested that the Zn film photoanode to be replaced with transparent fluorine-doped tin oxide (FTO) glass to activate the photocatalysts on both the front and rear sides of the film upon light irradiation, thus the performance of the PFC system was anticipated to be further improved.
3. The toxicity impact of treated POME to the environment should be evaluated through phototoxicity assessment to determine the possible usage of treated POME in agricultural field.

## REFERENCES

- Abdullah, M., Man, H. C., Idris, A. I., Yunus, K. F. and Abidin, Z. Z., 2018. Treatment of palm oil mill effluent using membrane bioreactor: novel processes and their major drawbacks. *Water* 2018, 10(9), 1165.
- Agustina, L., Suprihatin, Romli, M. and Suryadarma, P., 2021. Processing of palm mill oil effluent using photocatalytic: a literature review. *Journal of Ecological Engineering*, 22(11), pp. 43-52.
- Ahmad, A., Chong, M., Bhatia, S. and Ismail, S., 2006. Drinking water reclamation from palm oil mill effluent (POME) using membrane technology. *Desalination*, 191(1-3), pp.35-44.
- Akhbari, A. Kutty, P. K., Chuen, O. C. and Ibrahim, S., 2020. A study of palm oil mill processing and environmental assessment of palm oil mill effluent treatment. *Environmental Engineering Research* 2020, 25(2), pp. 212-221.
- Al-Amshawee, S. K., Yunus, M. Y. and Azoddein, A. A., 2020. A review on aerobic biological processes for palm oil mill effluent: possible approaches. *IOP Conference Series: Materials Science and Engineering, Energy Security and Chemical Engineering Congress*, 736, pp. 1-19.
- Albiss, B. and Dalo, M. A., 2021. Photocatalytic degradation of methylene blue using zinc oxide nanorods grown on activated carbon fibers. *Sustainability*, 13, 4729.
- Alhaji, M. H., Sanaullah, K., Salleh, S. F., Bains, R., Lim, S. F., Rigit, A. R. H., Said, K. A. M. and Khan, A., 2018. Photo-oxidation of pre-treated palm oil mill Effluent using cylindrical column immobilized photoreactor. *Process Safety and Environmental Protection*, 117, pp. 180-189.
- Alhaji, M. H., Sanaullah, K., Lim, S. F., Khan, A., Hipolito, C. N., Abdullah, M. O., Bhawani, S. A. and Jamil, T., 2016. Photocatalytic treatment technology for palm oil mill effluent (POME) – A review. *Process Safety and Environmental Protection*, 102, pp. 673-686.
- Anakhu, E. A. and Suleiman, A. I., 2021. Development and testing of a pilot scale anaerobic sequencing batch reactor (ASBR) for palm oil mill waste water treatment and biogas generation. *International Journal of Scientific Research and Engineering Development*, 4(5) pp. 1234-1240.

- Azad, A. K. and Rasul, M., 2019. *Advanced Biofuels: Applications, Technologies and Environmental Sustainability*. Sawston, United Kingdom: Woodhead Publishing. pp. 181-213.
- Baird, R. B., Eaton, A. D. and Rice, E. W., 2017, *Standard methods for the examination of water and wastewater*. 23<sup>rd</sup> ed. United States: American Water Works Association (APHA).
- Bala, J. D., Lalung, J., Al-Gheethi, A. A. S., Kaizar, H. and Ismail, N., 2018. Reduction of organic load and biodegradation of palm oil mill effluent by aerobic indigenous mixed microbial consortium isolated from palm oil mill effluent (POME). *Water Conservation Science and Engineering*, 3(3), pp. 139-156.
- Bandh, S. A., Shafi, S. and Shameem, N., 2019. *Freshwater Microbiology: Perspectives of Bacterial Dynamics in Lake Ecosystems*. Amsterdam, Netherlands: Elsevier.
- Bhosale, R., Jain, S., Vinod, C. P., Kumar, S. and Ogale, S., 2019. Direct Z-scheme g-C<sub>3</sub>N<sub>4</sub>/Fe<sub>2</sub>WO<sub>4</sub> nanocomposite for enhanced and selective photocatalytic CO<sub>2</sub> reduction under visible light. *ACS Applied Materials and Interfaces*, 11, pp. 6174-6183.
- Bokov, D., Jalil, A. T., Chupradit, S., Suksatan, W., Ansari, M. J., Shewael, I. H., Valiev, G. H. and Kianfar, E., 2021. Nanomaterial by sol-gel method: synthesis and application, *Advances in Materials Science and Engineering*, 2021, 5102014.
- Carmen G. T. F. D., Luis, C. L. J., Silvestre, L. R. A., Pio, S. G., Erik, R. M., Germán, P. H., Carlos, D. G. J. and Lorena, D. F. L., 2022. Sol-gel/hydrothermal synthesis of well-aligned ZnO nanorods. *Boletín de la Sociedad Española de Cerámica y Vidrio*, 346, pp. 1-9.
- Castillo-Blas, C., Montoro, C., Platero-prats, A. E., Ares, P., Amo-Ochoa, P., Conesa and J., Zamora, F., 2020. *Advances in Inorganic Chemistry: Nanoscale Coordination Chemistry*. 1<sup>st</sup> ed. Cambridge: Academic Press.
- Chen, Z. J., Guo, H., Liu, H. Y., Niu, C. G., Huang, D. W., Yang, Y. Y., Liang, C., Li, L. and Li, C. J., 2022. Construction of dual S-scheme Ag<sub>2</sub>CO<sub>3</sub>/Bi<sub>4</sub>O<sub>5</sub>I<sub>2</sub>/g-C<sub>3</sub>N<sub>4</sub> heterostructure photocatalyst with enhanced visible-light photocatalytic degradation for tetracycline. *Chemical Engineering Journal*, 438, 135471.
- Cheng, Y. W., Chong, C. C., Lam, M. K., Ayoub, M., Cheng, C. K., Lim, J. W., Yusup, S., Tang, Y. Y. and Bai, J. M., 2021. Holistic process evaluation of non-conventional palm oil mill effluent (POME) treatment technologies: A conceptual and comparative review. *Journal of Hazardous Materials*, 409, 124964.

- Chin, Y. H., Sin, J. C. and Lam, S. M., 2018. A facile route for fabrication of hierarchical porous Nb<sub>2</sub>O<sub>5</sub>/ZnO composites with enhanced photocatalytic degradation of palm oil mill effluent. *Materials Letters*, 216, pp. 8-11.
- Chin, Y. H., Sin, J. C., Lam, S. M., Zeng, H., Lin, H., Li, H. X. and Mohamed, A. R., 2022. 0-D/3-D heterojunction composite constructed by decorating transition metal oxide nanoparticle on peony-like ZnO hierarchical microstructure for improved photodegradation of palm oil mill effluent. *Optik*, 260, 169098.
- Ching, P. M. L., Zou, X., Wu, D., So, R. H. Y. and Chen, G. H., 2022. Development of a wide-range soft sensor for predicting wastewater BOD<sub>5</sub> using an extreme gradient boosting (XGBoost) machine. *Environmental Research*, 210, 112953.
- Chong, J. W. R., Chan, Y. J., Chong, S. H., Ho, Y. C., Mohamad, M., Tan, W. N., Cheng, C. K. and Lim, J. W., 2021. Simulation and optimisation of integrated anaerobic-aerobic bioreactor (IAAB) for the treatment of palm oil mill effluent. *Processes*, 9(7), 1124.
- Chung, C. Y., Selvarajoo, A., Sethu, V., Koyande, A. K., Arputhan, A. and Lim, Z. C., 2018. Treatment of palm oil mill effluent (POME) by coagulation flocculation process using peanut-okra and wheat germ-okra. *Clean Technologies and Environmental Policy*, 20, pp. 1951-1970.
- Commandeur, D., Brown, G., Hills, E., Spencer, J. and Chen, Q., 2019. Defect-rich zno nanorod arrays for efficient solar water splitting. *ACS Applied Nano Materials*, 2(3), pp. 1570-1578.
- Concina, I., Ibutoto, Z. H. and Vomiero, A., 2017. Semiconducting metal oxide nanostructures for water splitting and photovoltaics. *Advanced Energy Materials*, 7(23), 1700706.
- Crincoli, K. R. and Huling, S. G., 2021. Contrasting hydrogen peroxide- and persulfate-driven oxidation systems: Impact of radical scavenging on treatment efficiency and cost. *Chemical Engineering Journal*, 404, 126404.
- Crini, G. and Lichtfouse, E., 2019. Advantages and disadvantages of techniques used for wastewater treatment. *Environmental Chemistry Letters*, Springer Verlag, 17(1), pp.145-155.
- Dashti, A. F., Salman, N. A. S., Adnan, R. and Zahed, M. A., 2022. Palm oil mill effluent treatment using combination of low-cost chickpea coagulant and granular activated carbon: optimization via response surface methodology. *Groundwater for Sustainable Development*, 16, 100709.
- Da S. Pereira, W., Gozzo, C. B., Longo, E., Leite, E. R. and Sczancoski, J. C., 2019. Investigation on the photocatalytic performance of Ag<sub>4</sub>P<sub>2</sub>O<sub>7</sub> microcrystals for the degradation of organic pollutants. *Applied Surface Science*, 493, pp. 1195-1204.



- Du, H. L., Wang, F. L., Pan, B. Y., Dong, P. X and Qu, M. L., 2019. Preparation of zinc oxide nanorods array and its application in photocatalytic degradation of phenol wastewater. In: *2019 International Conference on Energy, Environmental and Civil Engineering*. Wuhan, China, 23-24 Jun 2019. U.S.A: DEStech Publications, Inc. Available at: <<https://www.dpi-proceedings.com/index.php/dteees/article/view/31521>> [Accessed 08 Feb 2022].
- El-Bindary, A. A., Ismail, A. and Eladi, E. F., 2019. Photocatalytic degradation of reactive blue 21 using Ag doped ZnO nanoparticles. *Journal of Materials and Environmental Science*, 10, pp. 1258-1271.
- Fu, S. Z., Deng, B. Q., Ma, D. M., Cheng, H. Q. and Dong, S. S., 2018. Visible-light-driven photocatalytic fuel cell with an Ag-TiO<sub>2</sub> carbon foam anode for simultaneous 4-Chlorophenol degradation and energy recovery. *Chemengineering*, 2(2), 20.
- Garrido-Cardenas, J. A., Esteban- García, B., Agüera, A., Sánchez-Pérez, J. A. and Manzano-Agugliaro, F., 2020. Wastewater treatment by advanced oxidation process and their worldwide research trends. *International Journal Environmental Research Public Health*, 17(1), 170.
- García-Betancourt, M. L., Jiménez, S. I. R., González-Hodges, A., Salazar, Z. E. N., Escalante-García, I. L. and Aparicio, J. R., 2020. Low dimensional nanostructures: measurement and remediation technologies applied to trace heavy metals in water. In: M. A. Murillo-Tovar, H. Saldarriaga-Noreña and A. Saeid, *Trace metals in the environment- new approaches and recent advances*. London: Intechopen.
- Gao, W., Liu, Y. and Dong, J., 2021. Immobilized ZnO based nanostructures and their environmental applications. *Progress in Natural Science: Materials International*, 31(6), pp. 821-834.
- Gawande, M. B., Goswami, A., Felpin, F. X., Asefa, T., Huang, X., Silva, R., Zou, X., Zboril, R. and Varma, R. S., 2016. Cu and Cu-based nanoparticles: synthesis and applications in catalysis. *Chemical Reviews*, 116, pp. 3722-3811.
- Ghauch, A., Tuqan, A. M. and Kibbi, N., 2015. Naproxen abatement by thermally activated persulfate in aqueous systems. *Chemical Engineering Journal*, 279, pp. 861-873.
- Ghosh, A. and Mondal, A., 2015. Fabrication of stable, efficient and recyclable p-CuO/n-ZnO thin film heterojunction for visible light driven photocatalytic degradation of organic dyes. *Materials Letters*, 164, pp. 221-224.
- Gonon, M., 2021. *Encyclopedia of Materials: Technical Ceramics and Glasses*. Amsterdam, Netherlands: Elsevier. pp. 560-577.

- Guan, K., Zhou, P. J., Zhang, J. Y. and Zhu, L. L., 2020. Catalytic degradation of acid orange 7 in water by persulfate activated with CuFe<sub>2</sub>O<sub>4</sub>@RSDBC. *Materials Research Express*, 7, 016529.
- HACH, 2017. Nitrogen, ammonia. *USEPA Nessler Method 8038*. 9<sup>th</sup> ed.
- HACH, 2021. Oxygen demand, chemical. *USEPA Reactor Digestion Method 8000*. 13<sup>th</sup> ed.
- Hamzah, M. H., Asri, M. F. A., Che Man, H. and Mohammed, A., 2019. Prospective application of palm oil mill boiler ash as a biosorbent: effect of microwave irradiation and palm oil mill effluent decolorization by adsorption. *International Journal of Environmental Research and Public Health*, 16(8), 3453.
- Han, J. H. and Liu, Z. F., 2021. Optimization and modulation strategies of zinc oxide-based photoanodes for highly efficient photoelectrochemical water splitting. *ACS Applied Energy Materials*, 4(1), pp. 1004-1013.
- Hashiguchi, Y., Zakaria, M. R., Maeda, T., Yusoff, M. Z. M., Hassan, M. A. and Shirai, Y., 2020. Toxicity identification and evaluation of palm oil mill effluent and its effects on the planktonic crustacean *Daphnia magna*. *Science of The Total Environment*, 710, 136277.
- Hashiguchi, Y., Zakaria, M., Toshinari, M., Yusoff, M. Z. M. Y., Shirai, Y. and Hassan, M. A., 2021. Ecotoxicological assessment of palm oil mill effluent final discharge by zebrafish (*Danio rerio*) embryonic assay. *Environmental Pollution*, 277, 116780.
- Hassan, H. H., Badr, I. H. A., Abdel-Fatah, H. T. M., Elfeky, E. M. S. and Abdel-Aziz, A. M., 2018. Low cost chemical oxygen demand sensor based on electrodeposited nano-copper film. *Arabian Journal of Chemistry*, 11(2), pp. 171 -180.
- Hayawin, Z. N., Ibrahim, M. F., Kamarudin, H., Norfaizah, J., Ropandi, M., Astimar, A. A. and Abd-Aziz, S., 2020. Production of a bioadsorbent from oil palm kernel shell, and application for pollutants and colour removal in palm oil mill effluent final discharge. *IOP Conference Series: Materials Science and Engineering*, 736, 022045.
- Hernández, S., Hidalgo, D., Sacco, A., Chiodoni, A., Lamberti, A. Cauda, V., Tresso, E. and Saracco, G., 2015. Comparison of photocatalytic and transport properties of TiO<sub>2</sub> and ZnO nanostructures for solar-driven water splitting. *Physical Chemistry Chemical Physics*, 17, pp. 7775-7786.
- Hu, H. D. and Xu, K., 2020. *High-risk pollutants in wastewater*. Amsterdam, Netherlands: Elsevier.
- Isa, M. H., Bashir, M. J. K. and Wong, L. P. 2022. Anaerobic treatment of ultrasound pre-treated palm oil mill effluent (POME): microbial diversity and enhancement of

- biogas production. *Environmental Science and Pollution Research*. 29(29), pp. 44779-44793.
- Jabeen, M. Iqbal, M. A., Kumar, R. V., Ahmed, M. and Javed, M., 2014. Chemical synthesis of zinc oxide nanorods for enhanced hydrogen gas sensing. *Chinese Physics B*, 23(1), 018504.
- Jouanneau, S., Recoules, L., Durand, M. J., Boukabache, A., Picot, V., Primault, Y., Lakel, A., Sengelin, M., Barillon, B. and Thouand, G., 2014. Methods for assessing biochemical oxygen demand (BOD): a review. *Water Research*, 49, pp. 62-82.
- Kanakaraj, D., Ahmad, N. B., Sedik, N. B. M., Long, S. G. H., Guan, T. M. and Chin, L. Y., 2017. performance of solar photocatalysis and photo-fenton degradation of palm oil mill effluent. *Malaysian Journal of Analytical Sciences*, 21(5), pp. 996-1007.
- Kaniapan, S., Hassan, S., Ya, H., Patma Nesan, K. and Azeem, M., 2021. The utilisation of palm oil and oil palm residues and the related challenges as a sustainable alternative in biofuel, bioenergy, and transportation sector: a review. *Sustainability*, 13(6), 3110.
- Kamyab, H., Chelliapan, S., Din, F.M., Rezania, S., Khademi, T. and Kumar, A., 2018. Palm oil mill effluent as an environmental pollutant, In: Waisundara, V., eds. *Palm Oil*; Rijeka: IntechOpen, pp. 13–28.
- Karimifard, S. and Moghaddam, M. R. A., 2018. Application of response surface methodology in physicochemical removal of dyes from wastewater: a critical review. *Science of The Total Environment*, 640 – 641, pp. 772-797.
- Kee, M. W., Lam, S. M., Sin, J. C., Zeng, H. H. and Mohamed, A. R., 2020. Explicating charge transfer dynamics in anodic TiO<sub>2</sub>/ZnO/Zn photocatalytic fuel cell for ameliorated palm oil mill effluent treatment and synchronized energy generation. *Journal of Photochemistry and Photobiology A: Chemistry*, 391, 112353.
- Kee, M. W., Lam, S. M. and Sin, J. C., 2019. Concurrent palm oil mill effluent degradation and power production by photocatalytic fuel cell. *AIP Conference Proceedings*, 2157(1), 020001.
- Kee, M. W., Wen, J., Lam, S. M., Sin, J. C. and Mohamed, A. R., 2018. Evaluation of photocatalytic fuel cell (PFC) for electricity production and simultaneous degradation of methyl green in synthetic and real greywater effluents. *Journal of Environmental Management*, 228, pp. 383–392.
- Kee, W. C., Wong, Y. S., Ong, S. A., Lutpi, N. A., Sam, S. T., Chai, A. and Eng, K. M., 2022. Photocatalytic degradation of sugarcane vinasse using ZnO photocatalyst:

operating parameters, kinetic studies, phytotoxicity assessments, and reusability. *International Journal of Environmental Research*, 16, 3.

Kemacheevakul, P. and Chuangchote, S., 2021. Photocatalytic remediation of organic pollutants in water. In: Inamuddin, M. I. Ahamed, E. Lichtfouse, eds. *Water Pollution and Remediation: Photocatalysis. Environmental Chemistry for a Sustainable World*, vol 57. Denmark: Springer Cham.

Khalik, W. F. W. M., Ho, L. N., Ong, S. A., Voon, C. H., Wong, Y. S., Yusoff, N. N. A. N., Lee, S. L. and Yusuf, S. Y., 2017. Optimization of degradation of reactive black 5 (RB5) and electricity generation in solar photocatalytic fuel cell system. *Chemosphere*, 184, pp. 112-119.

Kokkinos, P., Venieri, D. and Mantzavinos, D., 2021. Advanced oxidation processes for water and wastewater viral disinfection. a systematic review. *Food and Environmental Virology*, 13, pp. 283-302.

Lam, S. M., Choong, M. K., Sin, J. C. and Zeng, H. H., 2020. Synchronous organics removal and copper reduction in semiconductor wastewater with energy recuperation via photocatalytic fuel cell. *E3S Web of Conferences*, 167, 01002.

Lam, S. M., Sin, J. C., Lin, H., Li, H., Lim, J. W. and Zeng, H., 2020. A Z-scheme WO<sub>3</sub> loaded-hexagonal rod-like ZnO/Zn photocatalytic fuel cell for chemical energy recuperation from food wastewater treatment. *Applied Surface Science*, 514, 145945.

Lanan, F. A. B. M., Selvarajoo, A., Sethu, V. and Arumugasamy, S. K., 2021. Utilisation of natural plant-based fenugreek (*Trigonella foenum-graecum*) coagulant and okra (*Abelmoschus esculentus*) flocculant for palm oil mill effluent (POME) treatment. *Journal of Environmental Chemical Engineering*, 9(1), 104667.

Lebeau, B., Jonas, F., Gaudin, P., Bonne, M. and Blin, J. L., 2020. Dyes depollution of water using porous TiO<sub>2</sub>-based photocatalysts. *Environmental Nanotechnology*, 4, pp.35-92.

Lee, J., Gunten, U. V. and Kim, J. H., 2020. Persulfate-based advanced oxidation: critical assessment of opportunities and roadblocks. *Environmental Science and Technology* 54, pp. 3064-3081.

Lee, S. L., Ho, L. N., Ong, S. A., Wong, Y. S., Voon, C. H., Khalik, W. F., Yusoff, N. A. and Nordin, N., 2017. A highly efficient immobilized ZnO/Zn photoanode for degradation of azo dye reactive green 19 in a photocatalytic fuel cell, *Chemosphere*, 166, pp. 118-125.

Lee, Z. S., Chin, S. Y., Lim, J. W., Witoon, T. and Chin, K. C., 2019. Treatment technologies of palm oil mill effluent (POME) and olive mill wastewater (OMW): A brief review. *Environmental Technology & Innovation*, 15, 100377.

- Li, J. W., Li, R. Z., Zou, L. M. and Liu, X. Y., 2019. Efficient degradation of norfloxacin and simultaneous electricity generation in a persulfate-photocatalytic fuel cell system. *Catalysts*, 9(10), 835.
- Li, M. H., Liu, Y., Dong, L. M., Shen, C. S., Li, F., Huang, M. H., Ma, C. Y., Yang, B., An, X. Q. and Sand, W., 2019. Recent advances on photocatalytic fuel cell for environmental applications—The marriage of photocatalysis and fuel cells. *Science of The Total Environment*, 668, pp. 966-978.
- Li, N., Tang, S., Rao, Y., Qi, Y., Wang, P., K., Jiang, Y., Huang, H. M., Gu, J. M. and Yuan, D., 2018. Improved dye removal and simultaneous electricity production in a photocatalytic fuel cell coupling with persulfate activation, *Electrochimica Acta*, 270, pp. 330-338.
- Li, X. and Wang, J., 2019. One-dimensional and two-dimensional synergized nanostructures for high-performing energy storage and conversion. *InfoMat*, 2(1), pp. 3-32.
- Li, Z. C. and Yang, P., 2018. Review on physicochemical, chemical, and biological processes for pharmaceutical wastewater. *IOP Conference Series: Earth and Environmental Science*, 113, 012185.
- Liang, C. J., and Lei, J. H., 2015. Identification of active radical species in alkaline persulfate oxidation. *Water Environment Research*, 87 (7), pp. 656-659.
- Lim, K. S., Sethu, V. and Selvarajoo, A., 2021. Natural plant materials as coagulant and flocculants for the treatment of palm oil mill effluent. *Materials today: Proceedings*, 48(4), pp. 871-887.
- Lui, G., Jiang, G., Fowler, M., Yu, A. and Chen, Z., 2019. A high-performance wastewater-fed flow-photocatalytic fuel cell. *Journal of Power Sources*, 425, pp. 69-75.
- Marcello, B. A., Correa, O. V., Bento, R. T. and Pillis, M. F., 2020. Effect of growth parameters on the photocatalytic performance of TiO<sub>2</sub> films prepared by MOCVD. *Journal of Brazilian Chemical Society*, 31, pp. 1-14.
- Masuda, R., Kowalski, D., Katino, S., Aoki, Y., Nozawa, T. and Habazaki, H., 2020. Characterization of dark-colored nanoporous anodic films on zinc. *Coatings*, 10, 1014.
- Mayahhi, A. A. and Al-Asadi, H. A. A., 2018. Advanced oxidation processes (AOPs) for wastewater treatment and reuse: a brief review. *Asian Journal of Applied Science and Technology*, 2(3), pp. 18-30.

- Medel, A., Treviño-Reséndez, J., Brillas, E., Meas, Y. and Sirés, I., 2020. Contribution of cathodic hydroxyl radical generation to the enhancement of electro-oxidation process for water decontamination. *Electrochimica Acta*, 331, 135382.
- Meng, Y., Lin, Y. and Lin, Y., 2014. Electrodeposition for the synthesis of ZnO nanorods modified by surface attachment with ZnO nanoparticles and their dye-sensitized solar cell applications. *Ceramics International*, 40, pp. 1693-1698.
- Mohamad, Z., Razak, A. A., Krishnan, S., Singh, L., Zularisam, A. W. and Nasrullah, M., 2022. Treatment of palm oil mill effluent using electrocoagulation powered by direct photovoltaic solar system. *Chemical Engineering Research and Design*, 177, pp. 578-582.
- Mohamed, R. M. and Harraz, F. A., 2020. Mechanistic investigation and photocatalytic activity of yttrium vanadate (YVO<sub>4</sub>) nanoparticles for organic pollutants mineralization. *Journal of Materials Research and Technology*, 9(3), pp. 5666-5675.
- Mohammad, S., Baidurah, S., Kobayashi, T., Ismail, N. and Leh, C. P., 2021. Palm oil mill effluent treatment processes—a review, *Processes*, 9(5), 739.
- Moksin, N. S. A., Ong, Y. P., Ho, L. N. and Tay, M. G., 2021. Optimization of photocatalytic fuel cells (PFCs) in the treatment of diluted palm oil mill effluent (POME). *Journal of Water Process Engineering*, 40, 101880.
- Momoh, Y. and Naeyor, B., 2016. A novel electron acceptor for microbial fuel cells: nature of circuit connection on internal resistance. *Biochemical Journal*, 2(4), pp. 216-220.
- Mustapha, S., Ndamitso, M. M., Adbulkareem, A. S., Tijani, J. O., Shuaib, D. T., Ajala, A. O. and Mohammed, A. K. 2020. Application of TiO<sub>2</sub> and ZnO nanoparticles immobilized on clay in wastewater treatment: a review. *Applied Water Science*, 10, 49.
- Nasrullah, Q., Zularisam, A. W., Krishnan, S., Sakinah, M., Singh, L. and Yap, W. F., 2019. High performance electrocoagulation process in treating palm oil mill effluent using high current intensity application. *Chinese Journal of Chemical Engineering*, 27(1), pp. 208-217.
- Nawaz, R., Kait, C. F., Chia, H. Y., Isa, M. H. and Huei, L. W. 2019. Glycerol-mediated facile synthesis of colored titania nanoparticles for visible light photodegradation of phenolic compounds. *Nanomaterials*, 9(11), 1586.
- Nazri, N. A. B. A., Chong, C. H. and Nithyanandam, R., 2018. Ammoniacal nitrogen removal in synthetic wastewater using seaweed-based ionic liquid and bacillus spp. *Journal of Engineering Science and Technology*, Special Issue August, pp. 112-122.

- Oluwole, A. O., Omotola, E. O. and Olatunji, O. S., 2020. Pharmaceuticals and personal care products in water and wastewater: a review of treatment processes and use of photocatalyst immobilized on functionalized carbon in AOP degradation. *BMC Chemistry*, 14, 62.
- Ong, Y. P., Ho, L. N., Ong, S. A., Banjuraizah, J, Ibrahim, A. H., Thor, S. H. and Teoh, T. P., 2021. Dye decolourisation and energy recovery of photocatalytic fuel cell subjected to optimization of supporting electrolyte concentration and external resistance. *Journal of Environmental Chemical Engineering*, 9(4), 105794.
- Oyekanmi, A. A., Alshammari, M. B., Ibrahim, M. N. M., Hanafiah, M. M., Elnaggar, A. Y., Ahman, A., Oyediran, A. T., Rosli, M. A., Setapar, S. H. M., Daud, N. N. N. and Hussein, E. E., 2021. Highly effective cow bone based biocomposite for the sequestration of organic pollutant parameter from palm oil mill effluent in a fixed bed column adsorption system. *Polymers*, 14(1), 86.
- Oyekanmi, A. A., Latiff, A. A. A., Daud, Z., Mohamed, R. M. S. R., Aziz, N. A. A., Ismail, N., Rafatullah, M., Ahmad, A. and Hossain, K., 2019. Adsorption of pollutants from palm oil mill effluent using natural adsorbents: optimization and isotherm studies. *Desalination and Water Treatment*, 169, pp. 181-190.
- Pan, D. L., Xiao, S. N., Che, X. F., Li, R. P., Cao, Y. N., Zhang, D. Q., Pu, S. S., Li, Z. C., Li, G. S. and Li, H. X., 2019. Efficient photocatalytic fuel cell via simultaneous visible photoelectrocatalytic degradation and electricity generation on a porous coral-like WO<sub>3</sub>/W photoelectrode. *Environmental Science & Technology*, 53, pp. 3697-3706.
- Pandey, A., Höfer, R., Taherzadeh, M., Nampoothiri, K. M. and Larroche, C., 2015. *Industrial Biorefineries & White Biotechnology*. Amsterdam, Netherlands: Elsevier. pp. 575-605.
- Pandis, P. K., Kalogirou, C., Kanellou, E., Vaitsis, C., Savvidou, M. G., Sourkouni, G., Zorpas, A. A. and Argiris, C., 2021. Key points of advanced oxidation processes (AOPs) for wastewater, organic pollutants and pharmaceutical waste treatment: a mini review. *ChemEngineering*, 6(1), 8.
- Parvizi, T. and Parsa, J. B., 2021. High-efficient photocatalytic fuel cell integrated with periodate activation for electricity production by degradation of refractory organics. *Journal of Power Sources*, 484, 229264.
- Patel, H. and Vashi, R. T., 2015. *Characterisation of textile wastewater. Characterisation and treatment of textile wastewater*. Amsterdam, Netherlands: Elsevier. pp. 21-71.
- Patella, B., Moukri, N., Regalbuto, G., Cipollina, C., Pace, E., Vincenzo, S., D., Aiello, G., O’Riordan, A. and Inguanta, R., 2022. Electrochemical synthesis of zinc oxide

nanostructures on flexible substrate and application as an electrochemical immunoglobulin-g immunosensor, *Materials*, 15, 713.

- Pelaez, M., Falaras, P., Likodimos, V., O'Shea, K., de la Cruz, A. A., Dunlop, P. S. M., Bryne, J. A. and Dionysiou, D. D., 2016. Use of selected scavengers for the determination of NF-TiO<sub>2</sub> reactive oxygen species during the degradation of Microcystin-LR under visible light irradiation. *Journal of Molecular Catalysis A: Chemical*, 425, pp. 183-189.
- Poh, P. E. and Chong, M. F., 2014. Upflow anaerobic sludge blanket-hollow centered packed bed (UASB-HCPB) reactor for thermophilic palm oil mill effluent (POME) treatment. *Biomass Bioenergy*, 67, pp. 231-242.
- Priya, S. D., Nesaraj, A. S. and Selvakumar, A. I., 2021. Facile wet-chemical synthesis and evaluation of physico-chemical characteristics of novel nanocrystalline NdCoO<sub>3</sub>-based perovskite oxide as cathode for LT-SOFC applications. *Bulletin of Materials Science*, 44, 115.
- Rabé, K., Liu, L. F. and Nahyoon, N. A., 2020. Electricity generation in fuel cell with light and without light and decomposition of tetracycline hydrochloride using g-C<sub>3</sub>N<sub>4</sub>/Fe<sup>0</sup>(1%)/TiO<sub>2</sub> anode and WO<sub>3</sub> cathode. *Chemosphere*, 243, 125425.
- Ratnasari, A., Syafiuddin, A., Boopathy, R., Malik, S., Mehmood, M. A., Amalia, R., Prastyo, D. D. and Zaidi, N. S., 2022. Advances in pre-treatment technology for handling the palm oil mill effluent: Challenges and prospects. *Bioresource Technology*, 344, 126239.
- Rayaroth, M. P., Escobedo, E. and Chang, Y. S., 2020. Degradation studies of halogenated flame retardants. *Comprehensive Analytical Chemistry*, 88, pp. 303-339.
- Rioja-Cabanillas, A., Valdesuerio, D., Fern´andez-Ib´a˜nez, P. and Byrne, J. A., 2021. Hydrogen from wastewater by photocatalytic and photoelectrochemical treatment. *Journal of Physics: Energy*, 3(1), 012006.
- Saad, M. S., Wirzal, M. D. H., Halim, N. S. A. and Khan M. R., 2020. Removal color from palm oil mill effluent (POME): electrocoagulation method vs microfiltration using nanofiber membrane. *International Journal of Electrochemical Science*, 15, pp. 11283-11293.
- Saad, M. S., Wirzal, M. D. H. and Putra, Z. A., 2021. Review on current approach for treatment of palm oil mill effluent: Integrated system. *Journal of Environmental Management*, 286, 112209.
- Sadhukhan, J., Martnez-Hernandez, E., Murphy, R. J., Ng, D. K. S., Hassim, M. H. and Ng, K. S., 2018. Role of bioenergy, biorefinery and bioeconomy in sustainable



- development: Strategic pathways for Malaysia. *Renewable and Sustainable Energy Reviews*, 81, Part 2, pp. 1966-1987.
- Saha, D., Desipio, M. W., Hoinkis, T. J., Smeltz, E. J., Thorpe, R., Hensley, D. K., Fischer-Drowos, S. G. and Chen, J., 2018. Influence of hydrogen peroxide in enhancing photocatalytic activity of carbon nitride under visible light: An insight into reaction intermediates. *Journal of Environmental Chemical Engineering*, 6(4), pp. 4927-4936.
- Samanta, L. D., Sahu, S. J. and Roy, S., 2020. Photocatalytic removal of Malachite Green through ZnO/CeO<sub>2</sub> nanocomposite catalyst. *Turkish Journal of Computer and Mathematics Education*, 11(3), pp. 1886-1892.
- Saputera, W. H., Amri, A. F., Mukti, R. R., Suendo, V., Devianto, H. and Sasongko, D. 2021. Photocatalytic degradation of palm oil mill effluent (POME) waste using bivo<sub>4</sub> based catalysts. *Molecules*, 26, 6225.
- Sayed, M., Khan, J.A., Shah, L.A., Shah, N.S., Shah, F. and Khan, H. M., 2017. Solar light responsive poly(vinyl alcohol)-assisted hydrothermal synthesis of immobilized TiO<sub>2</sub>/Ti film with the addition of peroxymonosulfate for photocatalytic degradation of ciprofloxacin in aqueous media: a mechanistic approach. *The Journal of Physical Chemistry C*, 122 (1), pp. 406-421.
- Schnerder, J. T., Firak, D. S., Ribeiro, R. R. and Peralta-Zamora, P. 2020. Use of scavenger agents in heterogeneous photocatalysis: truths, half-truths, and misinterpretations. *Physical Chemistry Chemical Physics*, 22(27), pp. 15723-15733.
- Shmeis, R. M. A., 2018. Chapter one - water chemistry and microbiology. *Comprehensive Analytical Chemistry*, 81, pp. 1-56.
- Sia, Y. Y., Tan, I. A. W. and Abdullah, M. O., 2020. Palm oil mill effluent treatment using electrocoagulation-adsorption hybrid process. *Materials Science Forum*, 997, pp. 139-149.
- Singh, M P. and Pal, H., 2021. Concise overview of photocatalytic fuel cell technology for the generation of electricity and degradation of organic wastewater. *International Research Journal of Engineering and Technology (IRJET)*, 8(8) pp. 62-67.
- Sun, J., Liu, L. and Yang, F., 2022. A visible-light-driven photocatalytic fuel cell/ peroxymonosulfate (PFC/PMS) system using blue TiO<sub>2</sub> nanotube arrays (TNA) anode and Cu-Co-WO<sub>3</sub> cathode for enhanced oxidation of organic pollutant and ammonium nitrogen in real seawater. *Applied Catalysis B: Environmental*, 308, 121215.

- Syahin, M., Ghani, W.W.A.K. and Loh, S., 2020. Decolourisation of palm oil mill effluent (pome) treatment technologies: A review. *Journal of Oil Palm Research*, 32(1), pp. 1-15.
- Tan, Y. D. and Lim J. S., 2019. Feasibility of palm oil mill effluent elimination towards sustainable Malaysian palm oil industry. *Renewable and Sustainable Energy Review*, 111, pp. 507-522.
- Tan, X. H., Bai, J., Zheng, J. Y., Zhang, Y., Li, H. H., Zhou, T. S., Xia, L. G., Xu, Q. J. and Zhou, B. X., 2019. Photocatalytic fuel cell based on sulfate radicals converted from sulfates in situ for wastewater treatment and chemical energy utilization. *Catalysis Today*, 335, pp. 485-491.
- Tang, S., Li, N., Yuan, D., Tang, J., Li, X., Zhang, C. and Rao, Y., 2019. Comparative study of persulfate oxidants promoted photocatalytic fuel cell performance: simultaneous dye removal and electricity. *Chemosphere*, 234, pp. 358-667.
- Thor, S. H., Ho, L. N., Ong, S. A., Nordin, N., Ong, Y. P. and Yap, K. L., 2020. Explicating the importance of aeration and pH for amaranth degradation and electricity generation in a viable hybrid system of photocatalytic fuel cell and electro-fenton process. *Separation and Purification Technology*, 239, 116535.
- USDA, 2022. *Oilseeds: World Markets and Trade. United States Department of Agriculture (2022)*. [online] Available at: <<https://usda.library.cornell.edu/concern/publications/tx31qh68h?locale=en#release-items>> [Accessed 26 February 2022].
- Ushani, U., Lu, X. Q., Wang J. H., Zhang, Z. Y., Dai, J. J., Tan, Y. J., Wang, S., Li, W. J., Niu, C. X., Zai, T., Wang, N. and Zhen, G. Y., 2020. Sulfate radicals-based advanced oxidation technology in various environmental remediation: A state-of-the-art review. *Chemical Engineering Journal*, 402, 126232.
- Vasseghian, Y., Khatee, A., Dragoi, E., Moradi, M., Nabavifard, S., Conti, G. O. and Khaneghah, A. M., 2020. Pollutants degradation and power generation by photocatalytic fuel cells: A comprehensive review. *Arabian Journal of Chemistry*, 13(11), pp. 8458-8480.
- Vilar, R., 2016. *Laser Surface Modification of Biomaterials: Techniques and Applications*. Sawston, United Kingdom: Woodhead Publishing. pp. 77-125.
- Wei, J. X., Qin, F., Li, G., Li, X. J., Liu, X. B. and Dai, X. W., 2021. Chirp modulation enabled turbidity measurement for large scale monitoring of fresh water. *Measurement*, 184, 109989.
- Xiao, J. D., Xie, Y. B. and Cao, H. B., 2015. Organic pollutants removal in wastewater by heterogeneous photocatalytic ozonation. *Chemosphere*, 121, pp. 1-17.

- Xie, Y. D., Kocaefe, D., Chen, C. Y. and Kocaefe, Y., 2016. Review of research on template methods in preparation of nanomaterials. *Journal of Nanomaterials*, 8, 2302595.
- Xu, L. and Liu, L., 2022. Piezo-photocatalytic fuel cell with atomic Fe@MoS<sub>2</sub> on CFC helical electrode has enhanced peroxy monosulfate activation, pollutant degradation and power generation. *Applied Catalysis B: Environmental*, 304, 120953.
- Yan, A., Wang, Y., Tan, S. N., Yusof, M. L. M., Ghosh, S. and Chen, Z., 2020. Phytoremediation: a promising approach for revegetation of heavy metal-polluted land. *Frontiers in Plant Science*, 11, 359.
- Yong, Z. J., Lam, S. M., Sin, J. C., Mohamed, A. R. and Jaffari, Z. H., 2022. Boosting sunlight-powered photocatalytic fuel cell with S-scheme Bi<sub>2</sub>WO<sub>6</sub>//ZnO nanorod array composite photoanode. *Inorganic Chemistry Communications*, 143, 109826.
- Yong, Z. J., Lam, S. M., Sin, J. C. and Mohamed, A. R., 2021. Feasibility study of municipal wastewater removal synchronized with electricity generation via solar-driven photocatalytic fuel cell with Bi<sub>2</sub>WO<sub>6</sub>/ZnO nanorods array photoanode. *IOP Conf. Series: Earth and Environmental Science*, 945, 012004.
- Yu, Z. X., Moussa, H., Liu, M. M., Schneider, R., Moliere, M. and Liao, H. L., 2019. Heterostructured metal oxides-ZnO nanorods films prepared by SPPS route for photodegradation applications. *Surface and Coatings Technology*, 375, pp. 670-680.
- Yu, H. L., Zhou, Y. W., Xue, X. L., Liu, L. Q., Hong, J. Q., Liu, Z. Q., Chen, H. M., Shen, Y. G., Zheng, B. and Wang, J., 2021. Zg-modified ZnO nanorod array fabricated on polyester fabric and its enhanced visible-light photocatalytic performance by a built-in electric field and plasmonic effect. *ACS Omega*, 6 (22), pp. 14078 – 14089.
- Yunus, S. H. A., Sahdan, M. Ichmura, M., Supee, A. and Rahim, S., 2017. Structural studies of ZnO nanostructures by varying the deposition parameters. *AIP Conference Proceedings*, 1788(1), 030101.
- Yusoff, M. N. A. M., Zulkifi, N. W. M., Sukiman, N. L., Ong, H. C., Hassan, M. H., Hasnul, M. H., Zulkifli, M. S. A., Abbas, M. M. and Zakaria, M. Z., 2021. Sustainability of palm biodiesel in transportation: a review on biofuel standard, policy and international collaboration between malaysia and colombia. *BioEnergy Research*, 14, pp. 43-60.
- Zainuri, N. Z., Hairom, N. H. H., Sidik, D. A. B., Misdan, N., Yusof, N. and Mohammad, A. W., 2018. Reusability performance of zinc oxide nanoparticles for photocatalytic degradation of pome. *E3S Web of Conference*, 34(4), 02013.
- Zhao, Y. Q., Li, Y. C., Yang, Z and Fang, Y. J., 2011. A novel monitoring system for COD using optical ultraviolet absorption method. *Procedia Environmental*

*Sciences*, 10, pp. 2348-2353.

Zhou, J., Hou, C. and Liu, L. F., 2019. Persulfate enhanced pollutants oxidation efficiency and power generation in photocatalytic fuel cell with anodic BiOCl/BiOI and cathodic copper cobalt oxide. *Journal of the Taiwan Institute of Chemical Engineers*, 101, pp. 31-40.

Zulfahmi, I., Kandi, R. N., Huslina, F., Rahmawati, L., Muliara, M., Sumon, K. A. and Rahman, M. M., 2021. Phytoremediation of palm oil mill effluent (POME) using water spinach (*Ipomoea aquatica* Forsk). *Environmental Technology & Innovation*, 21, 101260.

## **AWARD**

**2<sup>nd</sup> Place** in Green Technology Category, awarded by 8<sup>th</sup> International Biotechnology Competition and Exhibition 2022 (IBCEx22) organized by Universiti Teknologi Malaysia (UTM), Johor via Cisco Webex online platform on 15 – 16<sup>th</sup> April 2022.

Title of Project: Photocatalytic Fuel Cell for Remediation of Environmental Pollutants and Sustainable Power Production.

Contributors: ChM. Ts. Dr. Lam Sze Mun, ChM. Ts. Dr. Sin Jin Chung, Warren Tong Meng Wei, Joyee Yap Chun Ting.